Copyright Warning & Restrictions

The copyright law of the United States (Title 17, United States Code) governs the making of photocopies or other reproductions of copyrighted material.

Under certain conditions specified in the law, libraries and archives are authorized to furnish a photocopy or other reproduction. One of these specified conditions is that the photocopy or reproduction is not to be "used for any purpose other than private study, scholarship, or research." If a, user makes a request for, or later uses, a photocopy or reproduction for purposes in excess of "fair use" that user may be liable for copyright infringement,

This institution reserves the right to refuse to accept a copying order if, in its judgment, fulfillment of the order would involve violation of copyright law.

Please Note: The author retains the copyright while the New Jersey Institute of Technology reserves the right to distribute this thesis or dissertation

Printing note: If you do not wish to print this page, then select "Pages from: first page # to: last page #" on the print dialog screen

ABSTRACT

APPLICATION OF INKJET PRINTING TECHNOLOGY TO FLEXIBLE BATTERIES

by
Yuan Gu

Printing technologies have been considered as alternative methods to fabricate thin films in recent years. More and more functional devices like resistors, sensors, antennas and even energy storage devices have been fabricated by printing technologies. As a typical digital printing technology, inkjet printing has much more advantages over the traditional mechanical printing technologies such as: low cost, computer controllable shape design and precise deposition. In this investigation, application of inkjet printing is used to fabricate conductive tracks and rechargeable lithium ion batteries.

Particle free silver ink is developed to solve this problem. In this research, silver complex solution is printed on polymer substrate and sintered in air. It is shown that the polymer additive could control the particle shape and size of silver produced during thermal sintering. Also, the silver particle size could be reduced furtherly with a certain amount of chemical reductant additive. Moreover, the chemical reductant additive can lower the sintering temperature effectively. High resolution silver conductive tracks are made by particle free silver ink by inkjet printing.

Constantan particle suspension ink is invented to make constantan sensors and resistors. A new chemical reducing sintering (CRS) is used to eliminate oxidation layers and sinter the constantan at low temperature. CRS is much safer and easier than other researches. This technology provides a general method to make metallic conductive tracks. Nickel and copper conductive tracks are also made by this method.

The nickel conductive film is made by CRS and used as the current collectors for the lithium ion batteries, which is cheaper than the traditional gold current collectors and more conductive than conventional carbon serious current collectors. Flexible rechargeable lithium ion batteries are made by inkjet printing layer by layer. Inkjet printing is a potential method to fabricate thin film designable batteries.

APPLICATION OF INKJET PRINTING TECHNOLOGY TO FLEXIBLE BATTERIES

by
Yuan Gu

A Dissertation
Submitted to the Faculty of
New Jersey Institute of Technology
in Partial Fulfillment of the Requirements for the Degree of
Doctor of Philosophy in Materials Science and Engineering

Interdisciplinary Program in Materials Science and Engineering

August 2016

APPROVAL PAGE

APPLICATION OF INKJET PRINTING TECHNOLOGY TO FLEXIBLE BATTERIES

Yuan Gu

Dr. John F. Federici, Dissertation Advisor Distinguished Professor of Physics, NJIT	Date
Dr. Zafar Iqbal, Committee Member Research Professor of Chemistry and Environmental Science, NJIT	Date
Dr. Reginald Farrow, Committee Member Research Professor of Physics, NJIT	Date
Dr. Robert B. Barat, Committee Member Professor of Chemical, Biological and Pharmaceutical Engineering, NJIT	Date
Dr. Keun Hyuk Ahn, Committee Member Associate Professor of Physics, NJIT	Date

BIOGRAPHICAL SKETCH

Author: Yuan Gu

Degree: Doctor of Philosophy

Date: August 2016

Undergraduate and Graduate Education:

- Doctor of Philosophy in Materials Science and Engineering,
  New Jersey Institute of Technology, Newark, NJ, 2016

- Master of Physical Chemistry of Metallurgy,
  China Automotive Battery Research Institute Co., Ltd., Beijing, P. R. China, 2012

- Bachelor of Metallurgy Engineer,
  University of Science and Technology Beijing, Beijing, P. R. China, 2009

Major: Materials Science and Engineering

Publications:

Gu, Y., Zhang, X., Lu, S., Zhao, T., Jiang, D., Yang, R., & Wu, A. (2012). $LiFePO_4$/C via fluoride doping. *Rare Metals, 31*(6), 573-577. doi:10.1007/s12598-012-0560-1

Gu, Y., Zhang, X., Lu, S., Jiang, D., & Wu, A. (2015). High rate performance of LiF modified $LiFePO_4$/C cathode material. *Solid State Ionics, 269*, 30-36. doi:http://dx.doi.org/10.1016/j.ssi.2014.11.007

Gu, Y., Zhang, X., Lu, S., Zhao, T., & Jiang, D. (2013). The study of structure and modification of $LiFePO_4$, *Chinese Journal of Power Source, 37*, No. 1.

Gu, Y., Wu, A., Sohn, H., Nicoletti, C., Iqbal, Z., & Federici, J. F. (2015). Fabrication of rechargeable lithium ion batteries using water-based inkjet printed cathodes. *Journal of Manufacturing Processes, 20, Part 1*, 198-205. doi:http://dx.doi.org/10.1016/j.jmapro.2015.08.003

Gu, Y., Yu, Z., Wang, D., & Federici, J. F. (2016). Fabrication of flexible current collector for lithium ion batteries by inkjet printing (waiting for sponsor's permission and patent application).

Gu, Y., Wu, A., & Federici, J. F. (2016). Comparison of thermal decomposition and chemical reduction of particle-free silver ink for inkjet printing (submitted to *Journal of Solid Thin Films*, under review).

Gu, Y., Wu, A., Federici, J. F., & Zhang, X., (2016). Fabrication of flexible constantan patterns by constantan ink (submitted *to Journal of sensors and actuators*, under review).

Wu, A., & Gu, Y. (2013). Study on electrochemical performance of carbon-coated $LiFePO_4$. *Emerging Materials Research, 2*(3), 133-137. doi:10.1680/emr.12.00014

Wu, A., Gu, Y., Beck, C., Iqbal, Z., & Federici, J. F. (2014). Reversible chromatic sensor fabricated by inkjet printing TCDA-ZnO on a paper substrate. *Sensors and Actuators B: Chemical, 193*, 10-18. doi:http://dx.doi.org/10.1016/j.snb.2013.10.130

Wu, A., Gu, Y., Stavrou, C., Kazerani, H., Federici, J. F., & Iqbal, Z. (2014). Inkjet printing colorimetric controllable and reversible poly-PCDA/ZnO composites. *Sensors and Actuators B: Chemical, 203*, 320-326. doi:http://dx.doi.org/10.1016/j.snb.2014.06.132

Wu, A., Gu, Y., Tian, H., Federici, J. F., & Iqbal, Z. (2014). Effect of alkyl chain length on chemical sensing of polydiacetylene and polydiacetylene/ZnO nanocomposites. *Colloid and Polymer Science, 292*(12), 3137-3146. doi:10.1007/s00396-014-3365-y

El, M. B., Gu, Y., Chou, T., & Wang, X. (2016). Cubic gauche polymeric nitrogen under ambient conditions (submitted to *nature communication*, under consideration).

Jiang, D., Zhang, X., Lu, S., Gu, Y., Cong, C., & Kan, S. (2012). Research on process of preparation and performance of iron phosphate as precursor of lithium iron phosphate. *Rare Metals, 30*(1), 52-54.

Cong, C., Zhang, X., Lu, S., & Gu, Y. (2012). Effect of different carbon sources on properies of $LiFePO_4$/C composites. *Chinese Journal of Power Source, 36*, No. 3.

Conferences:

Gu, Y., Zhang, X., Lu, S., Zhao, T., & Jiang, D. (2011). Effects of Fluorine Doping on the Electrochemical Behavior of $LiFePO_4$/C Cathode Materials. The 4th International Conference on Advanced Lithium Batteries for Automobile Application.

Gu, Y., & Federici, J. F. (2015). Environmentally-Friendly Flexible Lithium-Ion Battery by Inkjet Printing. TechConnect World Innovation Conference.

Gu, Y., & Federici, J. F. (2016). New Inks for Inkjet Printing of Electronic Circuits. 2016 TechConnect World Innovation Conference.

Carr, M., Gu, Y., & Federici, J. F. (2016). Application of Inkjet Printing. iMAPS New England 43th Symposium & Expo.

Carr, M., Gu, Y., & Federici, J. F. (2016). Application of Inkjet Printing. ATW on Additive Manufacturing.

Patents:

Gu, Y., Wu, A., & Federici, J. F. (2015). Fabrication of Strain Sensor by Inkjet Printing, (PRV-Provisiona).

Gu, Y., & Federici, J. F. (2015). Particle-Free Silver Ink for Inkjet Printing, (Disclosure filed).

Gu, Y., & Federici, J. F. (2016). Fabrication of Flexible Current Collector for Lithium Ion Batteries by Inkjet Printing, (Disclosure filed).

Wu, A., Gu, Y., & Federici, J. F. (2014). System and Method for Environmentally Friendly Inkjet Printing of Lithium Ion Battery Cathode with Aqueous Binder System, (PRV-Provisional).

Federici, J. F., Wu, A., Beck, C., Gu, Y., Iqbal, Z., & Zunino, J. (2014) "Poly-TCDA/ZnO Nano Composites Thin Film Sensor Fabricated by Inkjet Printing, (NPV-NonProvisional).

Zhang, X., Gu, Y., & Lu, S. (2012). A Method Used to Synthesize High Power $LiFePO_4$, (Chinese Patent, 201110459901.3).

Zhang, X., Gu, Y., & Lu, S. (2012). A Method Used to Improve Performance of $LiFePO_4$, (Chinese Patent, Submitted).

ACKNOWLEDGMENT

I would like to thank my dissertation Advisor, Professor John F. Federici for his enduring support and supervision through my research. Also, I would like to thank Professor Zafar Iqbal, Professor Reginald Farrow, Professor Robert B. Barat and Professor Keun Hyuk Ahn for their contributions to my research with their constructive suggestions.

I would like to acknowledge the US Army Armament Research, Department and Engineering Center (ARDEC) at Picatinny Arsenal, NJ for supporting this work financially through Mr. James Zunino.

Lastly, I would like to thank my parents, Jinbao Gu and Shuling Wang and my wife, Lijuan Xu for their infinite care and support.

TABLE OF CONTENTS

TABLE OF CONTENTS
(Continued)

Chapter **Page**

TABLE OF CONTENTS
(Continued)

TABLE OF CONTENTS
(Continued)

Chapter **Page**

LIST OF TABLES

LIST OF FIGURES

LIST OF FIGURES
(Continued)

LIST OF FIGURES
(Continued)

LIST OF FIGURES
(Continued)

LIST OF FIGURES
(Continued)

Figure **Page**

LIST OF FIGURES
(Continued)

Figure **Page**

LIST OF FIGURES
(Continued)

Figure **Page**

CHAPTER 1

INTRODUCTION

1.1 Background Introduction

Over the last twenty years, great interest in printed devices, electronics and circuits has been reached due to the development of and market for both various printers and inks. Novel manufacturing printing methods have been invented including mechanical (e.g., pad printing, gravure printing, screen printing, offset lithography and flexography), digital (e.g., inkjet-printing) and even 3D printing technologies. The basic principle of printing is the deposition process of functional "ink" on a substrate with designed patterns. The deposited ink then is dried or sintered to form stable and continue functional patterns for the further use. The goal of this thesis is to make flexible batteries by printing. In this chapter, the current printing technologies, properties of printable inks, sintering technologies and basic idea of printable batteries are introduced.

1.2 Current Printing Technologies

1.2.1 Pad printing

Pad printing is also known as tempo-graphic printing. It is the only printing method which is capable to print images on curved substrates. This technology can transform images from recessed areas (gravure) called the clichéfilled with ink and the excess is moved with a metal doctor blade. A flexible pad or tampon then pressed onto the clichéand deformed to pick up the images (pad is filled with ink with certain image), and the pad then is released and pressed on the substrate to transfer the images. The whole

printing process is displayed in Figure 1.1. The main feature of this printing method is the mobile and deformable pad, which catches images from clichéfilled with ink from ink pot, to transfer images to the substrate. Due to the flexibility of printing pad, the substrate can be 2D flat or 3D curved surface. Pad printing is used mainly on consumer goods, especially for logos and labelling printing on woods, metals, plastics and glass. It can also be applied on electrical and toys appliances such as portable machines ,video players and computer keyboard with various of surface conditions (Maideen, Sahudin, Yahya, & Norliawati, 2016).

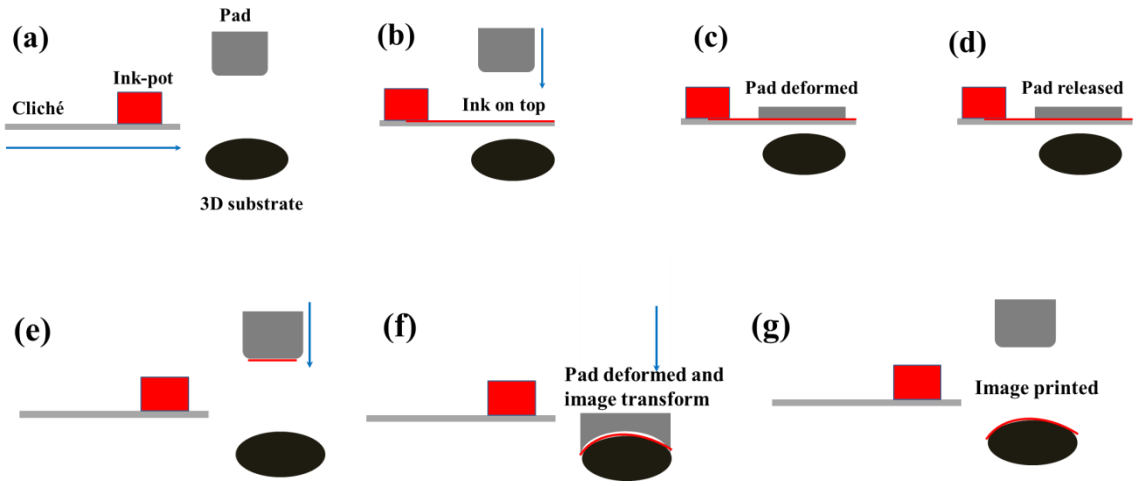

Figure 1.1 Schematics of pad printing process: (a)-(b) ink picking up on clichéé; (c)-(e) ink picking up by deformable pad; (f)-(g) image transfer from pad to 3D surface substrate.

Based on the working mechanism description above, the pad printing has several advantages:

(a) Printing on a variety of substrates: 3D objects can be used as substrate. This is the main advantage of pad printing. Based on the author's best knowledge, no printing technology can transfer 2D images on 3D substrate except pad printing.

(b) Economy and simple printing process: its machinery process is very simple and maneuverable; the machine is easy to set up and requires less training especially

for lab Research and Development (R&D).

(c) It can achieve multi-color printing: it is easy to set several ink pods working together to print layer by layer with different colors.

(d) Various inks can be used in pad printing: it have wide ranges of viscosity and surface tension due to the mechanical pressing.

As a mature technology, pad printing has already been applied in fabrication of electronics and energy storage devices. Peter Hahne studied the suitability of pad printing in connection with the printable solar cells. His work shows that pad printing is a simple, economic and high throughput method which offers lines with fine resolution even on uneven surfaces; this is impossible with other traditional printing (Hahne et al., 2001). Active layer in polymer solar cells are also achieved by pad printing as reported by Frederik and co-workers. In that research, a modified silicone rubber stamp is used as printing pad to pick up the ink from a gravure plate and transfer it to the substrate with certain patterns. The obtained devices had a good stability in air during storage and operation (Frederik C. Krebs, 2009b). Figure 1.2 (a) shows the pad printer and pad with different hardness; the pad hardness is crucial to the morphology of final printing. Mooring used a pad printing technique for the production of disposable electrode systems as shown in Figure 1.2 (b). The results have demonstrated behavior that is consistent with those obtained at conventional electrode substrates but with the advantage of disposability process. The approach is comparable to other printing technologies when considering the ease with which the ink formulations (and hence, electrode response) can be modified. They illustrate the capability of the pad printing over the other printing approach lies in the production of prototype detection/reagentless sensing systems where pad printing unquestionably provides a more rapid and economical method of production

with uncompromising electrode performance (Mooring et al., 2005).

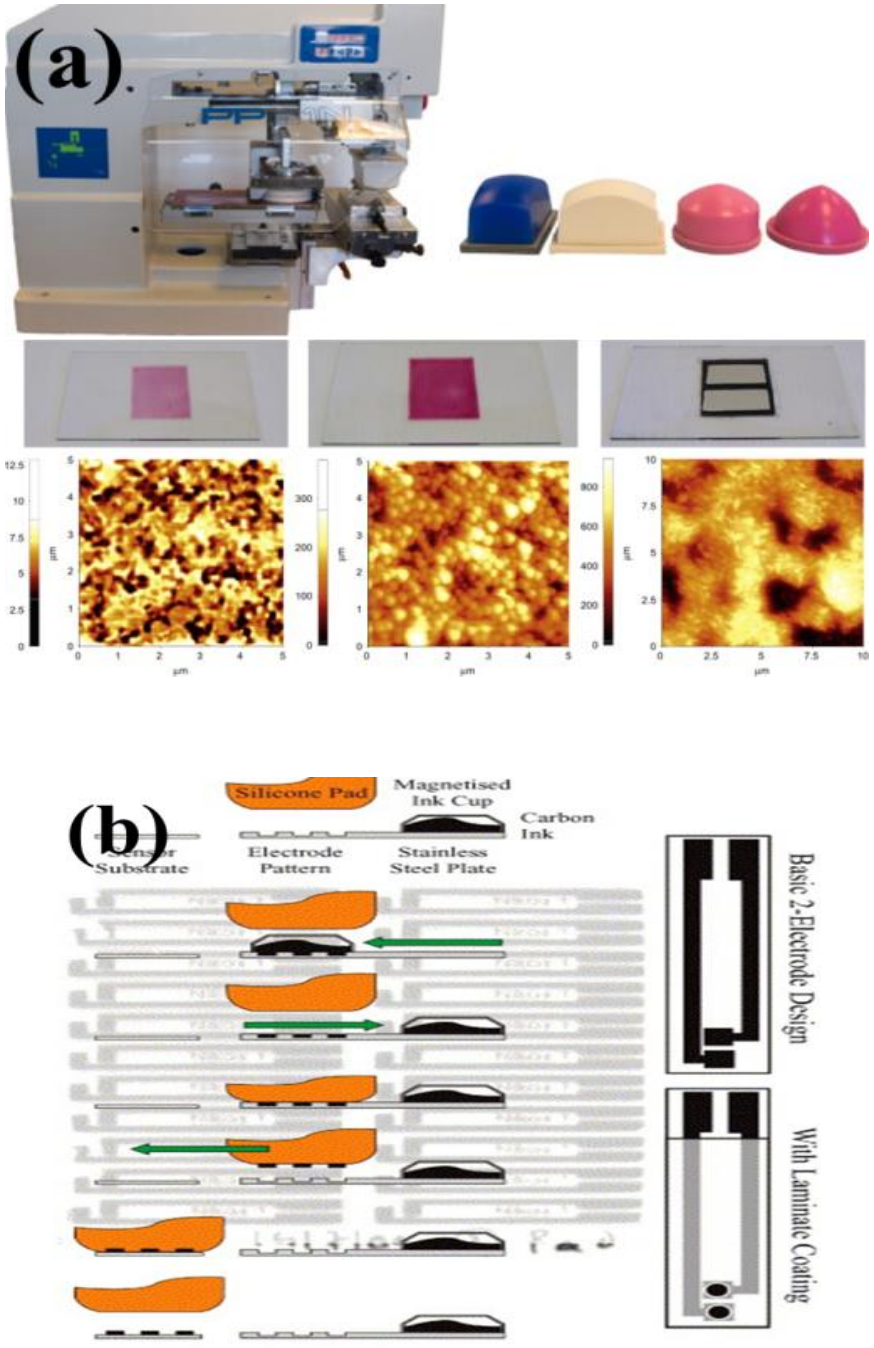

Figure 1.2 Schematic diagram of (a) the PP21N pad printer from Kent International (left) and examples of pads with different shapes (right), the bottom is the single, three layers and completed device of printed solar cell ; (b) pad printed electrode assemblies.

Source: (a) (Frederik C. Krebs, 2009b); (b) (Mooring et al., 2005).

However, as an easy mechanical printing process, pad printing also has disadvantages and limitations:

(a) Pad printing is less durable than other printing technologies. The clichéand pad-printed legends can be worn away by abrasion during the ink picking and printing deformation. Necessary maintains on the deformable pad are required in this technology.

(b) It is hard to produce large images. Large pads require a large press, and such a large pad has poorer durability caused by the movement of the press than is one of smaller mass. This means that pad printing cannot achieve large scale printing. This limits its application in industrial applications.

1.2.2 Gravure printing

Gravure printing is one of the simplest printing processes compared with other methods. It is a direct application process which transfers images on the substrate, meaning ink is placed directly onto the substrate without having to go through the complex image transfer methods that flexo and offset require which will be discussed in the following sections. The gravure printing system consists of a printing roller, an impression roller, a feed reservoir, and a doctor blade, as shown Figure 1.3. The printing roller, which is engraved or etched with the designed image and patterns on to the surface, picks up ink from the feed reservoir filled with ink. Then the extra ink on non-image areas is scraped off the printing roller by a doctor blade to the feed reservoir for the next printing. The ink on the printing roller then transferred to the substrate by the pressure from the press roller. Finally the ink is dried by drying system.

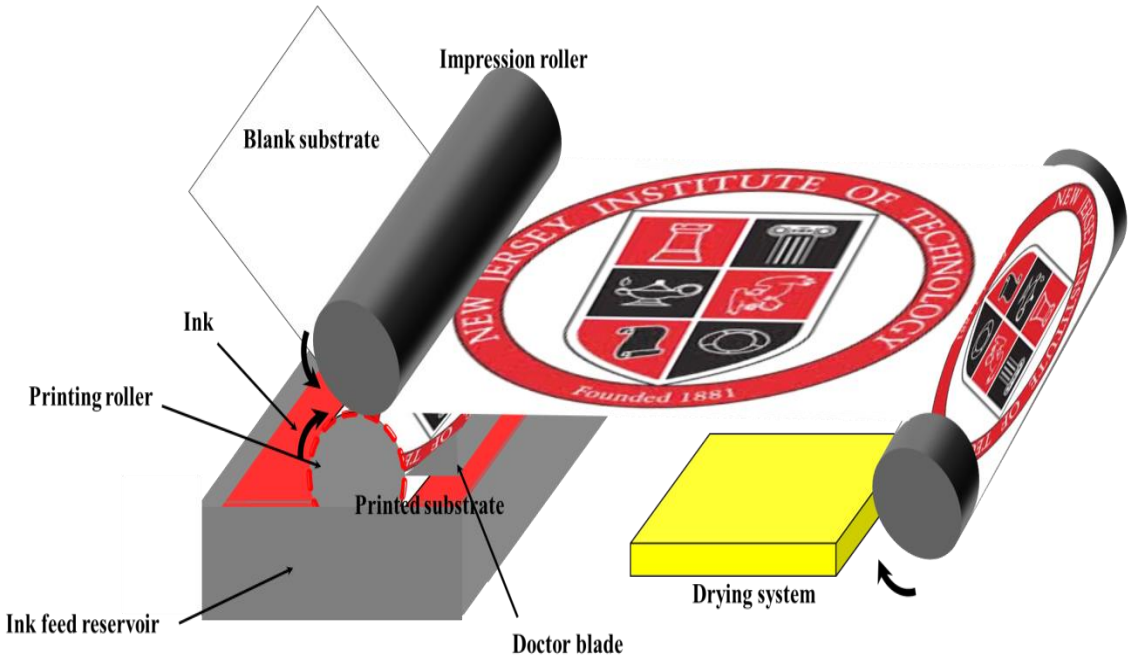

Figure 1.3 Schematics and structure of gravure printing process.

The advantages of gravure printing are summary below:

(a) Gravure printing can achieve roll-to-roll production easily: it is a highly consistent and continuously reproducible print process as shown in Figure 1.3. Gravure printing is the most popular printing method in industry before the flexo printing.

(b) Gravure printing is easy to set up and requires less training due to the simple structure of printer. It is easy to set up for R&D purpose.

(c) Multi-rollers can be mounted together in the same time to achieve front- and backside printing at the same time. Also, multi roller can achieve multi-color and multi-layer printing.

(d) Long lifetime of printing roller, unlike deformable pad in pad printing, the hard and durable nature of the metallic printing rollers used makes gravure printing an ideal process for providing high quality print on very long or regularly repeating runs, delivering cost advantages over other processes.

(e) Fast ink drying: the drying process of printed substrate is achieved by evaporation. The drying system is also mounted at the middle or end of the gravure printer. This contributes to an immediate post-finishing of the printed goods. The process is ideally suited to situations where there is a range of print designs but a constant carton construction and size.

Although gravure printing is no long as popular as past due to the other more advantageous printing technologies, it is still used widely in large runs for magazines, newspaper and books fabrication. But it is also applied in the fabrication of electronics and energy storage due to its roll-to-roll based continuous process which is an excellent economic method for industrial producing. Organic solar cells (OSCs) printed on a flexible PET substrate have been developed by Chung-Ki Cho. The printed PEDOT: PSS electrode has a relative low resistance (with a sheet resistance of 359 Ω/square) and 88.92 % transparency. This electrode shows outstanding flexibility irrespective of the bending test modes as shown in Figure 1.4 (a) (Cho et al., 2011). Compared with traditional ITO glass electrodes, this printing method has higher capability in massive production of electrodes on the flexible substrate with high quality resolution. Marko Pudas develops high conductive tracks (straight and curve) on paper and plastic substrate by gravure printing. For his research a metallic-organic suspension is synthesized as the ink. After deposition on the paper, the patterns are cured in temperatures of 70–120 ℃ (Figure 1.4 (b)) (Pudas, Halonen, Granat, & Vähäkangas, 2005) to achieve continuous and stable structures with high conductivity. Kopola also gravure prints organic solar cells based on poly-3-hexylthiophene (P3HT) and (6.6)-phenyl-C61-butyric acid methyl ester (PCBM) blend films with a module active area of 15.45 cm^2 prepared. The gravure printed solar cell modules exhibit good electrochemical and mechanical flexibility performance as shown in Figure 1.4 (c) (Kopola et al., 2011). Also, Hwang develops lithium-ion batteries by gravure printing. In his research, $LiNi_{0.5}Mn_{1.5}O_4$ protection layer are coated on $LiCoO_2$ cathode by printing to enhance the electrochemical stabilities. This battery has high stability during high rate charging and discharging; the Schematic of the Gravure

coating process is shown in Figure 1.4 (d) (Hwang, Cho, & Park, 2011).

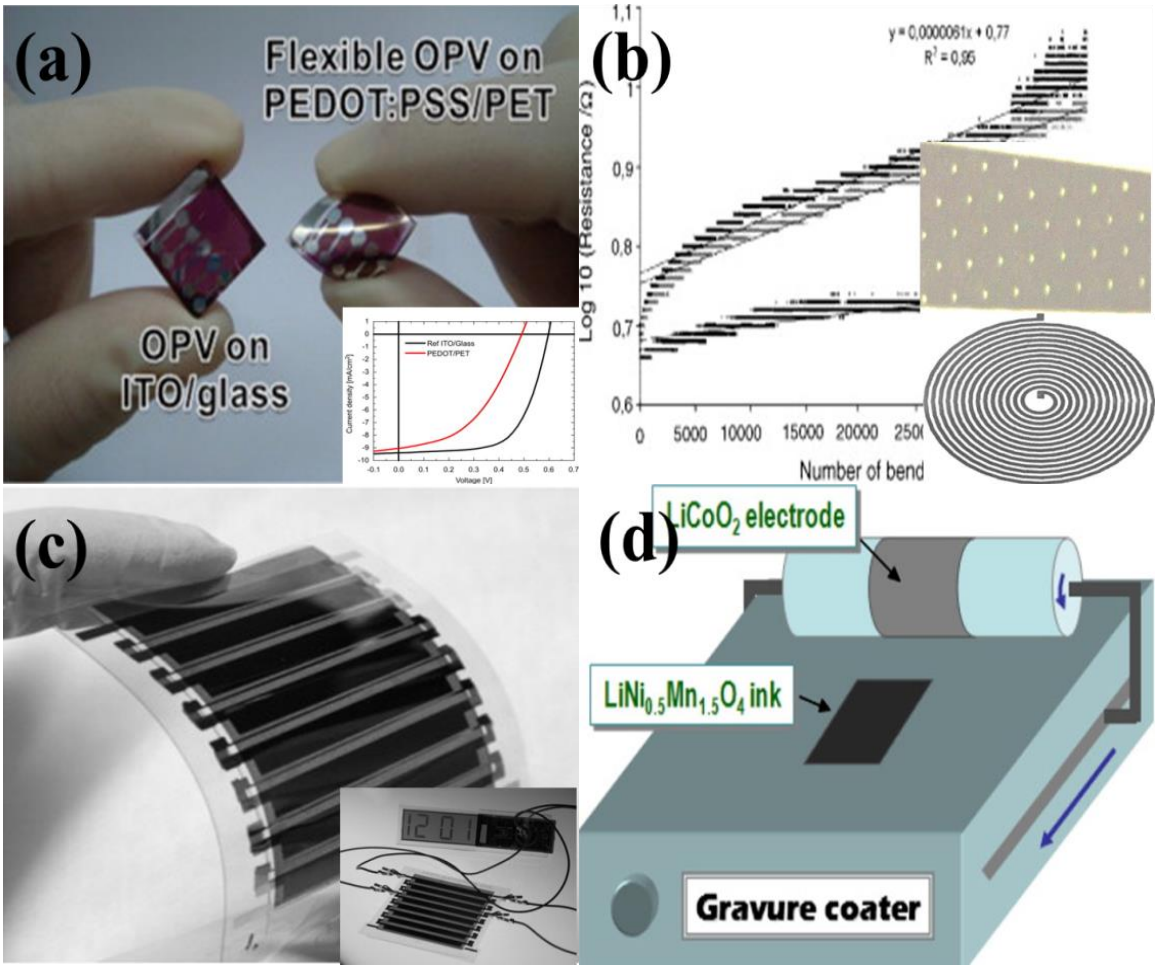

Figure 1.4 Schematic diagram of gravure printed (a) organic solar cells (OSCs) fabricated on rigid glass and flexible PET substrate, the insert is the performance of OSCs; (b) conductive tracks with folding data of customary office paper using XZ-250 ink, with maximum, median and minimum values of resistance variation; (c) flexible organic solar cell module, the insert is three cells connected in series used as a power source for a clock; (d) $LiCoO_2$/ $LiNi_{0.5}Mn_{1.5}O_4$ structure.

Source: (a) (Cho et al., 2011); (b) (Pudas et al., 2005); (c) (Kopola et al., 2011); (d) (Hwang et al., 2011).

Over the last centuries, more and more disadvantages of gravure printing have been discovered which limit the application of gravure printing. A summary of these

limitations are listed below:

(a) Limitation of the printed substrate: the substrate has to be 2D flexible substance with acceptable thickness. 3D subjects cannot be used in gravure printing due to the close distance between press roller and printing roller. Also, the substrate generally must be mechanical flexibility due to the roll-to-roll process.

(b) Only low viscosity ink can be used in gravure printing. Ink with high viscosity cannot be picked up very well by printing roller, which leads to a poor printing resolution.

(c) High startup costs: it is the method for mass production. Hundreds of thousands of copies are needed to make it profitable; this means it is not suitable for lab R&D.

(d) Long time and high cost to make, maintain and change the printing patterns on the printing rollers.

1.2.3 Screen printing

Screen printing is much more rapid and cost effective deposition method for both industrial producing and lab R&D. It is simple to begin and maintain. It is also an environment friendly printing method: only a small amount of chemical waste is produced per printing and the printing method is modular for actual production facilities. Basically, screen printing is hand making process due to its simple procedure; however, in recent years this technique can also be easily automated with a throughput exceeding 1,000 wafers per hour. There are two types of screen printing: flat bed and rotary screen printing.

Figure 1.5 shows a schematic of the flatbed screen printing process: during the actual printing, a squeegee moves the paste (ink) across the screen. This action causes a decrease in the viscosity of the paste, which in turn allows the paste to pass through the patterned areas on the screen and deposited onto the substrate. As the squeegee passes, the screen peels off and the paste viscosity returns to normal. Factors that affect the screen peel are the ink materials and viscosity, printing area, the mechanical flexibility

and tension of the screen, squeegee speed and the snap-off distance between the sample and the screen. The screen is made of an interwoven mesh kept at high tension, with an organic emulsion layer defining the printing pattern.

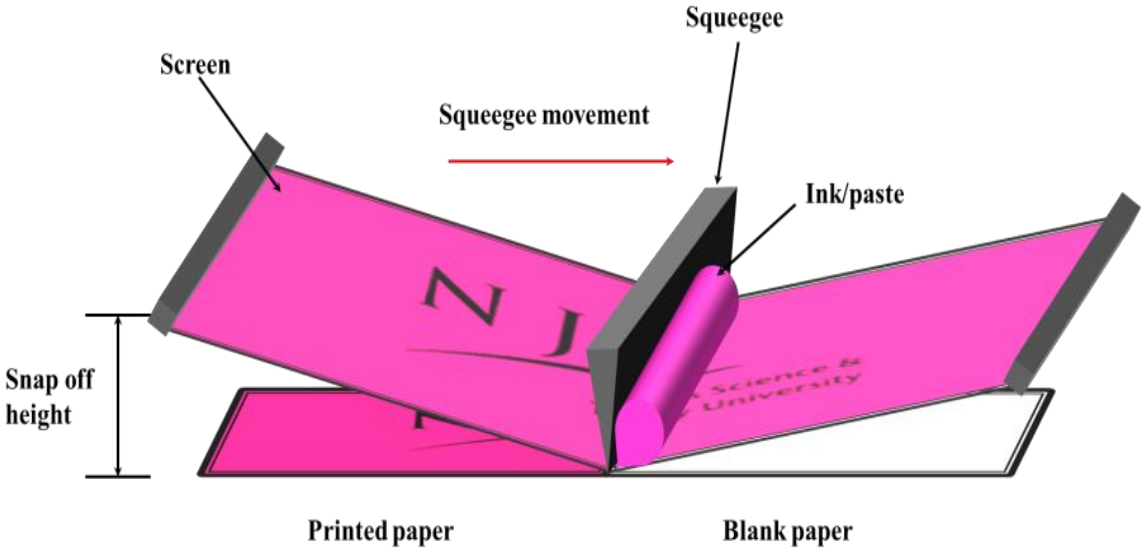

Figure 1.5 Schematics of flatbed screen printing process.

Another screen printing systems contains a fully continuous processing which is achieved through rotary screen printing as shown in Figure 1.6; this method is usually implied in massive production. The rotary printing process uses the same principle as flatbed printing but in this case the web of the screen is folded into a tube and the squeegee and the ink are placed inside of the rolling tube. As the screen rotates with the same speed as the substrate, the paste/ink is continuously pushed through the open area of the screen by the stationary squeegee, making a full print upon every rotation. Much higher processing speeds can be achieved by use of rotary screen printing (> 100 m/min) compared to flatbed (0–35 m/min), but the screens are quite expensive and they are much more difficult to clean because of the restricted curved access to the inside of the screen.

The process furthermore requires a longer adjustment run-in (adjusting the print with previously processed layers) compared to flat bed. This gives a higher initial waste, but once the process is running the procedure is very reliable.

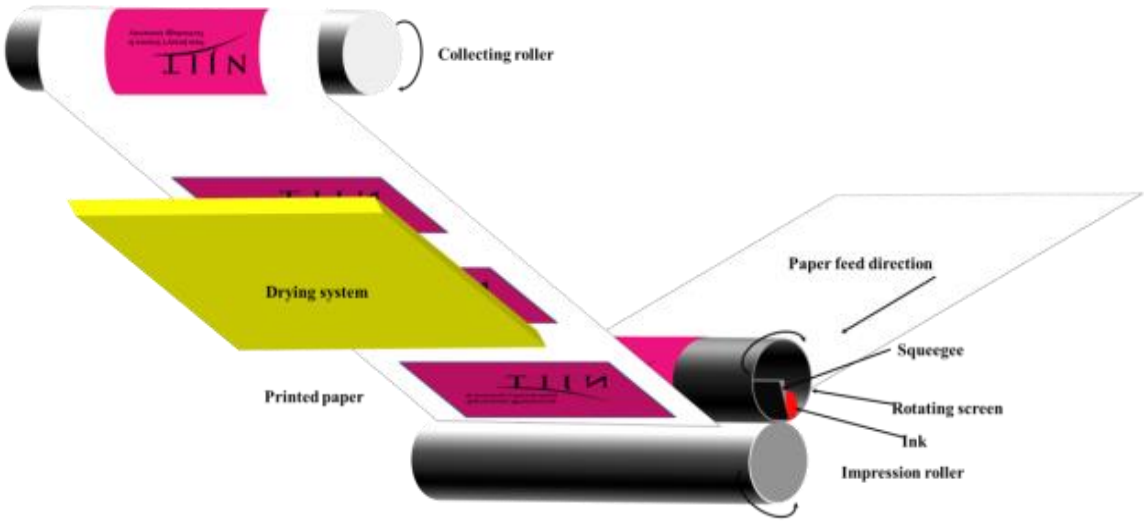

Figure 1.6 Schematics of rotary screen printing process.

The advantages of screen printing are listed below:

(a) Screen printing can accommodate a relatively wide range of print substrates especially for flatbed screen printing: hardness substrate and textile materials can be used to print. Right now, screen printing is used to print patterns on fabrics ranging from cotton and organza to silk and polyester.

(b) The size of screen printing can be scaled up to make large images in industries or scaled down in a lab research as mentioned above. This allows building a connection between lab research and industrial production.

(c) Low cost: as there is no complex machine required in screen printing and it is possible to print in a shorter space; the total investment in screen printing is comparatively lower than other printing systems. Also, screen printing requires less training.

(d) It enables the reproducible deposition of precise motifs, even free standing lines and dots, by the use of various mesh counts, coupled with the right screen coating on to a variety of substrates.

The main application of screen printing currently is on the textile printing. Screen-printing is also used in the fabrication of microelectronics and energy storage. This method is very easy to adjust and make thick film deposition compared than the other printing methods because of the adjustable snap off height, so it can control the precise amount of materials. Also, it is a simple and a relatively economical process to make 2D structures, especially for the flatbed screen printing because of the simple setting up and running. A recently developed flexible zinc-air battery has been produced by screen-printing. In this battery, a zinc/carbon/ polymer composite is used as anode ink, and a vapour polymerised PEDOT cathode ink is printed onto two sides of a photo paper, while silver layers are used as current collector. The structure of battery is shown in Figure 1.7 (a) (Hilder, Winther-Jensen, & Clark, 2009). Shaheen demonstrated the implementation of screen printing technology in the fabrication of an organic-based bulk heterojunction solar cell as shown in Figure 1.7 (b). However, this solar cell is made of inflexible glass (Shaheen, Radspinner, Peyghambarian, & Jabbour, 2001). It would be faster, cheaper and easier way to make solar cells on flexible substrates with different patterns. Figure 1.7 (c) (Suren & Kheawhom, 2016) shows the typical structure of the multilayers battery which has the similar structure as the zinc batteries in Reference 10. Some researchers (Sousa et al., 2016) even adopt this method to fabricate cathode electrode for lithium-ion batteries as shown in Figure 1.7 (d). The limitation in his research is the aluminum substrate which is not fully flexible. In recent years, screen printing has been developed as an ideal technology for large scale fabrication of multi-layer structure energy storage devices on both lab research and industrial production.

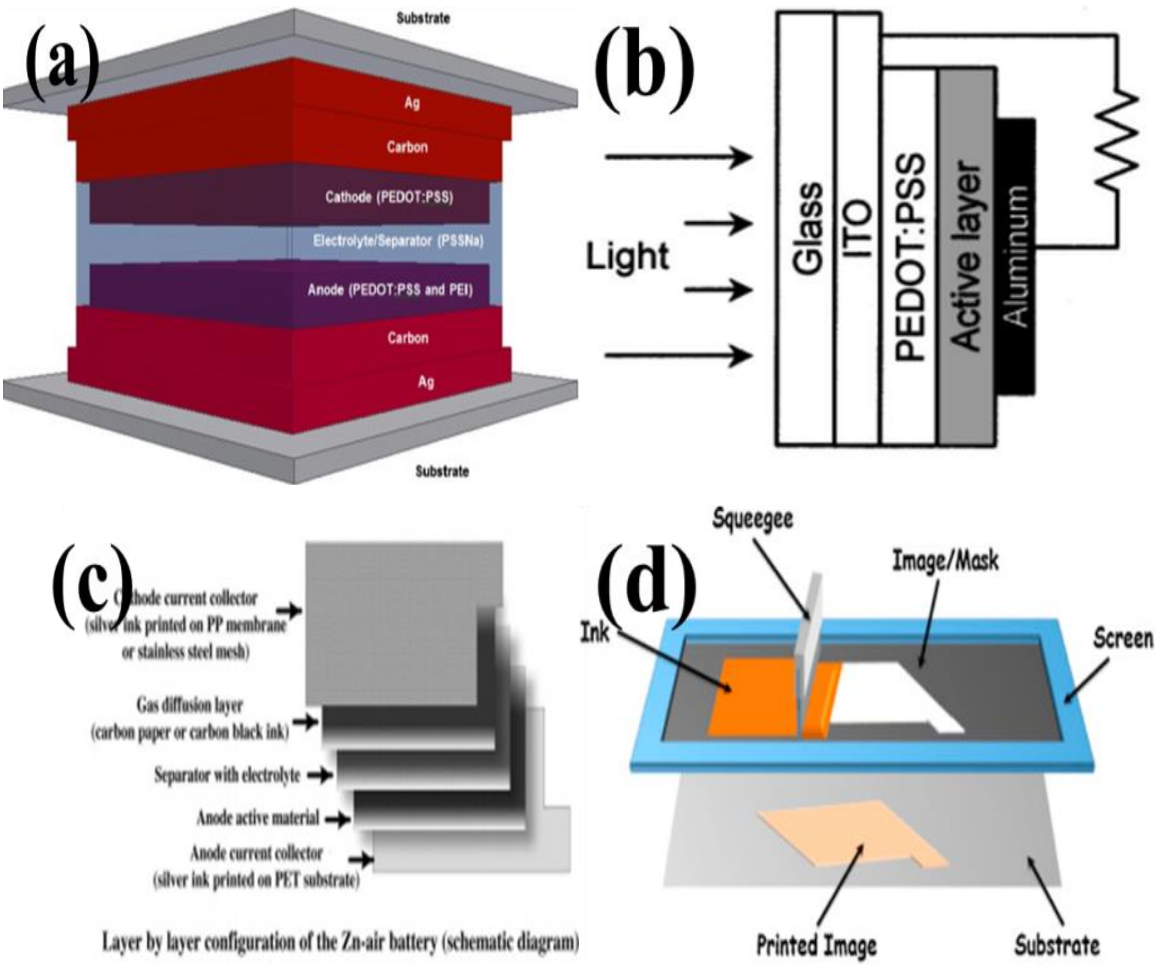

Figure 1.7 Schematic diagram of screen printed (a) polymer battery; (b) solar cell; (c) full cell structure and layer by layer configuration of the fabricated batteries; (d) lithium-ion batteries.

Source: (a) (Tehrani et al., 2015); (b) (Shaheen et al., 2001); (c) (Suren & Kheawhom, 2016); (d) (LiFePO4 electrodes) (Sousa et al., 2016).

As discussed above, screen printing is an outstanding deposition; however, it also has disadvantages:

(a) The main disadvantage of the screen printing process is that the ink must be pushed through the screens. This means that it is difficult to mix colors in an accurate amount in order to simulate smooth gradients and other effects. So most of items printed by screen printing are made from a combination color zones.

(b) Limited resolution: screen printing is not as high quality as gravure printing; it is not suitable for fine detailed reproductions such as micro devices. Also, the inks for screen printing are usually very thick which cannot be deposited very

uniformly and precisely.

(c) Screen printing requires multi printing process because it only prints one color at a time.

(d) Screen printing also requires time to maintain and make screens to change the patterns.

1.2.4 Flexographic printing

Flexographic printing (flexo printing below) is a high-speed rotational printing method, which is widely used in graphic arts and package printing on roll-to-roll process on various substrates such as cardboard, paper or plastic foil. In flexo printing, a flexible rubber or plastic plate is used to transfer the images. The schematics and structure of flexo printer is displayed in Figure 1.8: the printing plate is mounted onto the printing roller using an adequate substructure with defined height and compressibility. A steel roller with a finely surface referred to as anilox roller, transfers a precise amount of ink with a uniform layer thickness from the ink reservoir onto elevated areas of the printing plate. Excessive ink is removed by a doctor blade. Subsequently, the ink is transferred from the printing plate onto the substrate by the pressure of press roller. The ink is then dried by drying system and rolled by a collecting roller at the end of printing.

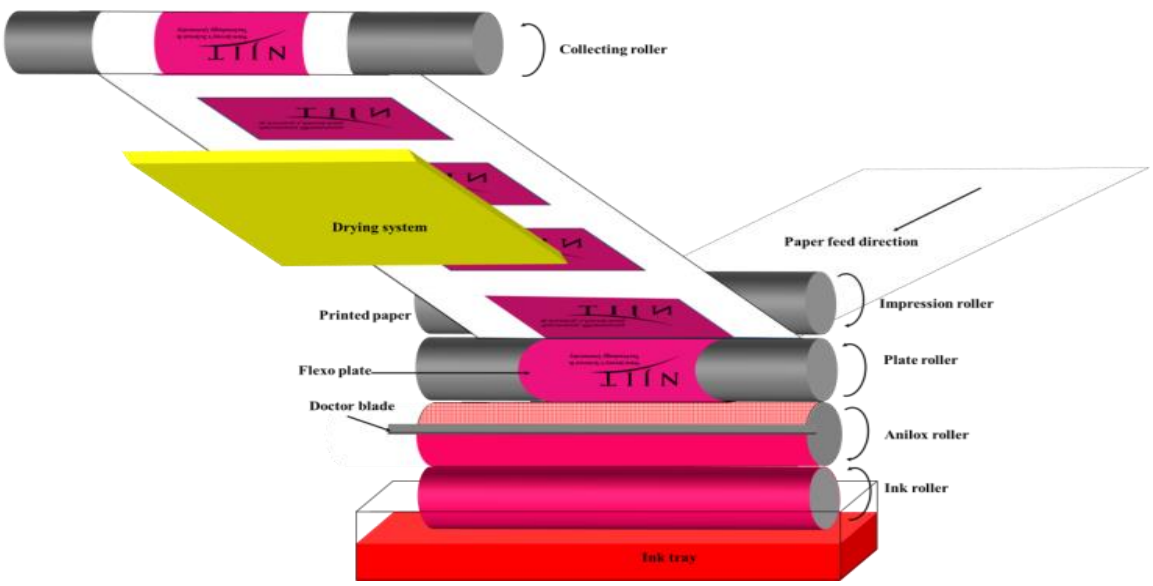

Figure 1.8 Schematics and structure of flexo printing process.

The structure of flexo printer is a kind of ink relief printing which is very similar to the intaglio printing (gravure printing) as shown from Figure 1.5. However, there are differences which affect the final printing quality. Using gravure printing and flexo printing as an example (Figure 1.9), details of printing roller exhibit different printing principles: in gravure printing, ink is picked up in cells on the surface of a metal roller; excess ink is removed with doctor blade. The ink remaining in the cells is transferred to the substrate (Figure 1.9 (a)). The substrate must be surface smooth and made of absorbent materials like paper, cloth and cardboard, which has ability to catch the ink from incurved cells uniformly. Gravure printing can produce high quality images due to the hardness and durability of steel roller. However, steel, wood and polymer cannot be used as the substrate in gravure printing due to the roughness surface and non-absorbent materials, which cannot catch inks from the cells very well. In contrast, flexo printing has wide range of substrate including non-absorbent materials, because this printing technology can press inks onto the rough substrates as shown in Figure 1.9 (b). However,

due to the flexibility of the plastic/robber plate on plate roller, the transferred images can be deformed and changed during the printing process because of the straining on the plate roller and the pressure on the substrate.

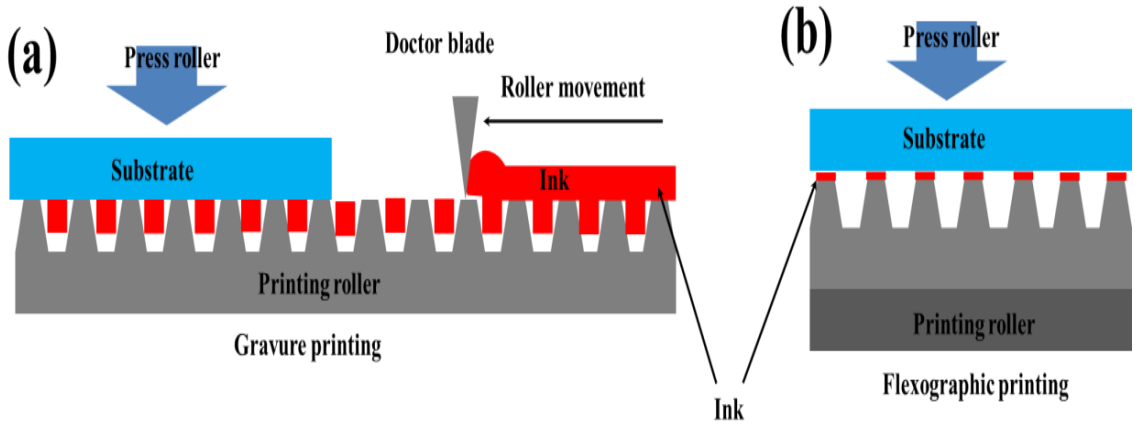

Figure 1.9 Details of gravure printing and flexo printing.

In the last decades, flexo printing has replaced gravure printing and became one of the most popular printing methods around the world. Based on the above discussion, the advantages of flexo printing are as follows:

(a) Flexo printing enables printing on a wide variety of surfaces. Inks can be pressed on rough surfaces, porous surfaces and non-absorbent materials. It is no longer limited to cardboard, paper and fabric when printing images using gravure printing, making this feature one of the top advantages of flexographic printing.

(b) Easy plate-making process: the patterned plate is using plastic or polymer, the plate created during the flexo printing process allows industry to change new patterns and images very easy and economy. In gravure printing, the patterns are etched on metallic roller which has more complicated process and higher costs.

(c) Flexo printing offers both short-run and long-run deposition method. Plate life is quite long, and flexo plates can be demounted to clean and saved for the next use.

Although flexo printing is currently used for a number of different products, it is dominant in the packaging printing area. The main reason is flexo printing has wider

range of substrates, including very rough surfaces like wood, shrink sleeves, cardboard and nonabsorbent plastics. But flexo printing is barely used in magazine and book printing due to its low resolution, however, flexo is also used on a limited basis in the newspaper industry which does not require high resolution quality. In the past decades, more and more interesting has been grown to apply flexo printing on the fabrication of electronics and energy storage devices because of its easy change plate process and high production process. A roll-to-roll printing process has been reported for the developed battery technology using commercially available flexographic printing presses, as shown in Figure 1.10 (a). Each part (cathode, separator, electrolyte, anode and current collector) of the batteries is controlled and deposited in a certain order by different rollers on flexible substrates using functional inks (Z. Wang et al., 2014). This process indicates a fast way to produce flexible batteries. Also, flexo printing can be expanded to solar cell and other energy storage devices by the same principle. For instance, Henrik F. Dam describes the fabrication of gradual bridging by flexo printing: this process can scale from the lab printing research to a true industrial roll-to-roll coating system where a special flexographic unit is central for printing of electrodes (Dam et al., 2015). Tim Wolfer showed that flexo printing can be employed as optical waveguides production as shown in Figure 1.10 (b) (Wolfer, Bollgruen, Mager, Overmeyer, & Korvink, 2014). Another example for the application on the solar cell fabrication by flexo printing is done by Jon E. Carle as shown in Figure 1.10 (c). The flexible P3HT: PCBM based polymer solar cells can be prepared entirely in air without vacuum steps and ITO while qualitatively similar performance can be achieved (Carl é et al., 2013).

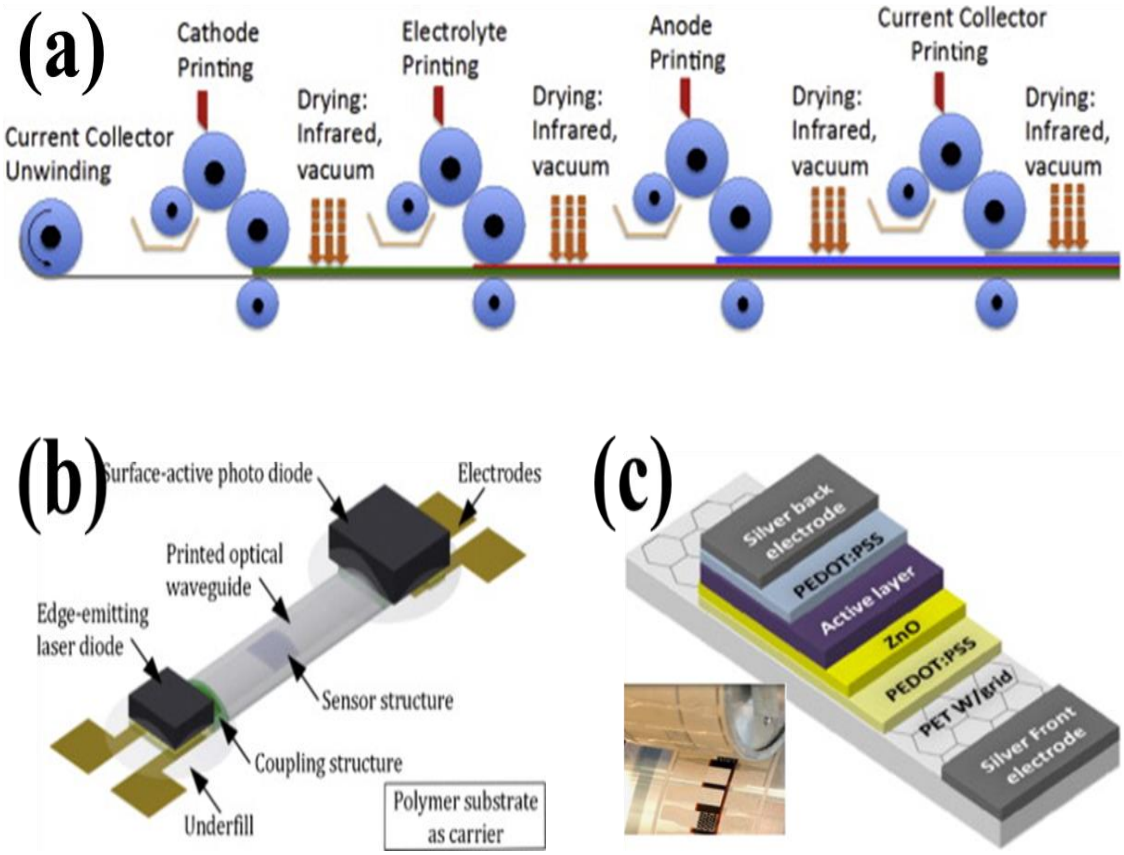

Figure 1.10 Schematic diagram of flexo printed (a) multi-station for large-scale battery production; (b) optical waveguides; (c) multi-layers structure of solar cell, the insert is the optical photo of printing process.

Source: (a) (Z. Wang et al., 2014); (b) (Wolfer et al., 2014); (c) (Carl é et al., 2013).

Flexo printing also has limitations and disadvantages descripted below:

(a) It cannot produce complicated and extensive artwork as compared to that produced by gravure printing. This is caused by the soft plastic pattern plate which cannot produce high quality images as hard metallic roller in gravure printing due to the deformation and long term wear.

(b) Flexo printing cannot produce thick layers of ink due to the direct impression process. In other words, the thickness of printed patterns cannot be controlled easily. It is especially bad for printed energy storage devices because thin layer only contains few active materials, which restricts the total energy storage of the device.

(c) The patterns on the plastic plate mounted on impression rollers are made by

lithographic printing and cannot stand for long time compared with metallic gravure roller.

1.2.5 Off-Set Lithographic printing

Basically there are two kinds of offset lithographic printing: conventional and waterless. Conventional lithographic printing is a 2-dimensional printing technique whose structure is unlike most other planographic techniques descripted above (i.e. both printed and non-printed areas are in the same plane). Basically, the offset lithography process is based on water based chemistry and creates images by having hydrophobic areas that are wetted by the water-based ink and hydrophilic areas that do not wet (as shown in Figure 1.11 white part is hydrophilic and red “NJIT” logo is hydrophobic). The already patterned ink then typically offset to a roller that transfers the images to the substrate by the press roller. Offset lithography is a fast roll-to-roll process of the high quality with relatively low cost compared with gravure and flexo printing. While it does have some advantages, it requires some development of ink systems with hydrophobic and hydrophilic properties before it can be envisaged for fabrication of polymer photovoltaics.

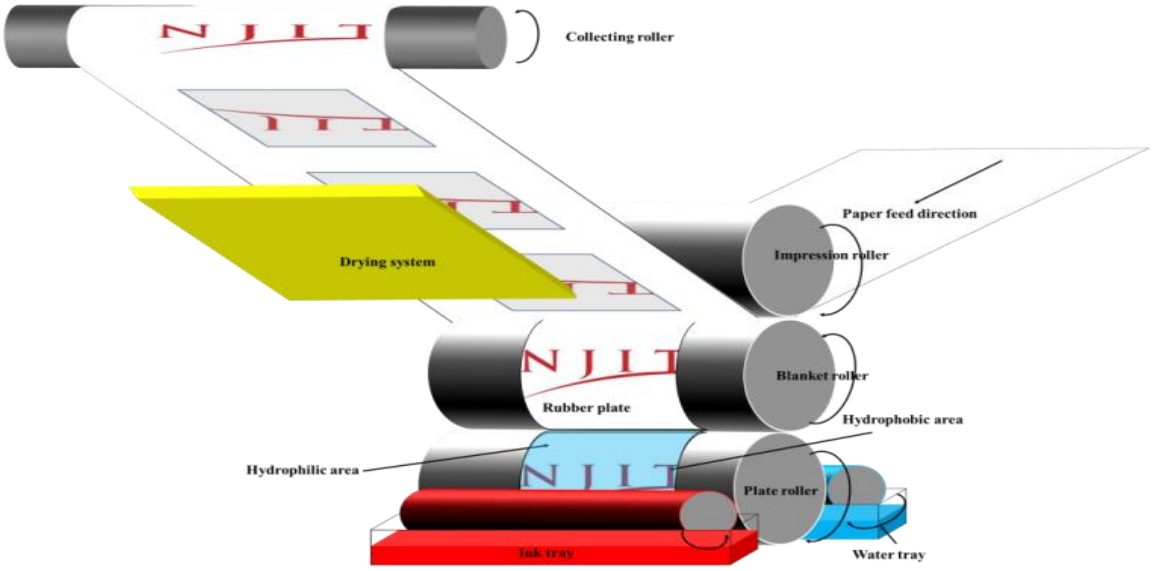

Figure 1.11 Schematics and structure of conventional lithographic printing.

With the development of lithographic printing, another new printing process is adopted which can print regular inks: waterless offset printing technology. Waterless is a lithographic process that does not use hydrophobic or hydrophilic solution (Figure 1.12 (a)). It is based on repulsion between the ink and siliconized areas as shown in Figure 1.12 (b). When the plates are exposed to light, siliconized and non-siliconized areas are formed according to the exposure mask. The ink is patterned by the repulsion from the siliconized zones towards the non-siliconized zones. The ink is then transferred onto the blanket and deposited on the substrate as shown in conventional lithographic printing. This process has fewer requirements as traditional lithographic printing.

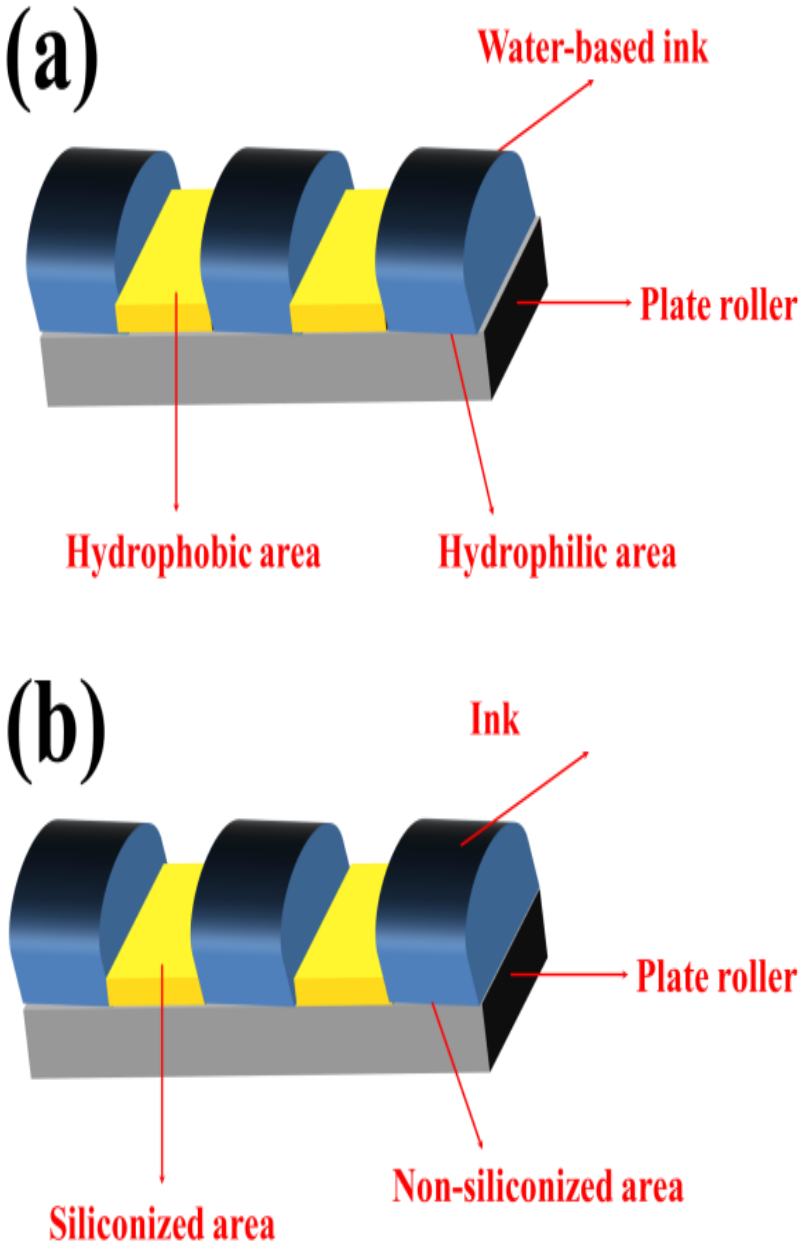

Figure 1.12 Plate roller details of (a) conventional and (b) water-less lithographic printing.

Offset lithographic printing can produce relative high quality images with less cost due to the following advantages descripted:

(a) It can produce higher quality images than flexo printing because the rubber

blanket conforms to the texture of the printing surface; also the images on the rubber blanket roller are renewed during each rotation of plate roller which means the image will not be damaged by impression as with flexo printing for instance.

(b) Offset printing has long durability. This is better than flexo printing because plates in offset printing only make contact with the printing blanket, which is much softer and less abrasive than paper, therefore the abrasion of plate image is reduced significantly.

(c) It is an excellent way to produce long run printing because it requires less maintenance and cost; it is a combination of gravure and flexo printing: easy changeable pattern plate with high resolution printing.

Lithographic printing is an economic printing process which can reach high resolution. It has been applied in wide areas like book, magazine and newspaper producing. In recent decades, more and more researchers report this method to fabricate functional devices and energy storage systems. Harrey fabricates humidity sensors by lithographically printing which forms conductive films on two sides of a moisture sensitive polymer like polyimide, the printed electrode films has excellent adhesion between the substrate and exhibits good stability in humid environments (90%RH). The printed sensors are displayed in Figure 1.13 (a) (Harrey, Ramsey, Evans, & Harrison, 2002). Dirk Zielke fabricated organic field-effect transistors using offset printed source/drain structures. The electrode are interdigitated by printing a poly (3, 4-ethylenedioxythiophene) (PEDOT) as shown in Figure 1.13 (b) (Zielke et al., 2005). This indicates that lithographic is a potential method to produce transistors massively. David made force sensitive resistors by lithographic printing. In his research, a carbon based suspension is used as lithographic ink that dried to form a film (Figure 1.13 (c) black squares) with controlled carbon content close to the percolation threshold for electrical conduction. Silver conductive ink is used for the electrodes and connecting leads (Figure 1.13 (c) metallic lines). Gloss art A4 paper is used as the substrate. The resistor is 23 KΩ

while the combined resistance of electrodes and leads is less than 2 Ω (Leyland, Evans, & Harrison, 2002). Darren Southee developed a process of using offset lithographic printing to form electrode structures suitable for voltaic cell fabrication in Figure 1.13 (d). Anode and cathode inks have been developed form polymeric resin. Inks developed attain hydrophobic and thixotropic properties necessary to facilitate lithographic printing as discussed above (Southee, Hay, Evans, & Harrison, 2007).

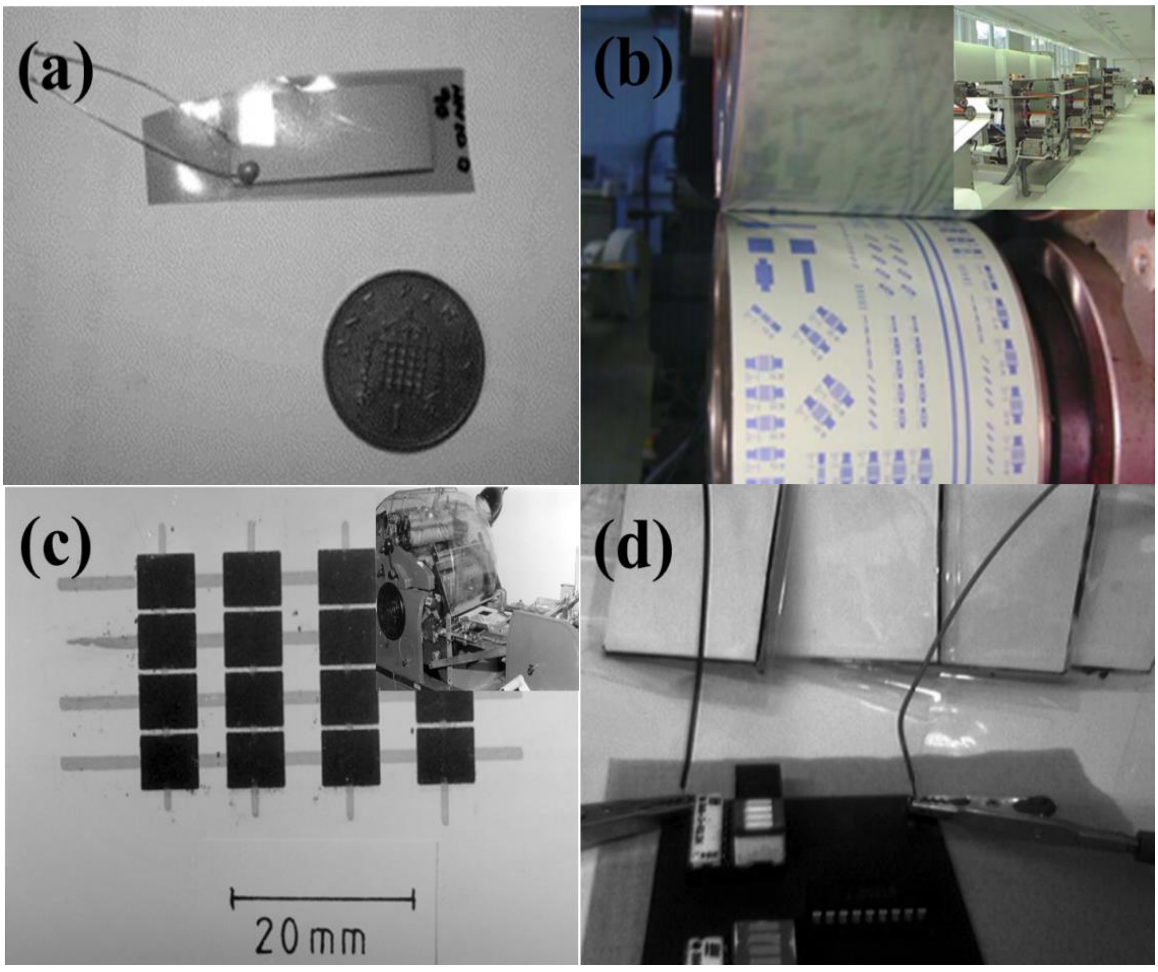

Figure 1.13 Schematic diagram of lithographic printed (a) sensor structure formed on polyimide film; (b) source/drain structures; (c) resistors with electroding grid, the insert is the small lithographic printer; (d) voltaic cells.

Source: (a) (Harrey et al., 2002); (b) (Zielke et al., 2005); (c) (Leyland et al., 2002); (d) (Southee et al., 2007).

Although lithographic printing combines advantages of gravure and flexo printing, it has some disadvantages as displayed below:

(a) Slightly poor resolution compared to rotogravure or photogravure printing. This is because of the soft pattern plate cannot transfer every details of the image precisely.

(b) Lithographic printing requires maintenance. Its relative costs are high to fabricate image patterns.

1.2.6 Digital printing (inkjet printing)

The printing methods mentioned above are all mechanical process. In these recent decades, digital printing's capabilities in device fabrication has grown. In this thesis, inkjet printing is emphasized. The main characteristics of inkjet printing technology are highlighted in the following:

(a) Inkjet printing permits the scalability of functional materials in a continuous reel-to-reel system.

(b) Inkjet printing offers the versatility to switch quickly the deposited materials and the pattern design. Functional inks can be printed on various substrates layers by layers.

Inkjet printing is a relatively novel process from the view of industrial printing and coating because of the easy set up and digital designable patterns. This technology has been driven forward by the typical low-cost ink jet printer. Figure 1.14 (a) and (b) show two types of commercial inkjet printing processes: drop on demand (DoD) inkjet printing and continuous inkjet printing (CIJ). In DoD inkjet printer, drops are only generated when given orders. The most widely used DoD printer uses piezoelectric materials to generate ink drops: a piezoelectric actuator is deformed by the image data signals to jet ink drops on the certain position, which is controlled by x-y mechanically moving plates and printing nozzles. DoD inkjet printing has more flexibility with ink and

system design. This inkjet printer requires inks with certain range of viscosity and surface tension in order to be emitted easily. In contrast, CIJ inkjet printer uses high voltage to control the path of ink drops, a chamber with a nozzle at one end is occupied by a plunger or a pump, Ink is continuously pressed to the nozzles and is charged before emitting out. The charged droplets are deflected by the electrode plates which are controlled by the computer with image data pulse. Unused inks are collected by a collecting tray and then pumped into the cartridge for the next printing. CIJ has higher drop ejection frequency which might be easy in high duty cycle applications. CIJ inkjet printer also has wider range of ink because it requires less for the viscosity and surface tension compared with DoD. But CIJ process also suffers disadvantages. The exposure of the recycle tray may contaminate and variate the concentration of the ink which can result into high risk of clogging; this is also very bad for metallic ink due to the oxidation of metallic particles in air. The oxidized metallic particles cannot be cured in the sintering process which will be discussed later in this chapter. Another disadvantage is ink waste: only a small fraction of inks are required in one printing cycle. The majority is recycled.

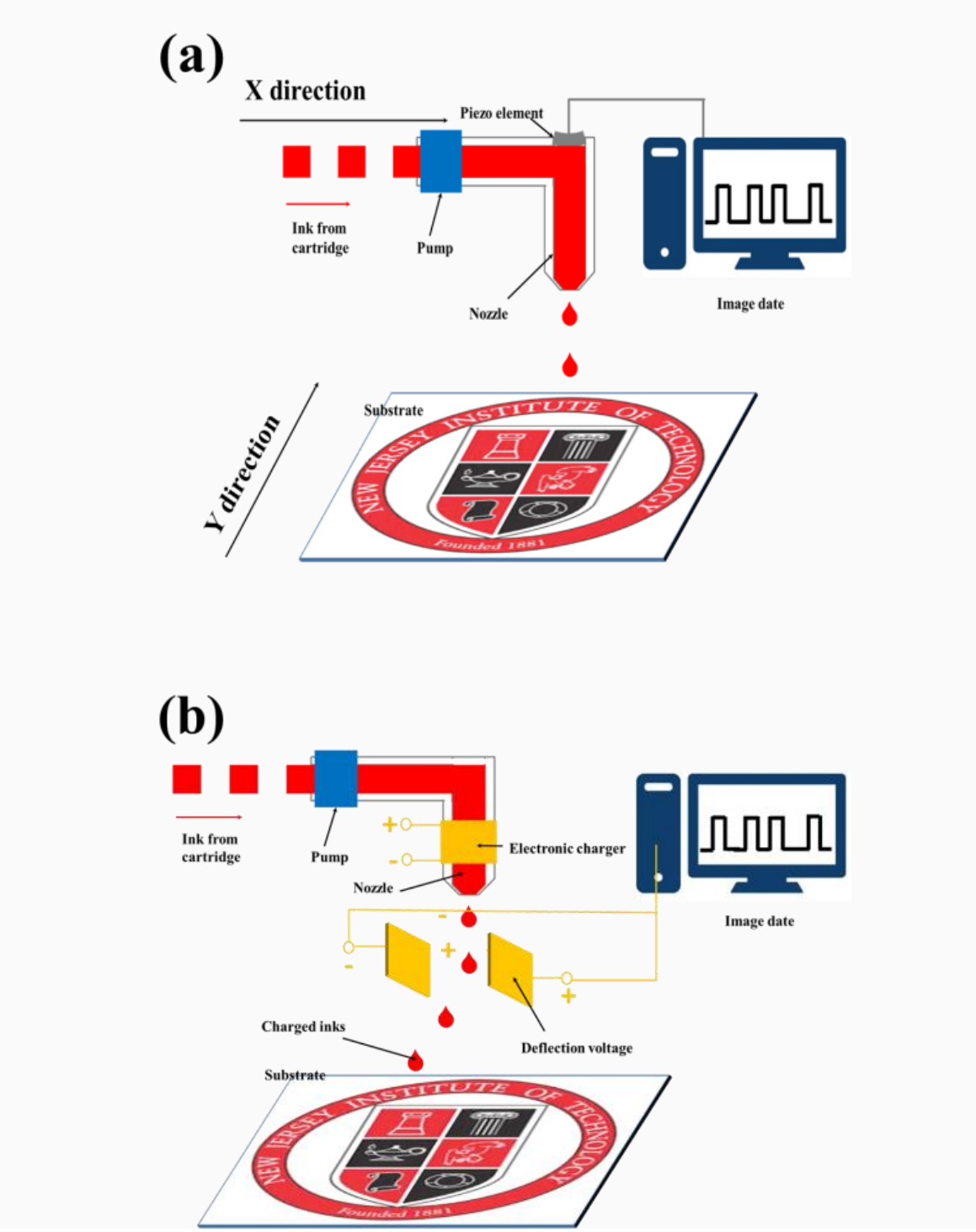

Figure 1.14 Schematics and structure of (a) drop on demand (DoD) and (b) continuous inkjet printing (CIJ).

Precise quantities of a wide range of materials (particle ink and particle free ink)

can be deposited in the form of single droplets or conducting lines on various substrates. It is an economic, non-contact technique to manufacture electronic circuits and energy storage devices. Costs are reduced owing to digital imaging, eliminating the multiple and consumable process steps including mask etching and plate fabrication and designs. As inkjet printing is a relatively fast technique, it potentially enables fast roll-to-roll patterning process.

As we discussed before, the key challenge in printing technology is suitable ink formulations development which determines the drop ejection properties and the evaporation behavior and orientation upon solvent evaporation which influences the printing quality. The resolution of inkjet printing can reach to 20 to 50 μm by statistical variations of the flight direction of droplets and their spreading on the substrate. Taking metallic conductive inks as an example, uniform and monodisperse metal nanoparticles in aqueous or organic solvent dispersions contribute to attain a high dispersion stability and low electrical resistivity at low curing temperatures. In recent years, metallic precursor ink can produce high conductive patterns with good resolution without nozzle clogging (nozzle clogging is a serious issue of inkjet printing and can interrupt the printing process) at relative low curing temperature. High sintering temperatures are incompatible with common plastic foils, such as PET and polycarbonate (PC) having a relatively low glass transition temperature. The choice of foil is therefore restricted to more expensive polymers such as polyimides (PI) whose working temperature can be as high as 400 ℃.

The advantages of digital printing process over mechanically printing are:

(a) The digital printing technology is cheaper and easier compared with mechanically printing available in the market. It requires smaller space to fit the machine. Also, digital printing uses a computer to generate image patterns, while mechanical printing technologies need to fabricate patterns roller, especially for gravure

printing needs to make metallic roller.

(b) Digital printing doesn't require long substrates to finish a printing cycle. Small piece of substrate can be fitted in the printer. This doesn't mean that digital printing is not suitable for industrial roll-to-roll production; it has been used in massive functional devices printing.

(c) The maintenance cost is low as compared to other printers. Also, less training is needed.

Digital printing has been applied in the fabrication of electronics and energy devices in recent years. A particle-free MOD ink (MOD = metal–organic-decomposition) of high silver content was directly used for inkjet printing silver conductive patterns on Polyimide (PI) substrate is reported by Dong Yue (Dong et al., 2015) in Figure 1.15 (a). Silver oxalate is used as silver precursor, ethylamine as a complexing ligand to increase the solubility of silver oxalate in order to increase the silver loading (27.6 wt. % in this case), ethyl alcohol and ethylene glycol as the solvent with suitable viscosity and surface tension. The deposited silver ink on PI substrate is thermally treated at different temperatures and times. The silver film cured at 170 ℃ for 30 min shows a best properties with a resistivity of 8.4 μΩ·cm (18.9 % of the bulk silver) and good adhesion on PI substrate. Zhang Weijun uses inkjet printing technology to replace the conventional photolithography to fabricate flexible electronics as shown in Figure 1.15 (b) (W. Zhang, Bi, Li, & Gao, 2016). In his research Ag/RGO (reduced graphene oxide) composite with good conductivity and dispersity is synthesized as conductive ink filler for inkjet printing. Inkjet printing is also a fantastic method for fabrication of energy storage devices. Carbon-based micro-supercapacitors in self-powered modules are fabricated with inkjet printing technology on silicon substrate (Figure 1.15 (c)) (Pech et al., 2010). The ink is first prepared by mixing an activated carbon powder with a PTFE polymer binder in

ethylene glycol, the system is stabilized with a surfactant, and then the mixture is deposited by inkjet on patterned gold current collectors in the serrated shape to increase the contact area between cathode and anode. The substrate is heated at 140 ℃ in order to assure a good homogeneity. These micro-devices show a high capacity behavior over a wide working potential range (2.5 V for a cell capacitance of 2.1 mF/cm^2). Matthew H. Ervin also reported fabrication of flexible supercapacitor (Figure 1.15 (d)) (Ervin, Le, & Lee, 2014): GO (graphene oxide) is dispersed in water as an active materials ink. The ink is then deposited onto a metal film which is stick on Kapton as current collectors by inkjet printing. After printing conductive graphene, electrodes are produced by reducing the graphene oxide at 200 ℃. These electrodes are sealed together with added electrolyte and separator with heat treatment, and the assembled supercapacitor performance is evaluated. The performance of the flexible packaged device works well with good specific capacity. But in the future, thicker graphene electrodes and further package optimization will be required to obtain good device-level performance. For instance, this capacitor is not fully inkjet printable: metal foil is used to act as current collector. The foil has to be stack on the Kapton film, and this step reduces the production efficient significantly.

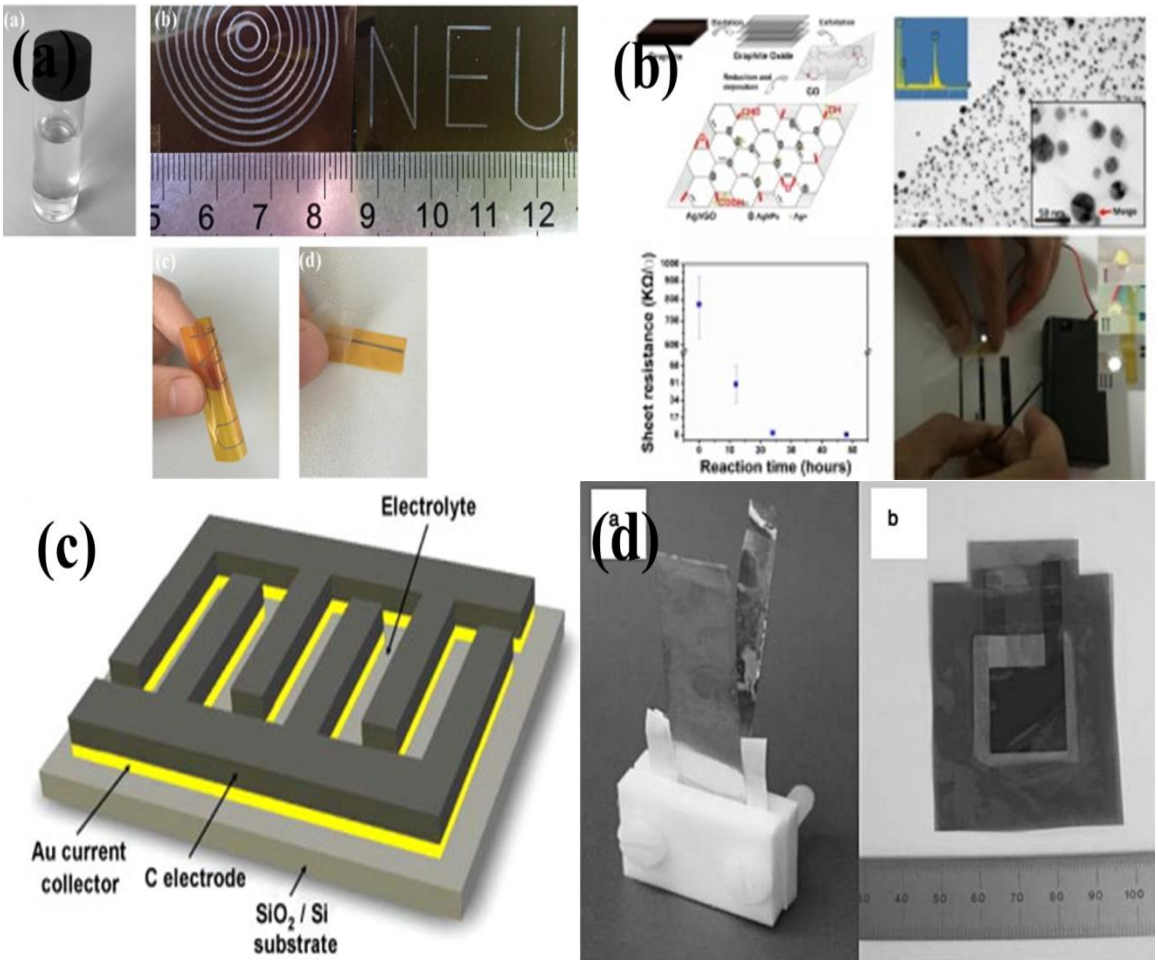

Figure 1.15 Schematic diagram of inkjet printed (a) silver conductive patterns by functional ink; (b) flexible electronics on PET film; (c) carbon-based supercapacitor; (d) supercapacitor prototypes on metal foil current collectors and heat sealed device.

Source: (a) (Dong et al., 2015); (b) (W. Zhang et al., 2016); (c) (Pech et al., 2010); (d) (Ervin et al., 2014).

Disadvantage of inkjet printing:

(a) Clogging of printing nozzles: This might be the main problem of inkjet printing. The inkjet printer requires fine and extremely small particle suspension inks. Even when printing with quality ink, the nozzles could be blocked easily.

(b) Consumption of cartridges: basically the cartridges cannot be cleaned and reused especially for the different inks. The cartridge cost increases the printing cost.

(c) This technology is not suitable for large volume printing. Due to the limitation of cartridge and printing speed.

(d) Inkjet printing requires time to dry the patterns. The substrate is placed on the printing plate which cannot reach high temperature to dry the patterns. Substrate needs to be removed to an individual drying system to remove the solvent.

Table 1.1 Comparisons of Various Printing Processes

Principle	Printing process	Main advantage	Main disadvantage
Mechanical	Pad printing	3D substrate	less durable and hard to scalable
	Gravure printing	High resolution	Can only be printed on smooth surface and printing plates
	Screen printing	Miniaturization	Hard to print multi colors
	flexo printing	Can be printed on rough surface	Low resolution and printing plates
	Lithographic printing	High resolution and can be printed on rough surface	Consumption of printing plates
Digital	Inkjet	Easy to setup and design	Nozzle clogging and consumption of cartridge

Table1.1 shows the main advantages and disadvantages for the different printing techniques. Mechanical printing is easy to achieve mass production especially for industrial processes. However, it requires time and financial resources to replace or make printing roller especially for gravure printing (metallic roller) and lithographic printing (hydrophilic and hydrophobic roller). In contrast, through inkjet printing changes in design can be implemented very easily through the computer design software. However, inkjet printing requires cartridge and printing head replacement with every print. Considering cartridges and nozzles are already commercial available, digital printing still shows outstanding properties compared to mechanical printing. In this research thesis we will discuss the application of inkjet printing in microelectronics and energy storage systems.

1.3 Inks for Printing

Generally the ink for printing can be classified into two types: nano particle suspension ink and particle-free ink. The surface tension and viscosity are two crucial factors for the printing process; they must meet the requirements of specific printers. A typical ink has a viscosity up to 2 cP but it depends on the specific printer. Some printers can be designed to handle liquids up to 100 cP. Additives such as glycerol and isopropanolare can be used to adjust viscosity. Polymeric additives such Polyvinylpyrrolidone (PVP), Poly (vinyl alcohol) PVA and sodium carboxymethyl cellulose (NaCMC) are used to improve dye bonding to the substrate.

1.3.1 Nanoparticle ink

Nanoparticle inks are the most widely used inks currently. Many of the materials previously discussed can be printed as fine particle/solvent (organic or aqueous) suspensions. The advantages of particulate suspensions are including the greater chemical stability of crystal and the higher concentration of active material loading over the other inks. However, particle sizes should be less than a micrometer (usually nanosized) to avoid sedimentation. Also, the dispersion must be very uniform to avoid any aggregation that would increase the viscosity and nozzle clogging during the printing. In order to make a stable and printable nanoparticle based ink, some chemicals are necessary to be added into the ink. Nanoparticles in dispersions approach other particles and stick together due to Brownian motion, and this may cause aggregation followed by further irreversible sedimentation because of the higher density of dispersed materials than the liquid “solvent”. This is especially important for the conductive nanoparticles because nano-sized particles tend to stick together to reduce the surface tension.

In order to prevent the aggregation of nanoparticle based ink, surfactants and stabilizers are necessary to add into the ink, to enhance the shelf life and performance of inks. Basically, the stabilization of nanoparticles against aggregation is achieved by two main mechanisms: electrostatic and steric. Electrostatic stabilization is achieved by electrostatic repulsion between electrical double layers which are adsorbed on the nanoparticles' surface as shown in Figure 1.16 (a) and (b). The value of the electric potential of the nanoparticles is known as zeta potential: higher absolute electrical potential values can give a larger electrostatic repulsion which can make the suspension system more stable. The electrosteric mechanism is especially effective when stabilizing nanoparticles in aqueous dispersions. The disadvantage of electrostatic stabilization is its sensitivity to electrolyte concentration (which is caused by the salts or polar solvent concentration), which strongly affects the thickness of the electrical double layers; this limits the application and stability of nanoparticle inks. Also, it is hard to achieve electrostatic layers in nonpolar solvents systems. To overcome this problem, steric stabilization is another alternative method to make stable suspensions. Steric stabilization is achieved by surrounding the particle with an adsorbed layer of sterically bulky molecules, such as polymers (Figure 1.16 (c)) and surfactant (Figure 1.16 (d)). The polymer/surfactant coated nanoparticles will no longer stick together. Static stabilization is very effective in highly loaded metal nanoparticles dispersions: non-ionic amphiphilic polymers containing both hydrophobic and hydrophilic components. Their molecules are capable of binding to the surface of metallic nanoparticles thus providing effective steric stabilization. The most frequently used is poly (N-vinyl-2-pyrrolidone) (PVP), Poly (vinyl alcohol) (PVA) and Carboxymethyl cellulose (CMC) of various molecular weights,

which exhibit a highly effective protective function in both organic and aqueous media. PVP has been shown to be an effective stabilizer for Ag and Cu NPs in both aqueous and organic solvents (Joshi & Banerjee, 2015; Sarkar, Mukherjee, & Kapoor, 2008; Slistan-Grijalva et al., 2008; Hongshui Wang, Qiao, Chen, Wang, & Ding, 2005). There is much interest in conventional inkjet printing of conductive nanoparticle inks to make conductors, resistors and circuits for electronics (Chung, Ko, Bieri, Grigoropoulos, & Poulikakos, 2004; Hsien-Hsueh, Kan-Sen, & Kuo-Cheng, 2005; Jin Sung Kang et al., 2010; Kraus et al., 2007; B. K. Park, Kim, Jeong, Moon, & Kim, 2007; Perelaer, de Gans, & Schubert, 2006).

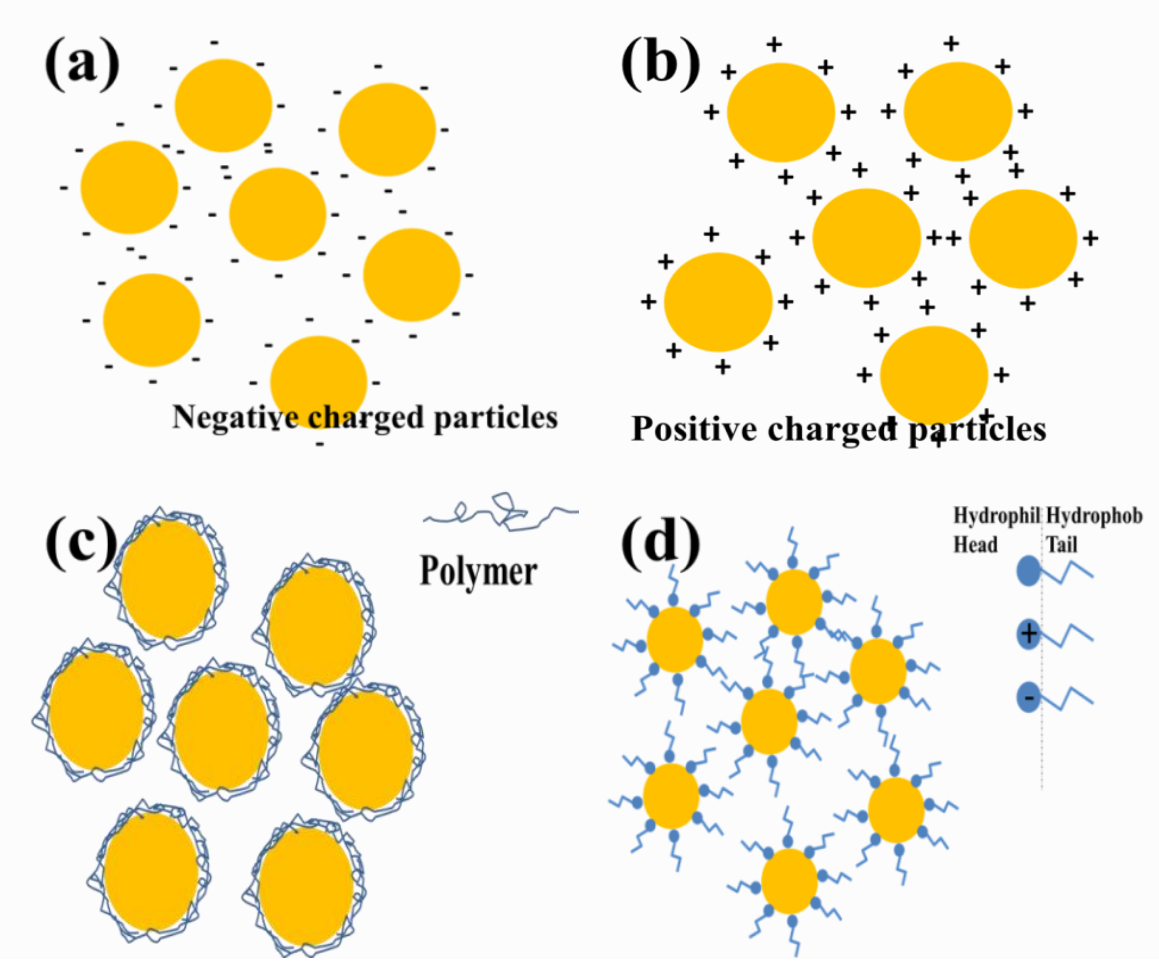

Figure 1.16 (a) Negative and (b) Positive charged electrical double layer stabilized nanoparticle suspension; (c) Polymer surrounded stabilized nanoparticles; (d) Structure of surfactant and stabilized nanoparticles. The yellow sphere is conductive nanoparticles.

1.3.2 Particle-free ink

Particle free ink uses specific solvents to make a stable solution which can be deposited on substrate by printing technologies. The deposited materials are then precipitated by evaporation or chemical reaction at a proper sintering temperature in a certain atmosphere environment. Particle free ink is an excellent choice for printing especially in inkjet printing because of no clogging risk. The particle free ink includes particle free metallic ink and particle free polymer ink (most of the time this means UV-Curable Ink).

The particle free metallic ink has two principles: thermal decomposition and chemical

reduction. Metal-organic decomposition ink (MOD ink) dissolves metallic salts into specific solvents. Usually, since metallic organic salts have poor solubility, chelating agents are necessary to increase the solubility (Figure 1.17 (a) and (b)). After ink deposition on substrate (Figure 1.17 (c)), the printed patterns are dried in certain environment to evaporate solvent and chelating agents and leave the metallic organic salts (Figure 1.17 (d)). The metal can be achieved by the disproportionation reaction a a certain temperature (Figure 1.17 (e)). The deposited metal is then sintered at high temperature to enhance the adhesion on substrate (Figure 1.17 (f)).

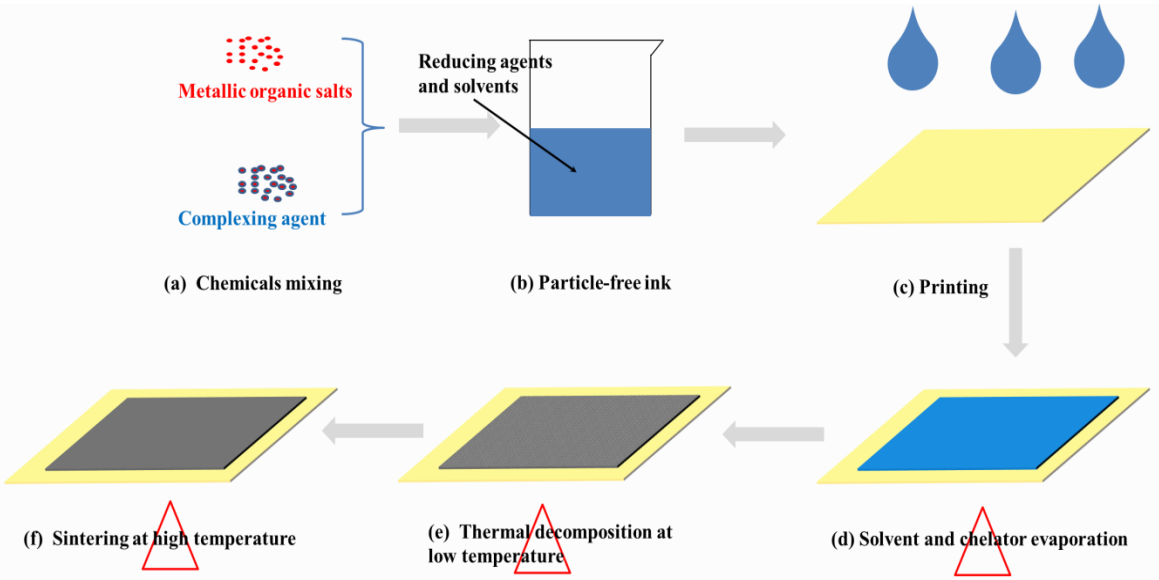

Figure 1.17 Schematics of thermal decomposition metallic organic ink printing process: (a) Chemicals; (b) Solution type ink; (c) Printing process; (d) Solvent evaporation; (e) Thermal decomposition; (f) Thermal sintering.

Another MOD ink use chemical reducing agents (most time solvent with reducing capability) mix with metallic organic salts and complexing agents to make a stable solution as shown in Figure 1.18 (a) and (b). The ink is then deposited on substrate by printing (Figure 1.18 (c)). The printed patterns then heated by thermal plate to evaporate

solvent, in the meantime the reducing agents reduce the metallic ions to form metallic nano particles which then settle on the substrate (Figure 1.18 (d)). The nano particles are then sintered at high temperature to make a continue film on the substrate (Figure 1.18 (f)).

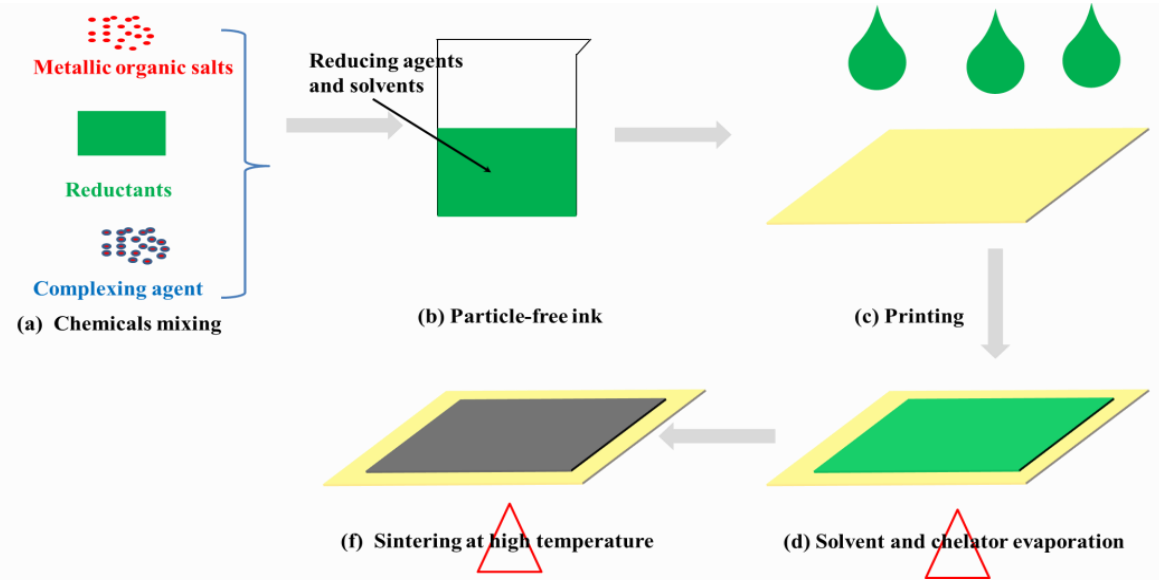

Figure 1.18 Schematics of chemical reducing metallic organic ink printing process: (a) Chemicals; (b) Solution type ink; (c) Printing process; (d) Solvent evaporation and chemical reducing; (e) Thermal sintering.

1.3.3 Ultraviolet (UV) curable ink

UV curing process is a photochemical process in which high intensity ultraviolet light is used to instantly cure inks. UV curable ink has many advantages over traditional inks, for instance: increase production speed, reduce risk of nozzle clogging due to particle free systems and facilitate superior bonding between active materials and substrate. UV curable inks are a better alternative to solvent-based products. Conventional thermal drying is achieved by solvent evaporation. This process shrinks the initial volume significantly which can cause space porous structure which lowers the contact areas

among the active materials; those porous structure leads to a poor conductivity in metallic conductive inks. What is more, organic solvent evaporation creates potential environmental pollutants issues. In contrast, no solvent evaporation in UV curable ink and any loss or shrinkage of coating thickness or volume of printed film.

A UV formulation consists of the following main parts: monomers, linker, photoinitiators (UV sensitive component) and other additives and stabilizers. The irradiation-sensitive element in the ink is the photo initiator which is affected by the UV irradiation. The ink is stable without dense UV shining and appears in liquid form as shown in Figure 1.19 (a). The photo initiator at a radical polymerization forms free radicals, which are able to split the double bonds within the oligomeres and monomers; this is a polymerization reaction in Figure 1.19 (b). Polymerization reaction transforms the fluid varnish film into a three-dimensional solid structure as shown in Figure 1.19 (c).

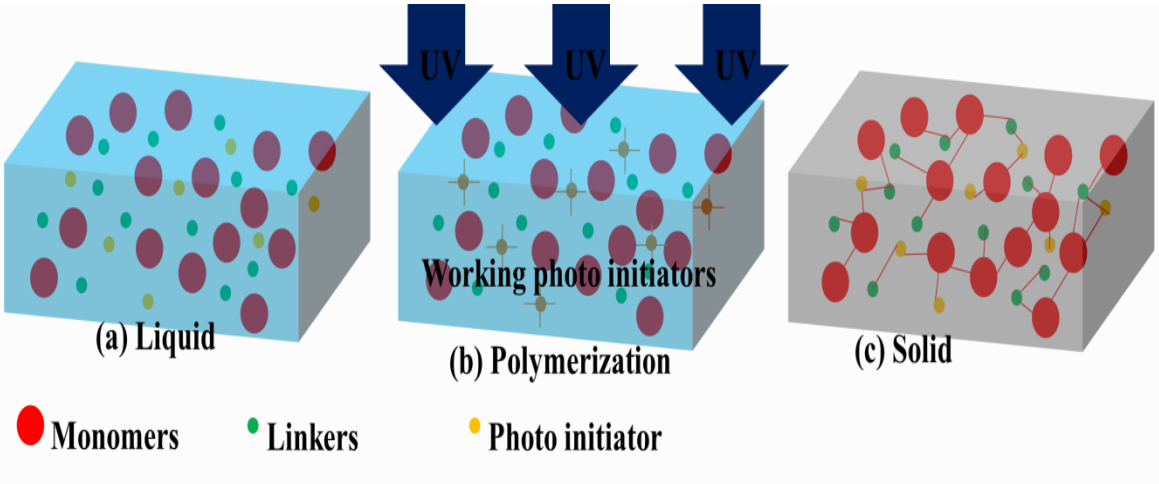

Figure 1.19 Drying process of UV curable ink.

1.3.4 Wettability, viscosity, adhesion and surface tension of ink

Physical properties such as viscosity η, surface tension γ, density ρ, contact angle θ of the

ink and adhesion on the substrate are the most important properties that affect ink and final products performance. The influences of each one on the inkjet printing process are descripted below:

Viscosity plays an important role in keeping the uniform shape of each drop and stabilizing the elongation drop by eliminating the oscillations after the fluid detaches from the nozzles. If the ink is too viscous, large pressure is needed to generate and jet droplets out from the nozzles. Nozzle clogging will happen if the pressure is not enough to shot the droplet especially in particle free ink which usually has high viscosity due to the large dissolved precursors (even though no particle blocking the nozzles, the ink is too thick to print). Another problem is high viscosities are usually caused by high molecular weight and polar solvents. Most of those solvents have a relative high evaporation point which means it will take a long time to dry the inks. On the other hand, if the ink is too thin (low viscosity), satellite spots would be formed due to the impact between the droplet and substrate; also, low viscous ink may easily spread out over the substrate after inkjet deposition as shown in Figure 1.20: the red dash line marks the original ink drop on the substrate after deposition. The rough edge is caused by ink spread out due to the low viscosity; the small satellites drops also formed during the ink deposition, both of satellite spots and rough edge lower the resolution of final patterns. Most of time, low molecular weight and non-polar solvents have low viscosity. These solvents with low vapor pressure can be evaporated very quickly. Fast evaporation of solvent too rapidly destroys the uniformities of ink formula, and potentially partially or totally clogs the nozzles due to the solute precipitation before droplet ejection. In order to make an ink with a property viscosity, ethanol, methanol, ethylene glycol, glycerol and

polymers are used as viscosity adjusters. The recommended viscosity of inkjet printer in this research is 10-12 cp.

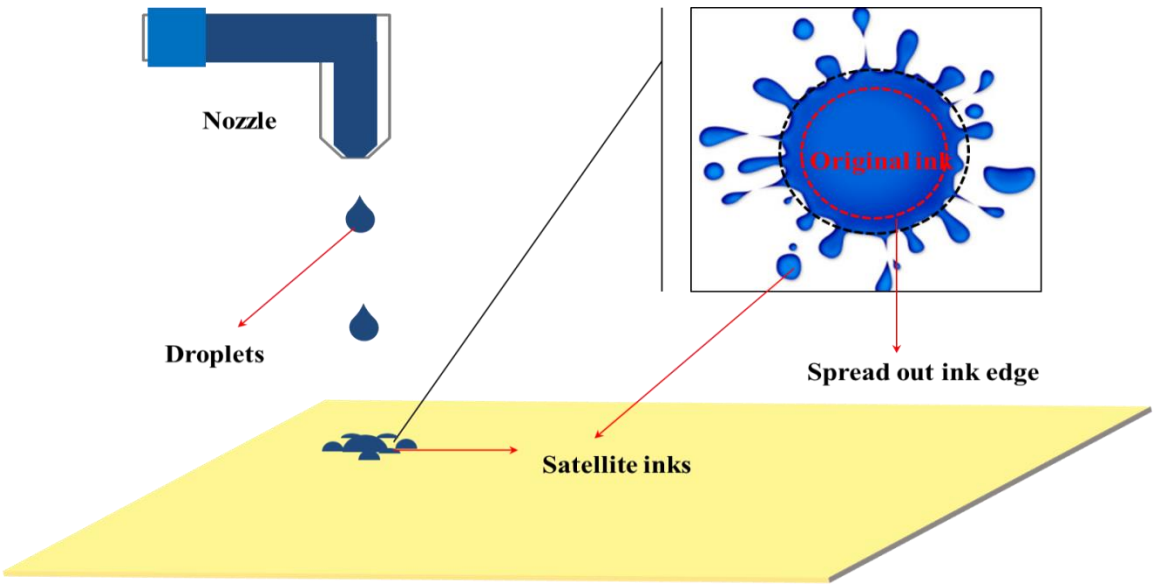

Figure 1.20 Schematics of satellite drops formation and rough edge caused by ink spreading over from printing low viscosity ink.

The extented area that a drop wets the surface is usually described by its equilibrium contact angle (θ_{eq} in Figure 1.21), which is defined as the angle between the liquid and solid interface as ink contact with the substrate. The liquid takes the shape which minimizes the surface energy of the system. Gibbs demonstrated that minimizing the free energy requires the minimization of the sum (ψ) of three energies contributed by the three interfaces.

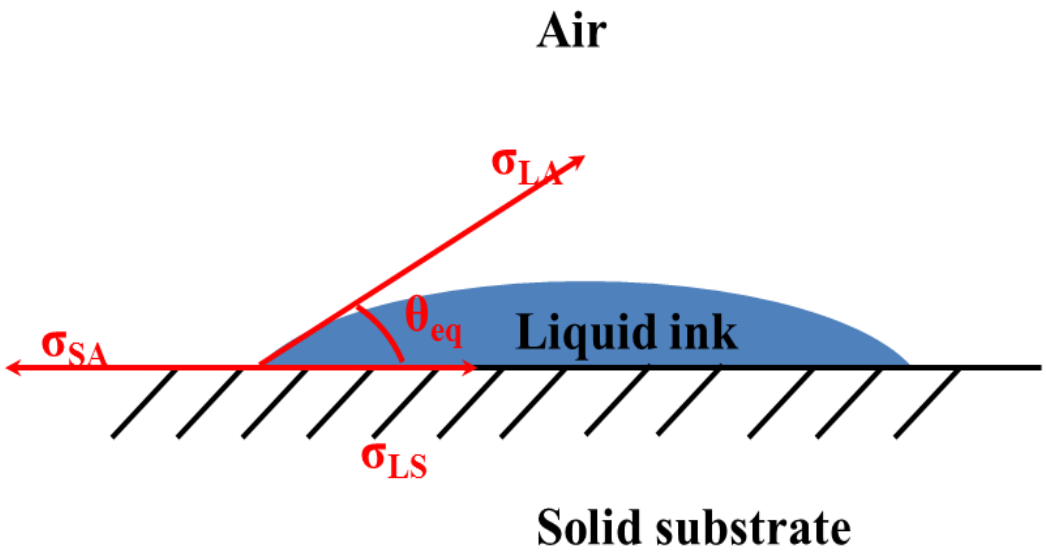

Figure 1.21 Contact angle between liquid drops and substrate.

$$\Psi = \sigma_{LA}A_{LA} + \sigma_{SA}A_{SA} + \sigma_{LS}A_{LS} \quad (1.1)$$

Where σ is the surface tension and A is the contact area (interface), the subscript LA, SA and LS are the liquid-air, solid-air and liquid-solid, respectively. For a plane, homogeneous surface, the minimization yields, where contact angles can be expressed as:

$$\cos\theta_{eq} = \frac{\sigma_{SA} - \sigma_{LS}}{\sigma_{LA}} \quad (1.2)$$

This equation is known as Young's Equation. The shape and size of the droplets on the substrate are controlled by the surface tension. The wetting situations after inkjet deposition are descripted in Figure 1.22 and the ideal wetting situation is marked by red line where the contact angle is between 0 ~90 .

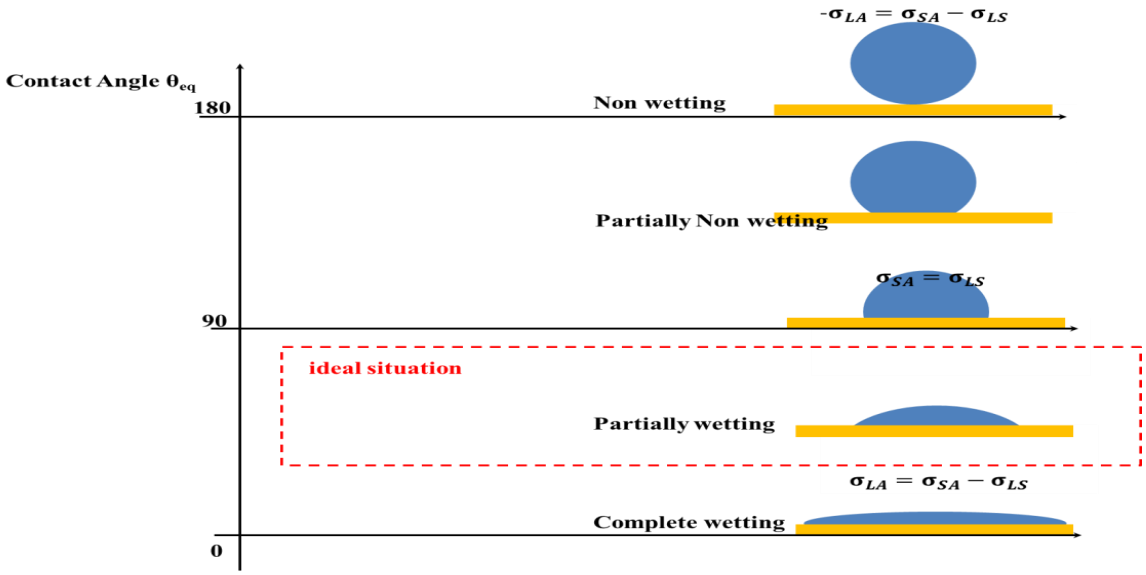

Figure 1.22 Wetting behavior of a liquid drop according to the contact angle (θ).

In order to make a low contact angle, other chemical additives are necessary to adjust the surface tension of ink such as low surface tension solvent and surfactants.

1.4 Sintering Technologies

To form a continuous, stable and flexible film, particles/particles precipitate from the solution must be sintered. Sintering is a process of joining particles together at a temperature below the melting point of the materials (Nir et al., 2010). The sintering process is especially important for conductive patterns fabrication. Good conductive cannot be achieved without sintering due to the huge physical contact resistance among particles (this is the reason of low conductivity of carbon based ink, because carbon based materials cannot be sintered easily). The conventional method to sinter metal nanoparticles is thermal heating. Because of the high surface-to-volume ratio due to the nano size effect, they are characterized by decreased melting temperatures (temperature

depression) (Nanda, Sahu, & Behera, 2002; Zolriasatein & Shokuhfar, 2015). For example, for silver and gold particles with a diameter around 2.5 nm, a reduction in melting point is estimated to be around 400 ℃ and 500 ℃, respectively (Qi, 2005; Skripov, Koverda, & Skokov, 1981; Younan Xia et al., 2003). However, the melting temperature for 1.5 nm gold particles is found to be as low as 380 ℃ (the melting point of bulk gold is 1063 ℃). Even for particles of 20 nm diameter, the melting point was found to be significant lower than that of the bulk metal. Such a depression of the melting point makes metallic nanoparticles much "softer" than large particles at a certain temperature range which is below the melting point, and enhanced solid diffusion of the metal atoms induces initial neck formation between Nano particles (NPs) thus causing the emerging of particles to each other Then the bonded particles are followed by grain growth and shrinkage with formation of a bulk phase.

For conventional thermal sintering of metallic nanoparticles, three steps are possible: (a) after the evaporation of solvent, metallic nanoparticles settle down on the substrate. Some of them contact with each other while others do not as shown in Figure 1.23 (a); (b) with the temperature rising, nanoparticles become much softer and getting closer to each other due to the volume expansion; in this time solid diffusion or plastic flow is activated near the grain boundaries, neck formation occurs between two particle as shown in Figure 1.23 (b), but the existence of porosity among particles still make the film nonconductive; (c) with the temperature continuing to increase, pore shrinkage occurs because particles tend to merge together. Particle contact each other further and further in Figure 1.23 (c).

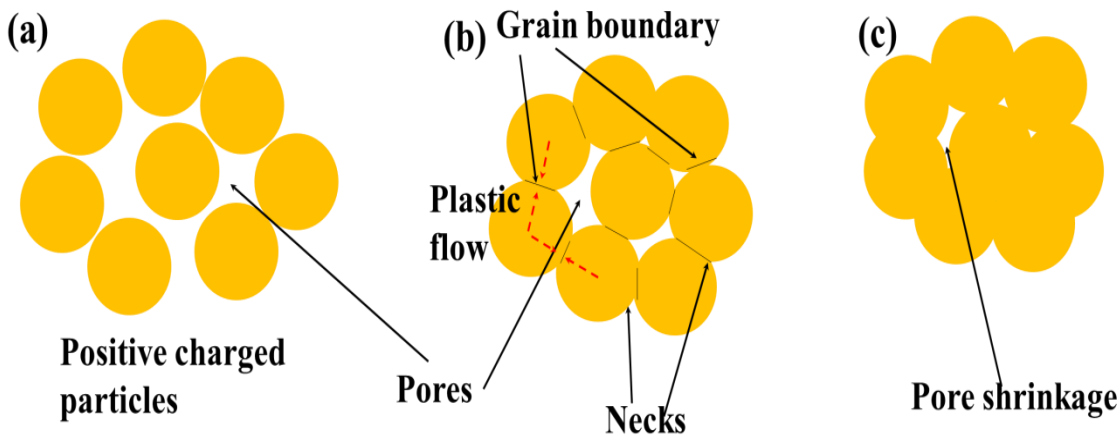

Figure 1.23 Thermal sintering processes of metallic particles: (a) Stable particle suspension; (b) Neck formation and solid diffusion at temperature below the melting point; (c) Volume shrinkage and grain growth.

Nanoparticles are need to formulate conductive ink particle suspension not just only to prevent nozzle clogging but also to enable easy sintering at relative low temperatures. Low temperature sintering is necessary for inkjet printing because commonly used substrates are flexible polymers which cannot survive at high temperatures. However, nanoparticles may cause a serious problem: surface oxidation, which is caused by high chemical reactivity at nano size. The high melting temperature oxidized layers prevent particle sintering and also lower the thermal and electronical conductivivty of the particle. New sintering technologies have been developed to promote sintering and eliminate oxidations in nanoparticle inks as introduced follow.

1.4.1 Plasma sintering

Plasma sintering can anneal metals at low temperature. Figure 1.24 shows the schematics of the plasma reduction and sintering process after inkjet printing. After inkjet printing, the patterns are transferred to vacuum ovens to evaporate the binder and thickener to increase the contact among nanoparticles (Figure 1.24 (a) and (b)). The dried patterns are

treated under H_2/Ar plasma for a while to remove the oxidized layer as shown in Figure 1.24 (c). Also, during this process, the bombardment in the plasma can connect individual particles together (neck formation). This plasma "sintering" process (Figure 1.24 (d)) can anneal metallic nanoparticles patterns without damaging polymer substrates. Plasma sintering technology has been used to fabricate silver conductive tracks successfully (Ma, Bromberg, Egitto, & Singler, 2013; Ma et al., 2014; Reinhold et al., 2009; Wünscher, Stumpf, Perelaer, & Schubert, 2014); other metals have not been reported. Plasma sintering depends strongly on the hardness of materials because it highly depends on the bombardments between the metallic particles and plasma ions. Silver is soft and exhibits a low melting temperature which make is ideal for plasma sintering; other metals usually have relative higher melting temperature or hardness.

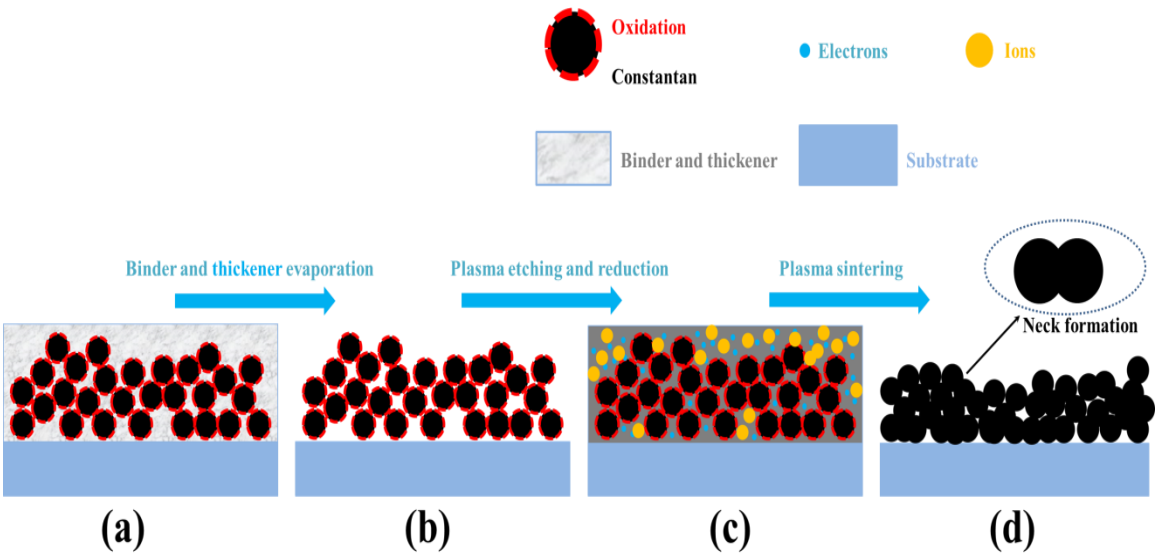

Figure 1.24 Schematics of plasma reduction and sintering process: (a)-(b) Evaporation of organic binder and thicker from the ink; (c) Plasma reducing/etch process; (d) Neck formation due to the particle bombardment.

1.4.2 Electrical sintering

In this method, the sintering is achieved by applying a voltage over the dried printed structure which causes current flow through the printed particles, leading to a local heating at particle-particle boundary (Mark et al., 2008). The whole process is shown in Figure 1.25. When current passes through the nanoparticles, heating occurs between the interfaces of particles due to the high contact resistance. After the voltage pulse, necks can be formed among the particles due to the local thermal heating. In order to enhance the sintering effect, pressure is applied on the printed patterns to eliminate the space voids among the particles. The main advantages of this method are the short sintering time (from microseconds to tens of seconds) and room temperature processing which means this sintering method can be expanded to a range of printing substrates. However, the main disadvantage of this sintering method is obvious: it can only be applied on the conductive materials. Isolated materials cannot be sintered. Lots of metallic inks like copper and nickel are surrounded by non-conductive oxidation layers.

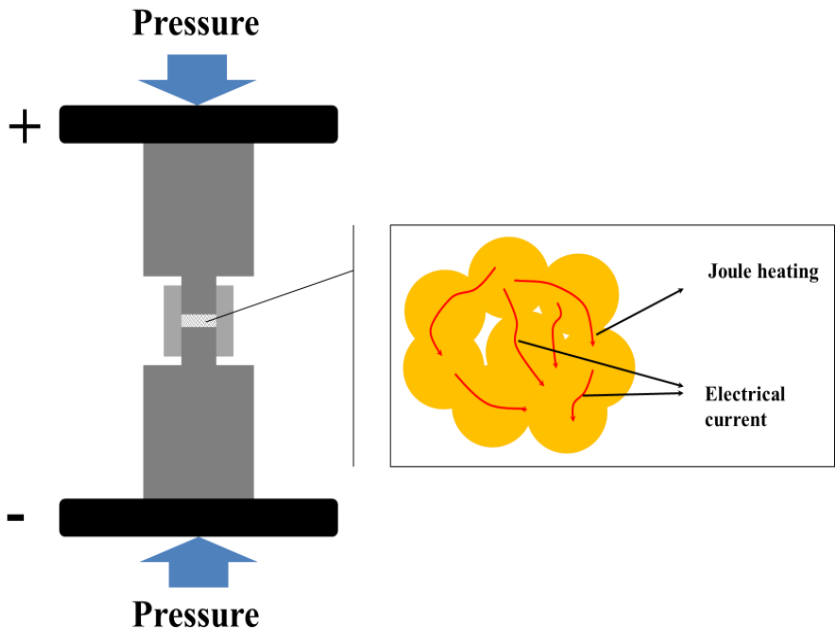

Figure 1.25 Schematics of electrical sintering.

1.4.3 Photonic sintering

Photonic sintering is a low thermal exposure sintering method developed to sinter nanoparticle based thin films. The process uses a xenon flash lamp to deliver a high intensity, short duration (< 1 ms) pulse of light to the deposited patterns. Subsequently light absorption by the printed metallic layer results in its heating which leads into evaporation of liquid, and nanoparticles sintering as displayed in Figure 1.26. This method is mainly used to sinter silver and copper nanoparticles which have relative low melting temperature (Hyun-Jun, Wan-Ho, & Hak-Sung, 2012; J. S. Kang, Ryu, Kim, & Hahn, 2011; H.-S. Kim, Dhage, Shim, & Hahn, 2009; Norita et al., 2015; Ryu, Kim, & Hahn, 2010). Generally, the metallic nanoparticles are surrounded by oxidation layers due to the Nano sized effect. The oxidation has high melting point and poor thermal and electrical conductivity which makes particle impossible to sinter and have poor properties after sintering. In order to remove the oxidation layers and enhance the sintering result,

suitable amounts of reducing capability polymers are added to the ink. Oxidation reduction occurs when intense pulse light passes the printed patterns (Figure 1.26). The advantages of photonic sintering are it can be operated at room temperature in a short time. Also, photonic sintering can achieve roll to roll processing which makes it excellent sintering method in industrial production.

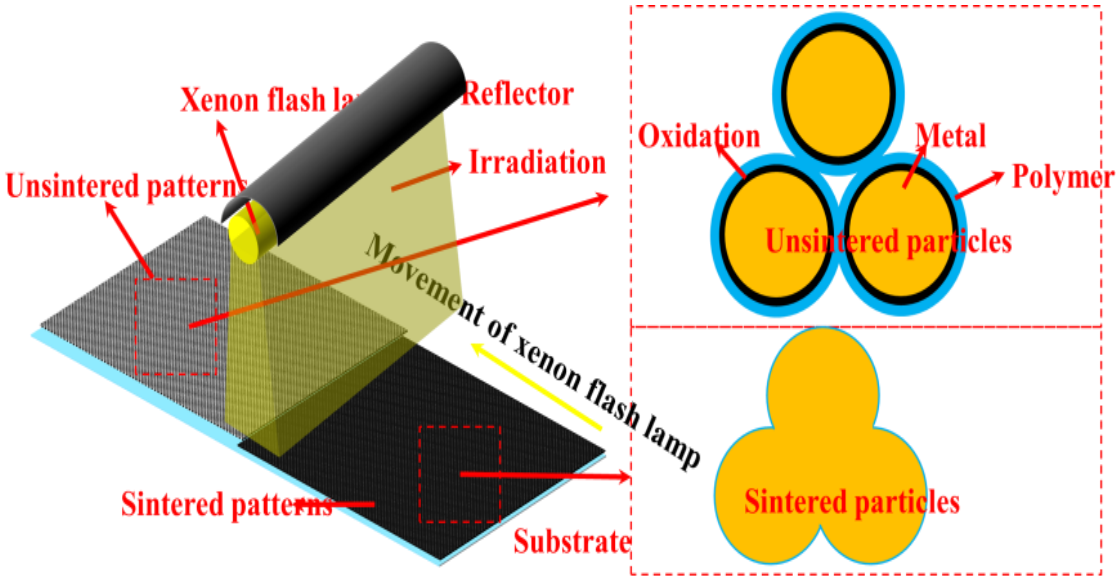

Figure 1.26 Schematics of photonic sintering.

1.4.4 Microwave sintering

A new flash microwave sintering process is developed to sinter printed patterns as shown in Figure 1.27 (Roy, Agrawal, Cheng, & Gedevanishvili, 1999; Stanciu, Raether, & Groza, 2016; S.-H. Wu & Chen, 2004). Metals can be sintered by microwave radiation in a short time. Another advantage of this sintering method is it combines chemical reduction when microwave is illuminating the pattern. However, this method has a very small penetration depth: the penetration depth at 2.54 GHz for Ag, Au, and Cu ranges

from 1.3 to 1.6 μm (Kamyshny, Steinke, & Magdassi, 2011). The printed thickness must smaller than the penetration of the microwave in order to cure the inner materials. Since inkjet printed conductive tracks meets this requirement, it is expected that this technology will be adapted for industrial manufacturing.

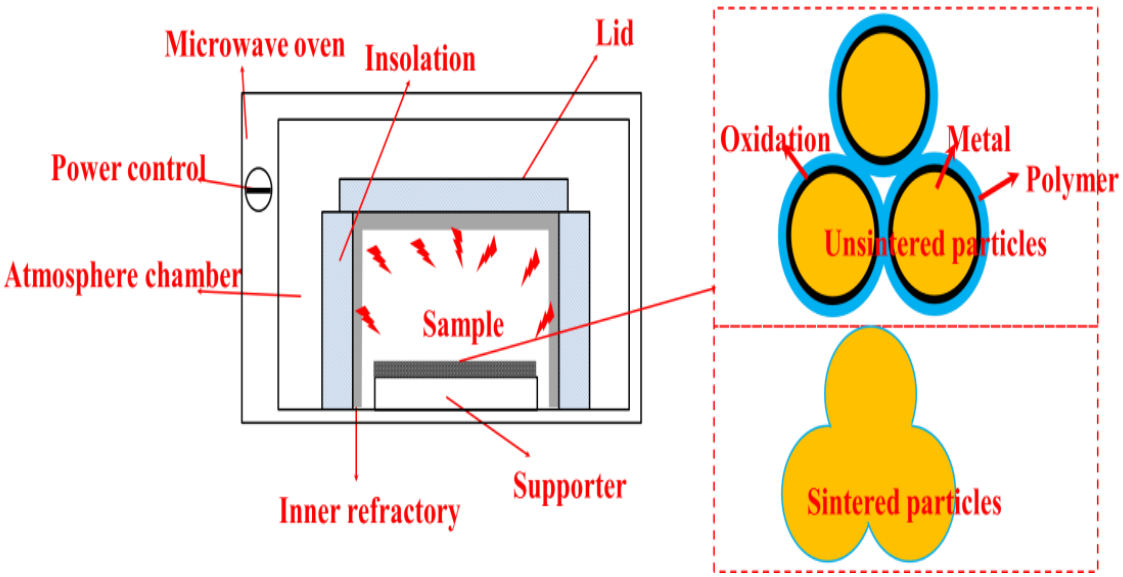

Figure 1.27 Schematics of microwave sintering.

1.5 Inkjet Printing Conductive Films

In recent years, there has been more attention to the fabrication of conductive inks with the development of printing technology in electronic industry (Daniel & Astruc, 2004; Herrmann et al., 2007; B. K. Park et al., 2007; Shipway, Katz, & Willner, 2000). Generally, nanoparticle suspensions (S.-H. Park, Chung, & Kim, 2014) and particle-free inks (Nie, Wang, & Zou, 2012) have all been developed to make conductive tracks. The basic fabrication process of suspensions is to disperse solid metallic particles in organic/inorganic solvents. Solid particles are deposited on flexible substrate by printer,

and then the printed pattern is sintered to make crackless films. Traditional methods require ultra-small (below 50 nm) solid particles and high sintering temperature., because the working temperature of substrates for conductive ink is usually below 400 ℃ which is a relative low temperature for thermal sintering, the temperature depression for sintering in nano-sized particles is advantageous for processing on plastic substrates. This limits the application of conductive ink due to the complexity of the synthesis of size qualified particles especially for alloy particles. However, metallic nanoparticles can oxide in the air very easily, so typically the sintering process is performed in hydrogen reducing atmosphere which is a high flammable gas with safety issues. Various sintering methods are developed to cure conductive inks such as microwave, plasma and photonic sintering to interconnect particles as mentioned above. All those sintering methods need complex instruments and safety protection. Another approach is a particle-free ink; soluble metal source precursors and reducer are dissolved in solvent. After deposition by printer, conductive track is formed during thermal sintering process by chemical reducing reaction. Particle-free ink depends on the solubility of metal precursor in solvent; it is not effective scalable pathway for massive products in industry. On the other hand, particle-free conductive inks can only make pure metal tracks; it is impossible to make particle free alloy ink.

The most printable conductive inks are summered in Table 1.2. To the best knowledge of our research, the most conductive metal is gold which can be sintered very easily (thermal sintering in air). However, gold ink suffers the expensive cost which can only applied in small amounts. Aluminum ink is fabricated from aluminum hydride which is a very unstable (air and water sensitive) and chemically flammable. This makes

aluminum ink impossible to print in air. Carbon black, carbon nanotubes and graphene inks have high resistance due to non-sintered property of carbon. Silver, copper and nickel inks are promising for the conductive tracks: silver has relative high conductivity per volume and mass; also silver ink requires simple sintering process without protecting atmosphere. Compared with silver, copper and nickel inks have much lower cost without sacrificing too much conductivity. However, both of copper and nickel needed to been sintered with protecting atmospheres.

Table 1.2 Summaries of Various Inks Developed in Recent Years

	Relative conductivity per unit volume	Relative conductivity per unit mass	Surface Resistance (printed) Ω/sq
Gold	0.7	0.33	5×10^{-3} (Bishop et al., 2010)
Silver	1.05	0.9	5×10^{-2} (Merilampi, Laine-Ma, & Ruuskanen, 2009)
Copper	1	1	10 (Y. Kim et al., 2012)
Aluminum	0.4	1.3	1.5 (H. M. Lee et al., 2012)
Nickel	0.24	0.25	50 (D. Li, Sutton, Burgess, Graham, & Calvert, 2009)
Carbon black	0.00001	0.00004	132 (Tortorich, Song, & Choi, 2014)
Graphene	0.0003	0.0012	65 (Shin, Hong, & Jang, 2011)

1.6 Inkjet Technology for Flexible Lithium-Ion Batteries

In recent decades, more and more energy storage devices are required in both industrial and people's daily life as shown in Figure 1.28 (a). Based on the currently known power

sources, shown in Figure 1.28 (b), Li-ion batteries are the prime candidate to meet these requirements. Rechargeable lithium-ion batteries have a higher energy density than most other types of rechargeable batteries. This means that for the same volume or weight they can store more energy than other rechargeable batteries. Lithium-ion batteries are expected to provide an energy return factor higher than that assured by conventional batteries, e.g., lead-acid batteries which are shown in Figure 1.28 (b). Lithium-ion batteries also have a lower self-discharge rate than other types of rechargeable batteries. This means that once they are charged they will retain their charge for a longer time than other types of rechargeable batteries. NiMH and NiCd batteries can lose anywhere from 1-5 % of their charge per day, (depending on the storage temperature) even if they are not installed in a device. Lithium-ion batteries will retain most of their charge even after months of storage. Also, the energy efficiency of a lithium-ion battery is typically over 90 %, but lead-acid batteries may be only 75 % efficient. Lithium-ion batteries typically can charge between 500-1500 cycles (Mukhopadhyay & Sheldon, 2014). They can also be recharged relatively quickly: typically 85 % of full charge capacity in less than 30 minutes.

Based on the advantages mentioned above, the lithium-ion battery is one of the most promising energy storage systems for portable computers, mobile devices, hybrid electric vehicles, and plug-in hybrid electric vehicles (Scrosati & Garche, 2010). Due to the high value of the energy density, lithium-ion batteries are the predominate power source for cell phones, lap-top computers, e-book readers, MP3 players, and most other portable electronic devices. (Mukhopadhyay & Sheldon, 2014) Indeed, lithium-ion batteries are today produced by the billions of units per year ("Global Battery Markets,"

2011), representing the major revenue (37 %) of the battery market.

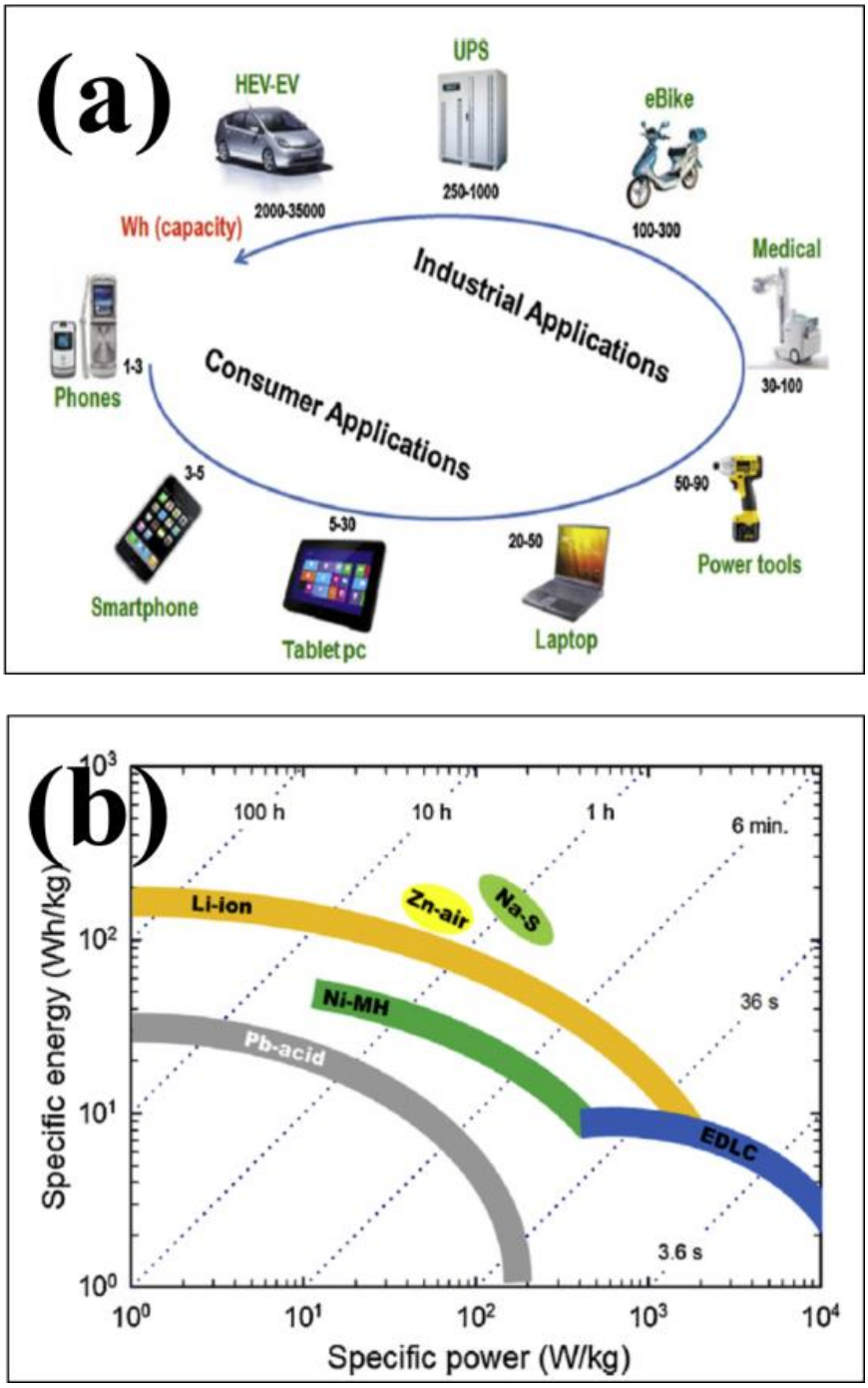

Figure 1.28 (a) The applications and associated energy capacity required for rechargeable batteries; (b) Comparison of energy and power capabilities of rechargeable batteries increasing specific energy implies longer battery runtime while increasing specific power implies increasing available current.

Source: (b) (Yoo, Markevich, Salitra, Sharon, & Aurbach, 2014).

In its most conventional structure, a lithium-ion battery (shown in Figure 1.29 (a)) contains an anode, a cathode formed by a lithium metal oxide or phosphate, and an electrolyte which is typically a lithium salt such as $LiPF_6$ dissolved in an organic solvent such as ethylene carbonate (Mukhopadhyay & Sheldon, 2014; Scrosati & Garche, 2010). Between the anode and cathode is a semipermeable separator. Figure 1.29 (a)**Error! Reference source not found.** shows a typical lithium-ion battery configuration. The graphite electrode is typically deposited on a copper current collector while the cathode material is typically deposited on an aluminum current collector. The cathode and anode react according to the Equations (1.3) and (1.4) reactions:

Cathode: $LiMO_2 \rightarrow Li_{1-x}MO_2 + xLi^+ + xe^-$ (1.3)

Anode:$xLi^+ + xe^- + 6C = Li_xC_6$ (1.4)

The electrolyte does not enable the conduction of free electrons; instead, the electrons that complete the half reaction move via an external wire providing power to an external load (de las Casas & Li, 2012). While charging and discharging, Li^+ ions move between the anode and cathode via the electrolyte. During the charging/ discharging processes, the movement of lithium ions between the cathode and anode result in intercalation/deintercalation of lithium ions into the electrodes and a commensurate physical volume change which mechanically fatigues the electrodes.

While Li-ion batteries have enabled the growth in the portable electronics, further improvements are needed to meet the high specific energy demands required by

uninterruptible power supplies and electric vehicles. To increase the capacity of Li-ion cells, materials with higher specific capacities than those currently used for the electrodes will be needed. Figure 1.29 (b) shows the effect of electrode capacity on the overall capacity of a cell, based on the work of Yoshi et al (M. Yoshio, T. Tsumura, & N. Dimov, 2005) (It should be noted that this estimation is based solely on the weights of the active materials, i.e., the weight of the cell case, separators, and current collectors, etc. are not considered. However, it provides a useful comparison of the effect of changing one or both electrodes.). Currently, Li-ion cells consist of a $LiCoO_2$ cathode (capacity of 155 mAh/g) and a graphite anode (capacity of 372 mAh/g) which is displayed in Figure 1.29 (b). The combination of these electrodes leads to a cell capacity of 109 mAh/g.

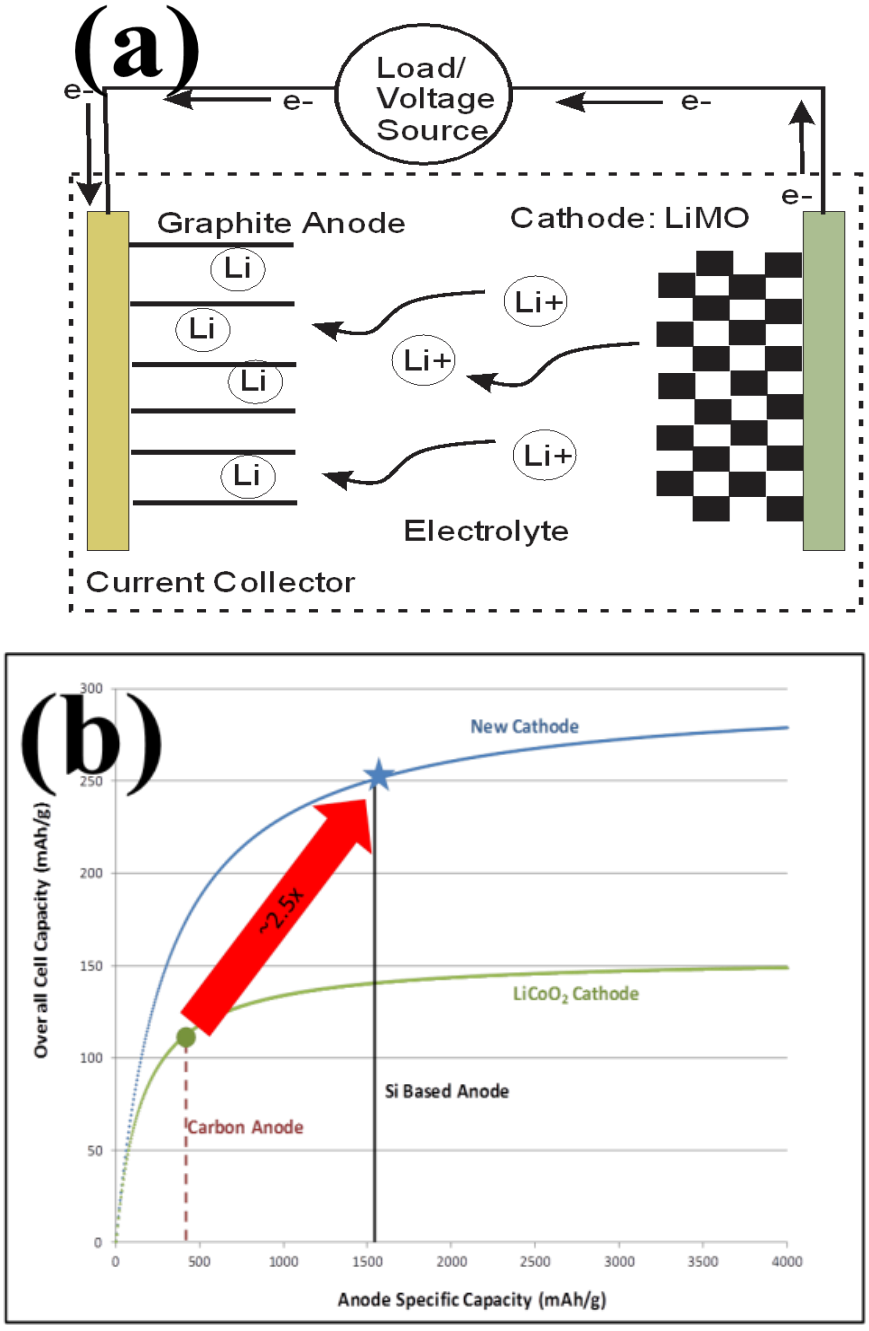

Figure 1.29 (a) Scheme of a common lithium-ion battery with a lithium metal oxide (LiMO) cathode; (b) Effect of Anode (x-axis) and Cathode (Curve) Specific Capacity on Overall Cell Capacity. The resultant cell specific capacity (y-axis) is based upon the active electrode materials only-no other materials e.g., electrolyte, separator, case are considered.

Source: (a) (de las Casas & Li, 2012); (b) (Masaki Yoshio, Takaaki Tsumura, & Nikolay Dimov, 2005).

In addition to the overall growth in the use of batteries, there is a parallel trend to develop mechanically flexible batteries. Form factor is becoming a major driver shaping innovation and transforming the energy storage industry through the emergence of new applications (X. He & Zervos, 2014) such as wearable electronic devices, flexible displays, conformal sensor networks, implanted medical devices (Koo et al., 2012; Nishide & Oyaizu, 2008), micro-vehicles (Rivera, 2012) and the Internet of Things, which demand thin profiles and flexibility. Mechanically flexible batteries are typically fabricated as thin flat sheets, enabling the batteries to conform to odd-shaped spaces. The mechanical flexibility of these batteries enables product designers with a range of possibilities. For example, electronically controlled drug delivery systems or wearable medical sensors could be wrapped around a wrist or arm (Jacoby, 2013). Conformal flexible battery sheets can be attached to or inserted into various shapes enabling them to conform to the packaging shape of a hand-held device thereby providing power for electronic devices. Flexible battery technology is already being used in the next generation of credit cards and security cards known as ‘smart cards’ or ‘powered cards’. These cards utilize the batteries to power embedded memory chips or microprocessors ("Flexion Batteries," 2013). Flexible batteries can also be used to power Radio Frequency Identification (RF-ID) sensory devices by providing local power for the integrated sensors. The main challenges in flexible energy storage devices are the design and mechanical properties of current collectors, as well as the fabrication of flexible electrode materials with high capacity and electrical conductivity. There are several approaches towards the flexible battery (X. Wang et al., 2014) development including paper-based batteries, polymer batteries, cellulose-based batteries, and soft packing batteries. The

mechanical flexibility of the batteries is predominately determined by electrodes/current collectors.

To meet the high cell capacity and mechanical flexibility requirements outlined above, we developed an inkjet printable high energy capacity cathode material in conjunction with high energy capacity silicon anode to increase the overall cell capacity. The second major theme of the battery development described in this thesis is to use inkjet printing technology to pattern electrode structures to improve battery cycling lifetime and flexibility. The third theme is to use water based processing for the inks to eliminate the need for organic solvents and binders. Below, an overview of the cathode, anode, and binder materials of the high energy batteries is presented.

1.6.1 Positive cathode materials

The conventional positive materials for lithium-ion batteries are: olivine, layered and spinel structured crystals are shown in Figure 1.30 (Christian M Julien, Mauger, Zaghib, & Groult, 2014). The classification of the structure is based on the lithium ion diffusion pathways inside the crystals (Goodenough, 1994).

The typical 1D structure positive material is $LiFePO_4$ (LFP) which is an excellent candidate material for Electric Vehicles (EVs) and Hybrid Electric Vehicles (HEVs) due to the relative easy obtain row materials and cheap cost of fabrication, high capacity, non-chemical toxicity and outstanding thermal stability. The main drawback of LFP positive material is poor rate capacity due to the limitation of lithium ion diffusion pathway. Also, LFP has very low electronic conductivity.

Typical 2D structure positive materials including: layered transition metal oxide materials, such as $LiCoO_2$, $LiNiO_2$, $LiNi_{1/3}Co_{1/3}Mn_{1/3}O_2$ and $LiNi_{0.8}Co_{0.2}O_2$, suffer a

drawback of oxygen evolution in the high delithiated state which - despite their high theoretical capacities - could cause severe thermal runaway of the cell leading to low practical energy capacity (Ammundsen, Jones, Rozière, & Burns, 1996; Boulineau, Simonin, Colin, Bourbon, & Patoux, 2013; Jarvis, Deng, Allard, Manthiram, & Ferreira, 2011). Consider the lithium rich manganese-based (LRM) layered materials $_xLi_2MnO_{3\cdot(1-x)}Li[Ni_{1/3}Co_{1/3}Mn_{1/3}]O_2$ as an example. These materials have attracted increasing attention as a promising high-capacity cathode (C. M. Julien, Mauger, Groult, Zhang, & Gendron, 2010; Qiao et al., 2013) with an anomalously high discharge capacity of more than 250 mA·h/g through the activation of Li_2MnO_3. However, the commercial application of LRM cathodes in Lithium-ion batteries is hindered by several drawbacks including poor cycle life, low thermal stability and a gradual voltage drop during cycling (Oishi et al., 2013; Yabuuchi, Yoshii, Myung, Nakai, & Komaba, 2011).

$LiMn_2O_4$ (LMO) is the typical 3D spinal cathode materials for lithium-ion batteries. The theoretical capacity is competitive with existing materials and in the 4V region. The 3D structure has relative high ion diffusion which flavors a high rate capacity. However, there are some problems with the material that leads to a slow capacity loss and need to be solved: the dissolution of divalent Mn and oxygen from the host structure in the high-voltage region, this can lead to a loss of active cathode material. LMO also suffers degradation during cycling over the high-voltage two-phase region (approx. $Li_{0.5}Mn_2O_4$ - λ-MnO_2) (Gao & Dahn, 1996; Hunter, 1981; Yongyao Xia & Yoshio, 1996).

The widely used method to modify cathode materials is the surface carbon coating in order to increase the electronical conductivity among particles during charging and discharging (H. Huang, Yin, & Nazar, 2001). However, the carbon coating method

obviously helps nothing in the lattice electronic conductivity or chemical diffusion coefficient of lithium within the crystal (Xie & Zhou, 2006). Another modification is ion doping: Substitution of a small quantity of elements inside positive materials by other ions to improve the kinetics of lithium ion diffusion and change the crystal lattice which can enlarger the pathway of lithium ion, this can improve the capacity delivery, cycle life, and rate capability (Liu, Wang, Tan, Yang, & Zeng, 2013; Myung, Kumagai, Komaba, & Chung, 2001; J. Xu & Chen, 2010). However, such doping usually lowers the battery's capacity due to the incorporation of inactive elements into the cathode. A coating approach can also improve rate capability and cycle stability for Li-rich layered oxides (Y.-K. Sun et al., 2012; F. Wu et al., 2013). But the highly continuous coating on the surface of particles is not realistic to obtain during practical processing.

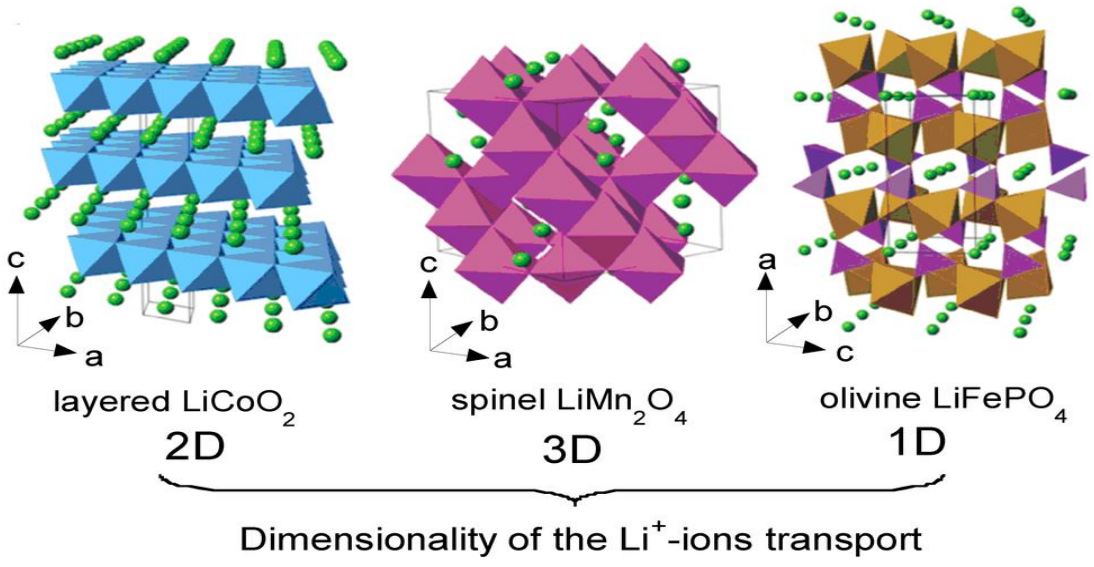

Figure 1.30 Crystal structure of the three lithium insertion compounds in which the Li^+ ions are mobile through the 2-D (layered), 3-D (spinel) and 1-D (olivine) frameworks.

Source: (Christian M Julien et al., 2014).

In this thesis, $LiNi_{1/3}Co_{1/3}Mn_{1/3}O_2$ (NMC) is used as the cathode materials to make printable positive electrode considering the stability and relative good performance.

1.6.2 Negative anode materials

Carbon-based anodes are the most popular for lithium-ion batteries. Lithium ions are basically stored inside the layers structure which is shown in Figure 1.31 (a) (Wen et al., 2014). In order to achieve higher energy density for lithium-ion batteries, there is great interest in replacing carbon-based anode materials with silicon or silicon-based compounds (Figure 1.31 (b)) (S.-P. Kim, Datta, & Shenoy, 2014). When compared to graphite-based Li_1C_6 with a specific capacity of 372 mAh/g, the fully lithiated lithium-silicon phase, $Li_{22}Si_5$, exhibits a theoretical specific capacity of ~4200 mAh/g (Teki et al., 2009). When cells are made with silicon-based anodes, high capacity is observed initially. However there is a significant decrease in capacity as the cells experience charge/discharge cycles. The decrease in capacity with cycling has been attributed to two main phenomena: decrepitation and continuous formation of an impermeable solid electrolyte interphase (SEI) layer which are descripted below.

In carbon based anodes, the Li^+ ions are intercalated between graphite planes, with minimal expansion. For silicon-based anodes, the Li forms a series of alloys with silicon (Mukhopadhyay & Sheldon, 2014), each with a different molar volume. As Li^+ enters and leaves the silicon material during cycling, there is a significant volume change as the alloy composition and associated molar volume varies. The fully lithiated alloy, $Li_{22}Si_5$, undergoes a > 300 % volume expansion compared to silicon alone. The main drawback to silicon anodes is its cycle performance. Failure of the Si anodes is mainly caused by the large volume expansion/contraction during lithium insertion/extraction

because the intermetallics of Li/Si have much greater molar volume than the nanostructure Si phase. Volume change can cause stress gradient inside Si particles. Large stresses induced by the repetitive volume expansion and contraction can cause cracking and pulverization of the Si anodes resulting in the loss of electrical contact between them (Huggins & Nix, 2000). Stress development in electrode materials is one of the primary causes of performance degradation (capacity fade) and failure of Li-ion batteries. It represents a major bottleneck in the development of new high-capacity electrode materials for Li-ion batteries (Mukhopadhyay & Sheldon, 2014).

Solid-electrolyte interphase (SEI) film formation which results from the decomposition of electrolytes is another important factor in the battery performance, which leads to irreversible capacity loss. Large volume changes crack the SEI films and expose Si to electrolytes repeatedly, thus facilitating the continued growth of SEI films. As a result, active Si particles are isolated by the electric-insulated SEI films and the anode's electrochemical activity degrades.

Another anode materials for lithium anode is $Li_4Ti_5O_{12}$ (LTO) (Yi et al., 2011) as displayed in Figure 1.31 (c). The theoretical capacity of LTO is around 175 mAh/g with a flat charge/discharge potential plateau at 1.55 V, the charge-discharge plate is due to the stable Ti^{4+}/Ti^{3+} redox couple versus and experiences zero-strain during lithium intercalation/deintercalation (Peramunage & Abraham, 1998; Zaghib, Simoneau, Armand, & Gauthier, 1999). LTO also has other advantages such as cheap and green raw materials, excellent safety, structural stability, high rate capabilities and long cycle life (Amatucci, Badway, Du Pasquier, & Zheng, 2001). Hence, $Li_4Ti_5O_{12}$ is used in this thesis.

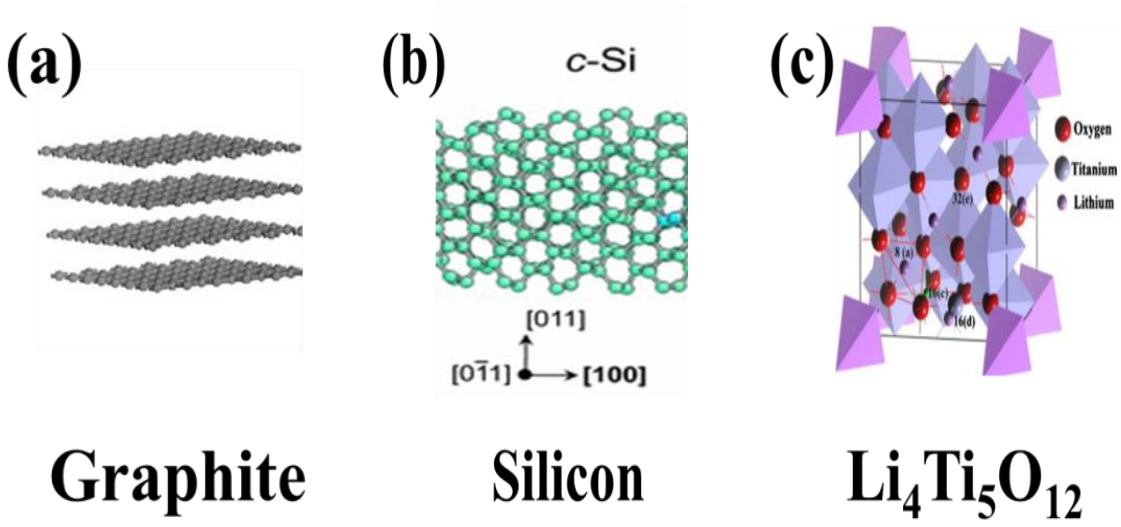

Figure 1.31 Crystal structures of the three anode materials for lithium-ion batteries: (a) conventional graphite; (b) silicon materials; (c) LTO ceramics.

Source: (a) (Wen et al., 2014); (b) (S.-P. Kim et al., 2014); (c) (Yi et al., 2011).

1.6.3 Binder system

For lithium-ion batteries, the binder serves two primary functions (Chong et al., 2011): (a) holding the active materials and conductive agent (e.g., carbon black) into a cohesive, conductive film; (b) adhering the conductive film to the current collector. Poly-vinylidene fluoride (PVDF) has been a widely employed as a binder for electrodes in Li-ion batteries due primarily to its electrochemical stability over a large voltage range (window voltage of the battery). PVDF is insoluble in water and slurries are prepared industrially with an organic solvent, N-methyl-pyrrolidone (NMP). Several studies show that NMP, while an excellent solvent for PVDF, is dangerous to humans and the environment ("United States Environmental Protection Agency ", 2006).

Traditional methods which use PVDF as a binder for lithium-ion batteries require a process of recovery and treatment for the organic vapors. Furthermore, the NMP solvent or another organic system is flammable which increases potential danger during

electrodes fabrication which means strict control must be introduced to ensure safety. Also, humidity is another problem for organic solvent system (water < 2 %) (Guerfi, Kaneko, Petitclerc, Mori, & Zaghib, 2007). This requires severe water control system and associated high costs. The last problem is PVDF itself: fluorine is one of the degradation products in the battery that produces a stable LiF phase. The choice of liquid electrolyte could accelerate the formation reaction of LiF and other harmful products with double bond (C=CF–) (Maleki, Deng, Kerzhner-Haller, Anani, & Howard, 2000). Furthermore, self-heating thermal runaway can be induced. Lastly, some research has indicated that PVDF has strong binding but low flexibility which limits its applicability as a mechanically flexible power source (Guerfi et al., 2007). The low flexibility of PVDF can easily deteriorate the battery's cycle life characteristics due to breaking of the mechanical bond between active materials during the expansion/contraction process which occurs during charging and discharging.

1.6.4 Batteries separator

Generally, the separator in battery is used to prevent circuit short due to contact between the anode and cathode while lithium ions can pass through the separator to achieve the electrochemical reaction. Also thermal stability and mechanical flexibility are also required to prevent some extreme conditions. The most commercially used porous polymer separators for lithium-ion batteries are made of polyethylene (PE) or polypropylene (PP). However, most polymer separators do not have thermal stability which can cause thermal deformation and lead to energy runaway or even worse accident. Additionally, polymer separators could easily be penetrated by lithium dendrite formed at high rates or long-term cycling uses (S. S. Zhang, 2007), which can cause circuit short or

possible fire eventually (Q. Wang et al., 2012). Moreover, polymer separators usually have poor wettability (Arora & Zhang, 2004; H. Lee, Yanilmaz, Toprakci, Fu, & Zhang, 2014) in organic solvent electrolytes due to their hydrophobic property. In order to overcome those problems, surface modification is introduced on the commercial polymeric separator (S. S. Zhang, 2007): (1) inorganic filled polymer composite separators (X. Huang & Hitt, 2013; F. Zhang, Ma, Cao, Li, & Zhu, 2014); (2) inorganic coating on polymer composite separators (M. Kim, Han, Yoon, & Park, 2010; J. Lee, Lee, Park, & Kim, 2014; Yang et al., 2015). Although the inorganic/organic separator can improve the safety and stability of batteries, the mixture still has low mechanical flexibility and thermal stability due to the polymer separator bulk. Other disadvantage of polymer separator is impossible to print polymers with micro porous structure. Recently, pure inorganic separators are reported to replace the polymer separator (J. Chen, Wang, Cai, & Wang, 2014; J. Chen, Wang, Ding, Jiang, & Wang, 2014; M. He, Zhang, Jiang, Wang, & Wang, 2015; Xiang, Chen, Li, & Wang, 2011). Also, inorganic materials can be adapted in to the printing technologies to make thin porous separator. In contrast, it is not easy to print porous organic separator. ZnO and ZrO_2 are used to make printable separators in this thesis.

1.7 Thesis Structure

In order to make printable batteries, conductive inks and battery inks are studied in this thesis as shown in Figure 1.32. Several metallic inks are studied like constantan ink, silver ink, copper ink and nickel inks.

(1) Constantan is an important electronic material widely used in sensors and resistors due to its unique physical properties: low temperature coefficient;

(2) Silver has high electronic conductivity which is a perfect materials for the conductive film, moreover, as an precious metals, silver shares lots common properties as gold like: high conductivity, relative low melting points which makes it easily to be sintered, chemical stability and high corrosion resistance in air;

(3) Copper is the most widely used materials in electronics due to high property price ratio;

(4) In order to meet the extreme condition inside the lithium-ion batteries (high operating voltage, chemical corrosion and conductivity requirements), nickel ink is also studied in this thesis.

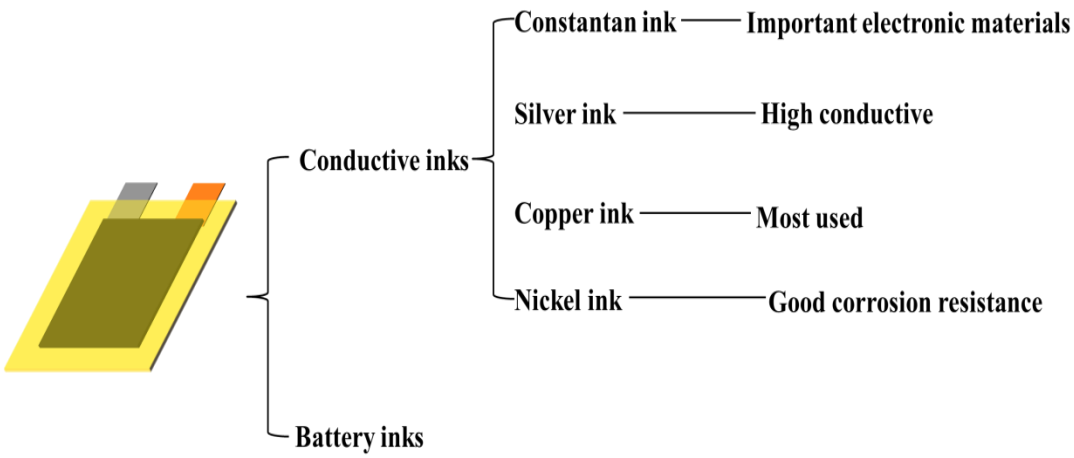

Figure 1.32 Structure of the thesis research.

The battery inks are made of battery active materials with carbon black conductive agent. Battery inks are deposited on the suitable conductive films based on the results of conductive inks research to make electrodes for the lithium-ion batteries.

CHAPTER 2

FABRICATION OF PARTICLE FREE SILVER INK

2.1 Introduction

Increasing attention has been devoted to printable circuit boards, sensors and smart ID cards by using conductive/functional ink (Fjelstad, 2008; Leung & Lam, 2008; Ng et al., 2009; Pudas, Hagberg, & Leppävuori, 2004; Sangoi et al., 2005; Xiao, Tong, Savoca, & van Oosten, 2001). The principle of printed electronics is to deposit conductive/functional ink on flexible substrate by printing technologies (inkjet or screen printing) (Frederik C Krebs, 2009; Van Osch, Perelaer, de Laat, & Schubert, 2008). The most used substrate is Kapton (polyimide) because of its stable physical and chemical properties especially at relative high temperature (Kensuke Akamatsu, Ikeda, & Nawafune, 2003; Kensuke Akamatsu, Ikeda, Nawafune, & Yanagimoto, 2004; Yi Li, Lu, Qian, Zhu, & Yin, 2004). The printed patterns are then treated with sintering processes to create bendable and continuous tracks. Various sintering processes have been studies like thermal, microwave, plasma and photonic sintering (Dong et al., 2015; Norita et al., 2015; Perelaer et al., 2006; Wunscher, Stumpf, Perelaer, & Schubert, 2014). Thermal curing is one of the easy, economical and scalable methods for industrial realization. The key step of making printable devices is ink fabrication. Right now the commercial available conductive/functional inks are metals such as copper (Y. Kim et al., 2012; B. Lee, Kim, Yang, Jeong, & Moon, 2009; Silverbrook, 2002), platinum (Kensuke Akamatsu et al., 2005), nickel (K. Akamatsu, Nakahashi, Ikeda, & Nawafune, 2003) and silver (Greer & Street, 2007; Volkman, Pei, Redinger, Yin, & Subramanian, 2004; Y. Zhang, Lei, & Kim,

2013)) organic or aqueous suspensions. Among those metallic nanoparticles, silver has high electronical conductivity, relative low melting point and excellent chemical stability at high temperature while sintered in air; those advantages make it the most widely used ink for printing conductive tracks. However, nanoparticle based ink requires a high temperature sintering temperature to join particles. Also, nanoparticle based ink is not suitable for high resolution printing due to nozzle clogging during printing. Alternative particle-free silver inks have been developed to avoid nozzle clogging and achieve high resolution printing. Generally, silver salt complex solution is used as particle free ink. After printing and curing, the organic silver complex can be transformed into highly conductive silver thin film; the thermal treating temperature is usually lower than nanoparticle based ink. Silver is produced by different chemical processes: thermal decomposition (Nie et al., 2012) or chemical reducing of silver complex (S.-P. Chen, Kao, Lin, & Liao, 2012). The former process usually occurs after evaporation of solvent, and then the silver complex degrades to silver by disproportionation reaction during sintering. In contrast, the latter one happens in the solution. Both methods can produce high quality silver conductive film.

In this chapter, silver film made by thermal decomposition and chemical reduction are compared. The effect of additive of sodium carboxymethyl cellulose in the silver ink is also investigated. Silver citrate is used as silver precursor which can be decomposed to silver above 100 ℃. Silver citrate is much safer than silver nitrate in making silver ink because it will not produce explosive silver iodide, and it has almost the same silver content (silver citrate: 63 wet. %, silver nitrate: 64 wet. %). Dimethylformamide (DMF) is used as a mild reductant to reduce silver complex in

aqueous solution by silver mirror reaction.

2.2 Experimental Section

2.2.1 Materials

All of the chemical reagents used in the experiments were purchased from commercial sources with analytical purity and used without further purification. Silver citrate, ammonia, propanol alcohol, sodium carboxymethyl cellulose (NaCMC) and dimethylformamide (DMF) were purchased from Sigma Aldrich, USA. Kapton was from Dupont Company, USA.

2.2.2 Synthesis of particle free silver ink

(a) Thermal Decomposable Silver Ink without NaCMC:

The solvent for ink was made by mixing 0.01 g deionized (DI) water and 0.01 g ammonia. 0.01 g silver citrate was added to the solvent, the mixture was bath ultrasonicated for 15 min to produce silver ammonia complex. The final viscosity was adjusted by adding propanol alcohol to meet the requirement of printer, volume ratio of water to propanol alcohol is fixed at 1:1. A clean and transparent particle free solution was formed.

(b) Thermal Decomposable Dilver Ink with NaCMC:

0.15 wet. % NaCMC solution was prepared by dissolving NaCMC in DI water at 50 ℃ and magnetic stirred for 30 min. 0.01 g of NaCMC solution, 0.01 g ammonia and 0.01 g silver citrate were mixed, the mixture was ultrasonicated for 15 min to produce silver ammonia complex. The viscosity of silver ink was adjusted by adding propanol alcohol. The final NaCMC concentration is 0.05 %. NaCMC was used as polymer capping agent and film former (Magdassi, Bassa, Vinetsky, & Kamyshny, 2003).

(c) Chemical Reductive Silver Ink with NaCMC:

The solvent for chemical reductive ink was prepared by dissolving NaCMC in ammonia, the concentration of NaCMC in ammonia is 0.15 wet. %. Then 0.01 g of NaCMC ammonia solution, 0.01 g DMF and 0.01 g silver citrate were mixed and ultrasonicated for 15 min to produce silver ammonia complex. The viscosity was adjusted by adding propanol alcohol to 10 cp. The final NaCMC concentration is 0.05 %.

2.2.3 Fabrication of conductive patterns by nanoparticle ink:

Conductive patterns were prepared from the particle-free inks by inkjet printing (DMP-2800, Fujifilm, USA) on a Kapton substrate. The substrate was washed by propanol alcohol and DI water to remove all the organic contaminants on the surface. The printed patterns were first dried in air at 100 ℃ for 30 min to evaporate liquid solvent. The dried patterns were then sintered at 225 ℃ in for 30 min on the thermal plate. The films then cooled to room temperature.

2.2.4 Characterization

X-Ray Diffraction (XRD)

XRD measurements were carried out on a Philips PW3040 X-Ray Diffractometer, 2θ ranges from 10 °to 80 ° with CuK_α radiation (λ= 15.4 nm) with a step size of 0.02 °and a time per step of 15 s.

Scanning Electron Microscope (SEM)

LEO 1530VP Field Emission SEM instrument was used to observe the surface morphology of printed patterns.

Resistivity Measurement

The resistivity of the patterns was measure by fore point probe (Jandel CYL-HM21,

USA). The thickness of the patterns is confirmed by SEM to calculate the resistivity.

Thermal Analysis

Thermogravimetric analysis (TGA) and Differential thermal analysis (DTA), STA 449 F1 Jupiter from Netzsch, Inc. USA, were used to study the thermal behavior of different inks and chemical reaction processes. Measurements were carried out in air with a temperature rise of 5 K/min.

Tape Testing

Adhesive strength is measured by tape testing. A scotch tape was sticked on the surface of the silver patterns and peeled off up to five times.

2.3 Results and Discussion

2.3.1 Effect of NaCMC surfactant

The effect of NaCMC surfactant on silver film fabrication is studied. CMC was found to be a very effective water soluble polymer stabilizer against aggregation. The main principle is negative charged carboxyl radicals (-COO-) in NaCMC solution bind on the positive charged metallic particles, the attached polymer layer can provide a strong electrostatic or steric repulsions to cancel the attractive van der Waals to prevent agglomeration.

Figure 2.1 shows the SEM images of silver film made by thermal decomposition without NaCMC and thermal decomposition with NaCMC at different magnifications. The particle size is not uniform without NaCMC additive from Figure 2.1 (a)-(b). Also the large particles are not sintered very well. The silver film becomes more uniform after adding NaCMC from Figure 2.1 (c)-(d). This can be explained by Ostwald ripening

process which occurs in drying process without NaCMC additive. Small silver citrate crystals dissolve, and redeposit onto larger silver crystals. In contrast, NaCMC can adsorb on silver citrate crystals and prevent Ostwald ripening, which can produce smaller crystals. The Ostwald ripening process is bad for film formation because it leads to an inhomogeneous structure and large silver citrate particles are hard to be sintered. However, the silver film still exhibits significant porosity after sintering even with the help of NaCMC. This is caused by the volume shrinkage of silver citrate after thermal decomposition. Generally, production of silver from silver citrate thermal decomposition has two steps: (a) deposition of silver citrate on the substrate; (b) disproportionation reaction of silver citrate to produce silver film. The volume of each silver particle from silver citrate disproportionation reaction can be calculated: the silver content is about 63 wt. % based on the calculation from the silver citrate chemical formula ($C_6H_5Ag_3O_7$), and the density of the silver is three times greater than silver citrate salt, so the volume of a single silver particle is only 20 % of the original silver citrate particle from the thermal decomposition. Even though the thermal decomposition can produce nano particles which require low sintering temperature, we still cannot get a dense structure due to the volume shrinkage of silver and mass of porosity during the disproportionation reaction; the space porosity structure makes the relative lower conductivity of final products.

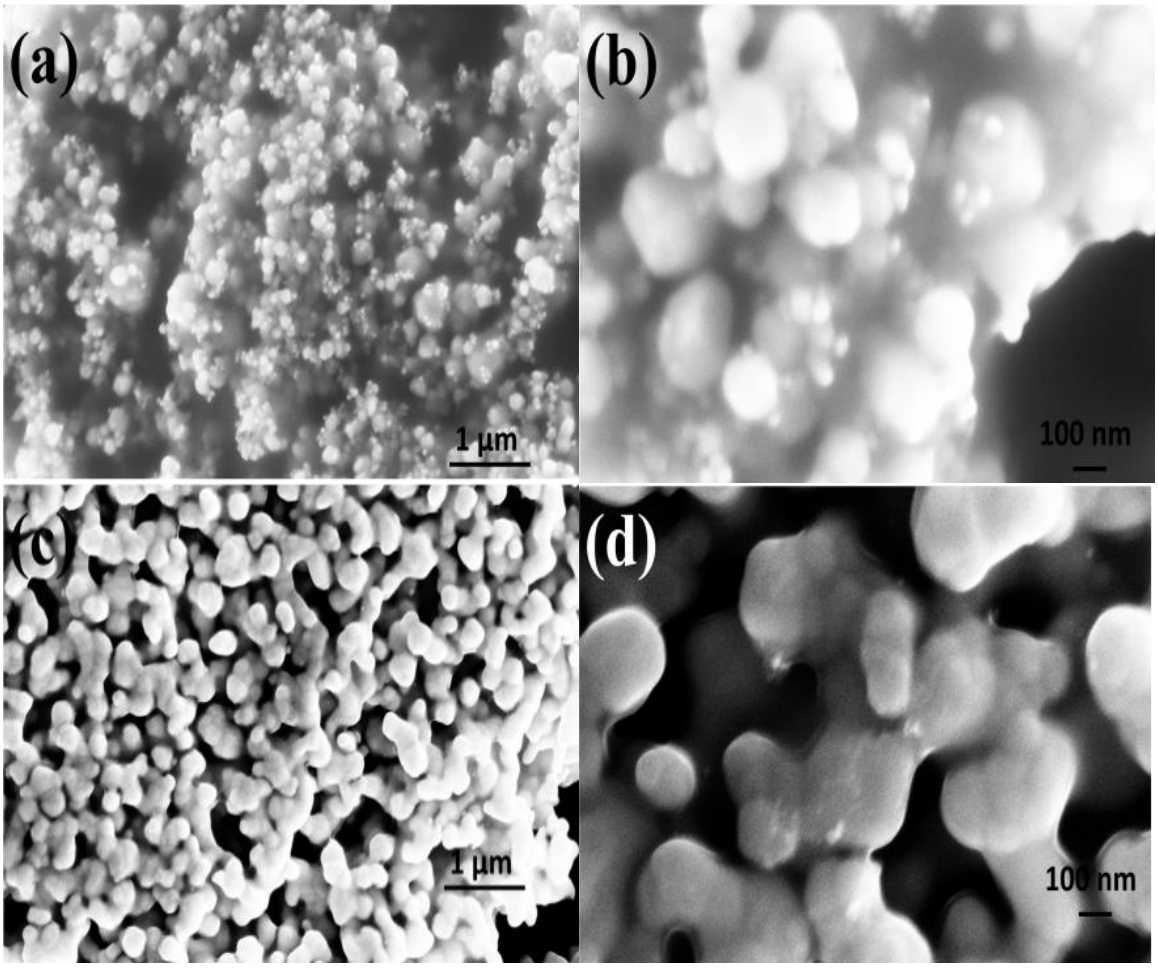

Figure 2.1 SEM images of silver made by: (a) and (b) thermal decomposition without NaCMC; (c) and (d) thermal decomposition with NaCMC.

Figure 2.2 shows the XRD patterns of silver after thermal sintering: silver films made by thermal decomposition of silver citrate without/without NaCMC additive are marked by #1, and #2, respectively. All of them show at 2θ of 38.1 º, 44.3 º, 64.4 º, 77.5 º, and 81.5 º index as (111), (200), (220), (311) and (222) (JCPDS file No. 04-0783) reflections of the Fm-3m space group without any significant impurities. This means slight NaCMC additive has no effect on the space structure of final silver. However, the intensity if XRD peaks drops significantly after adding NaCMC from #1 and #2 patterns. The particle size and the width of XRD peaks have a reciprocal relationship according to

Scherrer's Equation which means that larger particles give sharper signals (Patterson, 1939). This confirms the Ostwald ripening process with no NaCMC additive as mentioned above: NaCMC can reduce and unify particles size effectively.

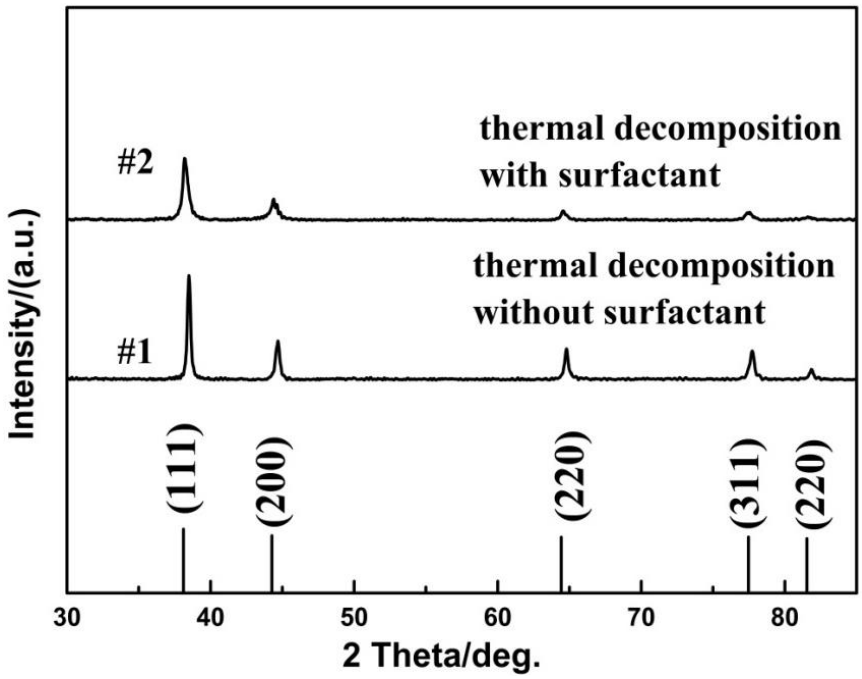

Figure 2.2 XRD patterns of silver made by thermal decomposition without/with NaCMC.

2.3.2 Effect of DMF reductant

Figure 2.3 (c) and (d) show the SEM morphologies of silver particles reduced by DMF. Silver particles synthesized by thermal decomposition are also displayed in Figure 2.3 (a) and (b) in order to compare. Volume shrinkage leads to the porous and discontinuous structure as discussed in Figure 2.4 (a). The most of inter porous structure disappears the conductivity of printed silver patterns. However, silver films made by chemical reduction are significantly denser with much smaller particle size than those made by thermal decomposition. The original particle size is below 50 nm which is half of the particle size

made from thermal decomposition. This suggests silver particles are formed in the solution as shown in Figure 2.4 (b). The chemical reduction has two steps: (a) silver reduction in the DMF solution during low temperature drying process; (b) deposition of silver instead of silver citrate on the substrate which can make denser and more continuous structure after solvent evaporation. Smaller size particles benefit from thermal sintering due to the temperature depression at nano size. Moreover, smaller particles can give a denser structure which can increase the conductivity of silver patterns.

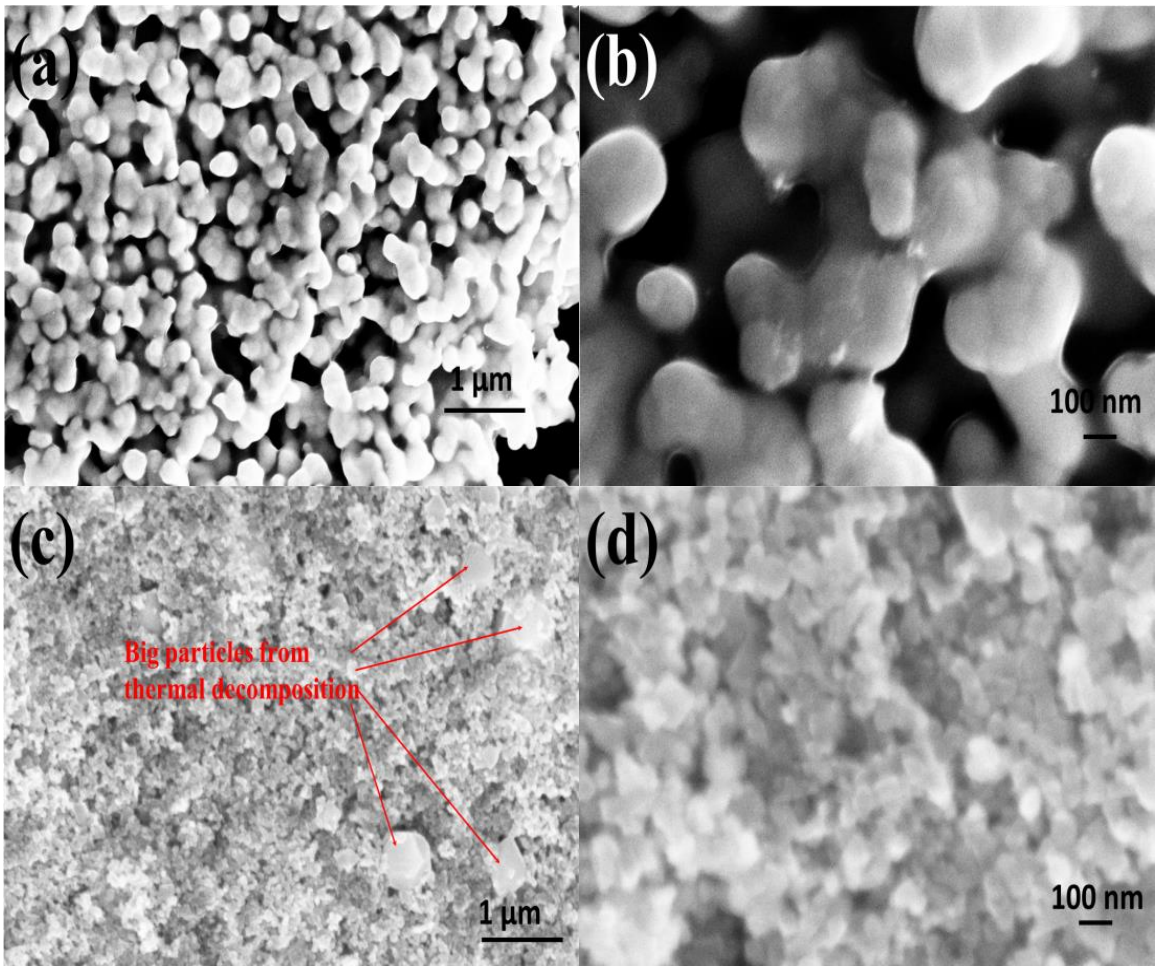

Figure 2.3 (a) and (b) Thermal decomposition with NaCMC; (c) and (d) Chemical reduced by DMF with NaCMC.

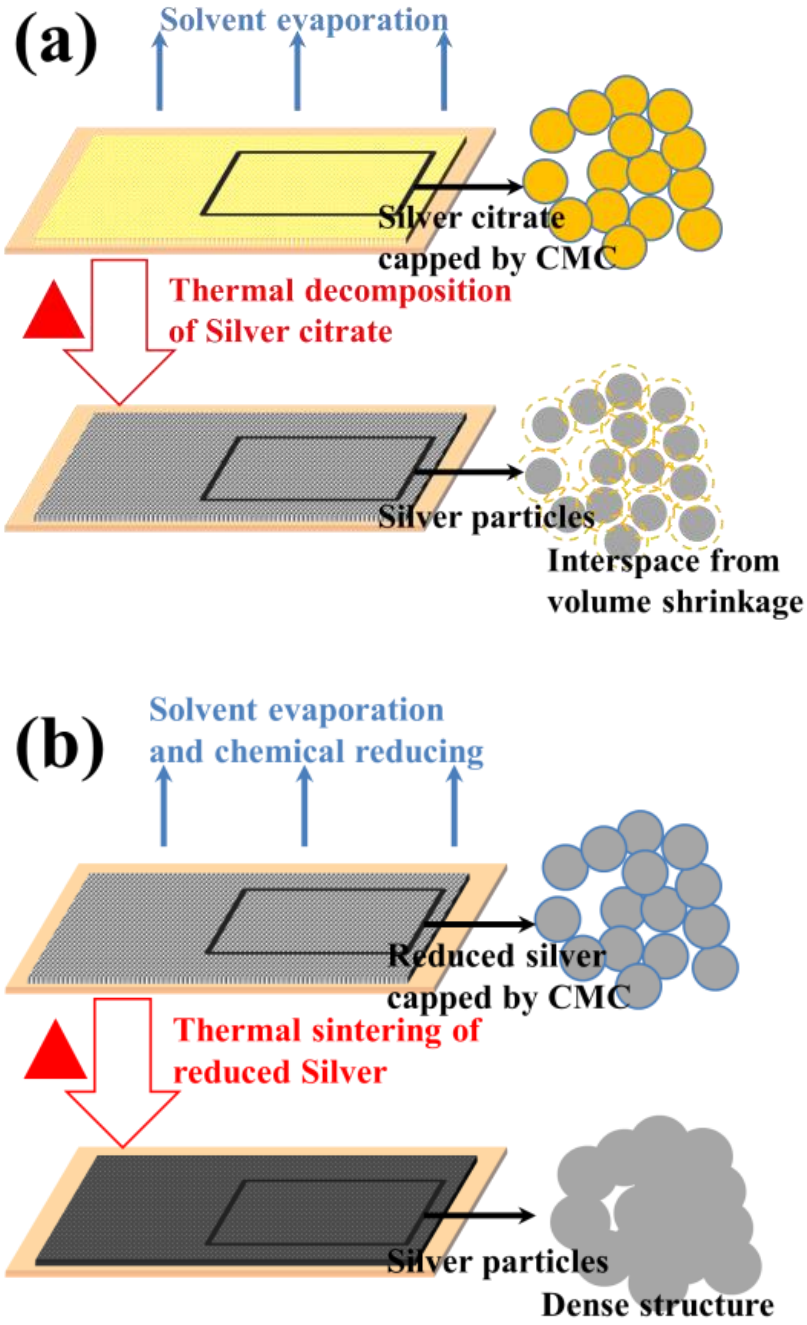

Figure 2.4 Scheme of silver films made by (a) thermal decomposition; (b) chemical reduction.

Figure 2.5 shows the XRD patterns of silver synthesized by thermal decomposition and DMF reduction. Both methods can produce pure silver without any

impurities. Figure 2.5 (b) presents the detail of XRD from 2θ=35 ºto 55 º, silver signals made by DMF reduction shift to higher degree than thermal decomposition as displayed in Figure 2.5 (b). The high angle shift indicates smaller crystal size which is confirmed by SEM results. Smaller crystals benefit thermal sintering and higher conductivity in the final printed patterns.

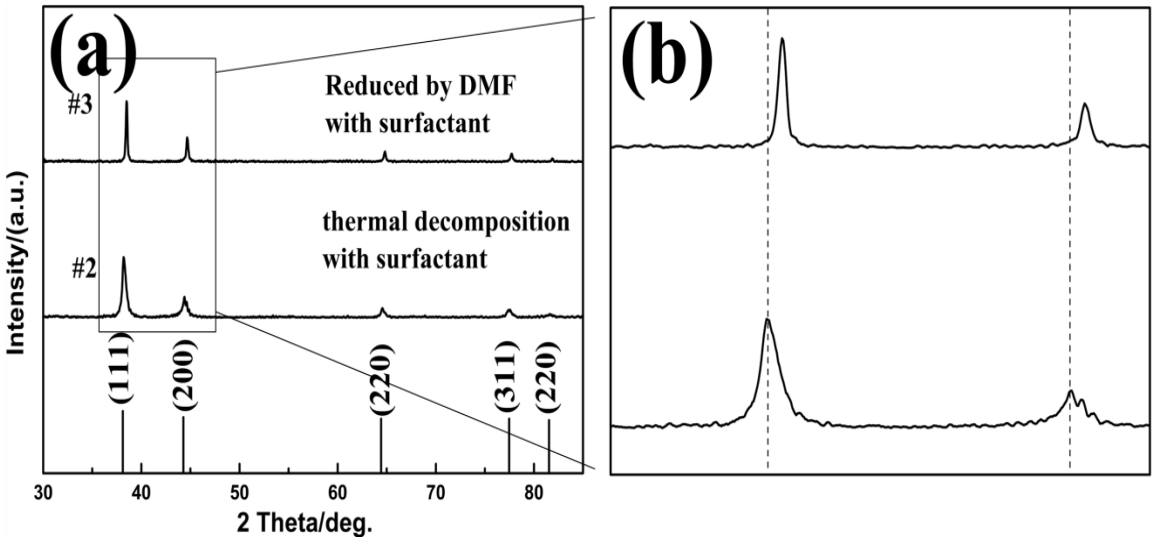

Figure 2.5 XRD patterns of silver made by: (a) thermal decomposition with NaCMC; (b) chemical reduced by DMF with NaCMC.

Thermogravimetric analysis (TGA) and Differential thermal analysis (DTA) are carried out to study the thermal decomposition and chemical reduction processes. Figure 2.6 (a) indicates that thermal decomposition temperature of silver citrate powder is at approximately 220 ℃ with heat releasing. DTA of silver citrate shows the mass loss is around 35 % which corresponds to elements loss in citrate $(C_6H_5O_7)_3$. DTA and TGA results are similar to a previous report (Nie et al., 2012). DTA in Figure 2.5 (b) shows that the chemical reduction of silver ions occurs at 95 ℃ which is even lower than the

evaporation temperature of water solvent, which means DMF can reduce silver ions very effectively. TGA in Figure 2.6 (b) displays two mass loss steps: the first mass loss is from 30-95 ℃ corresponding the formation of silver particles in water solvent; the second mass loss step between 95-160 ℃ attributes the evaporation of water solvent.

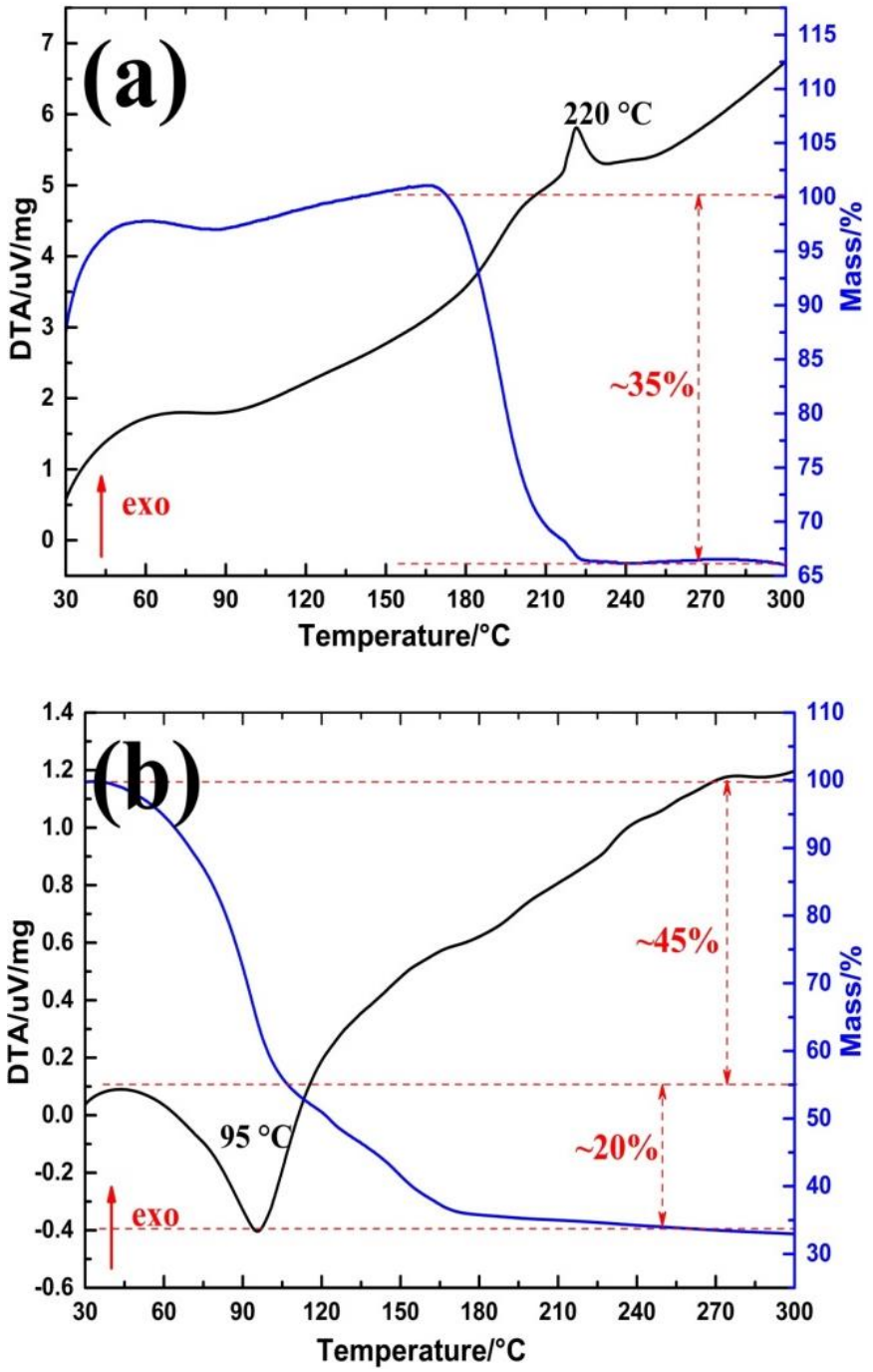

Figure 2.6 Thermogravimetric analysis (TGA) and Differential thermal analysis (DTA) of (a) silver citrate powder; (b) silver citrate conductive ink reduced by DMF with NaCMC. All samples are tested in air with temperature rise rate: 5K/min. In this figure, "exo" denotes an exothermic reaction.

The mass loss in two steps is not exactly equal to the water and citrate content

which might be associated with the dissolve of ammonia (formed from Equation (2.1)) and thermal decomposition of carbamic acid in Equation (2.2) (Pastoriza-Santos & Liz-Marzán, 2000). The silver remaining is around ~25 % which is close to the theoretical silver content 20 %.

$$HCONMe_2 + 2Ag(NH_3)_2^+ + H_2O = 2Ag \downarrow + Me_2NCOOH + 2H^+ + 2NH_3 \quad (2.1)$$

$$Me_2NCOOH \rightarrow CO_2 + Me_2NH \quad (2.2)$$

2.3.3 Compare with other researches

Previous reported data of silver patterns made by various silver inksare listed in Table 1 for comparison. The sintering temperature ranges from 75-300 ℃ (only one is sintered at 961 ℃) with sintering time 5-60 min. Silver particle-free ink requires lower sintering temperature compare with silver nanoparticle ink, and there is no concern for nozzle clogging during the printing. Silver particle free ink can also skip silver nano particles synthesis process which usually requires a strict chemical process. Silver citrate is an excellent precursor to make silver particle-free ink due to its high silver content compare with other precursors (Silver neodecanoate ($Ag(C_{10}H_{19}O_2)$): 39 wt. % silver; $AgO_2C(CH_2OCH_2)_3H$: 38 wt. % silver), the lower silver content gives the more porous final products (as shown in Figure 2.7 (a)) with poorer conductivity. The NaCMC additive also contributes to unify and reduce the particle size: NaCMC adsorption on silver particle controls the final shape and prevents aggregation (compare Figure 2.3 (b) and (d)); NaCMC is also a good film former contributes to the adhesion of silver patterns on polymer substrate. Chemical reducing is more efficiency to make dense silver patterns with high conductivity compared with thermal decomposition displayed in Figure 2.7 (c). The volume shrinkage and porous structure cannot be avoided due to the density

difference between silver precursor and silver. The silver patterns fabricated from this recipe have the lowest electrical resistivity although some researchers have more competitive sintering conditions (lower sintering temperature and shorter sintering time). The resistivity of silver made by chemical reducing process is almost half compared to the silver made by thermal decomposition, which is caused by less porosity.

Table 2.1 Resistivity of Silver Films Fabricated by Different Silver Inks

Silver source	Status	Sintering temperature (℃)	Sintering time (min)	Resistivity (μΩ·cm)	Source
Bulk silver	5-7 nm particles	300	10	3	Fuller et al. (Fuller, Wilhelm, & Jacobson, 2002)
Bulk silver	(1-10 nm) particles	300	15	35	Szczech et al. (Szczech, Megaridis, Gamota, & Zhang, 2002)
Bulk silver (10-50 nm)	(10-50 nm) particles	150-260	3	16	Hsien Hsueh Leeet al. (Hsien-Hsueh et al., 2005)
silver	Bulk	961	-	1.61	- (Dong et al., 2015)
Silver oxalate	Particle-free	150	30	8.6	Yue Dong et al. (Dong et al., 2015)
Silver nitrate	Particle-free	250	10	7.41	Jung Tang Wu et al. (J.-T. Wu, Hsu, Tsai, & Hwang, 2009)
Silver neodecanoate	Particle-free	150	5	9	Angela L. Dearden et al. (Dearden et al., 2005)
$AgO_2C(CH_2OCH_2)_3H$	Particle-free	130	30	9.1	Stephan F. Jahn et al. (Jahn et al., 2010)
Silver nitrate	Particle-free	100	60	13.7	Jung Tang Wu et al. (J.-T. Wu, Hsu, Tsai, & Hwang, 2011)
Silver citrate	Particle-free	150	50	17	Xiaolei Nie et al. (Nie et al., 2012)
Silver nitrate	Particle-free	200	30	8.5	Dongjo Kim et al. (D. Kim, Jeong, Lee, Park, & Moon, 2007)
Silver oxide	Particle-free	75	20	6.1	Shih Pin Chen et al. (S.-P. Chen et al., 2012)
This work (thermal decomposition)	Particle-free	225	30	5.7	
This work (reduced by DMF)	Particle-free	225	30	3.1	

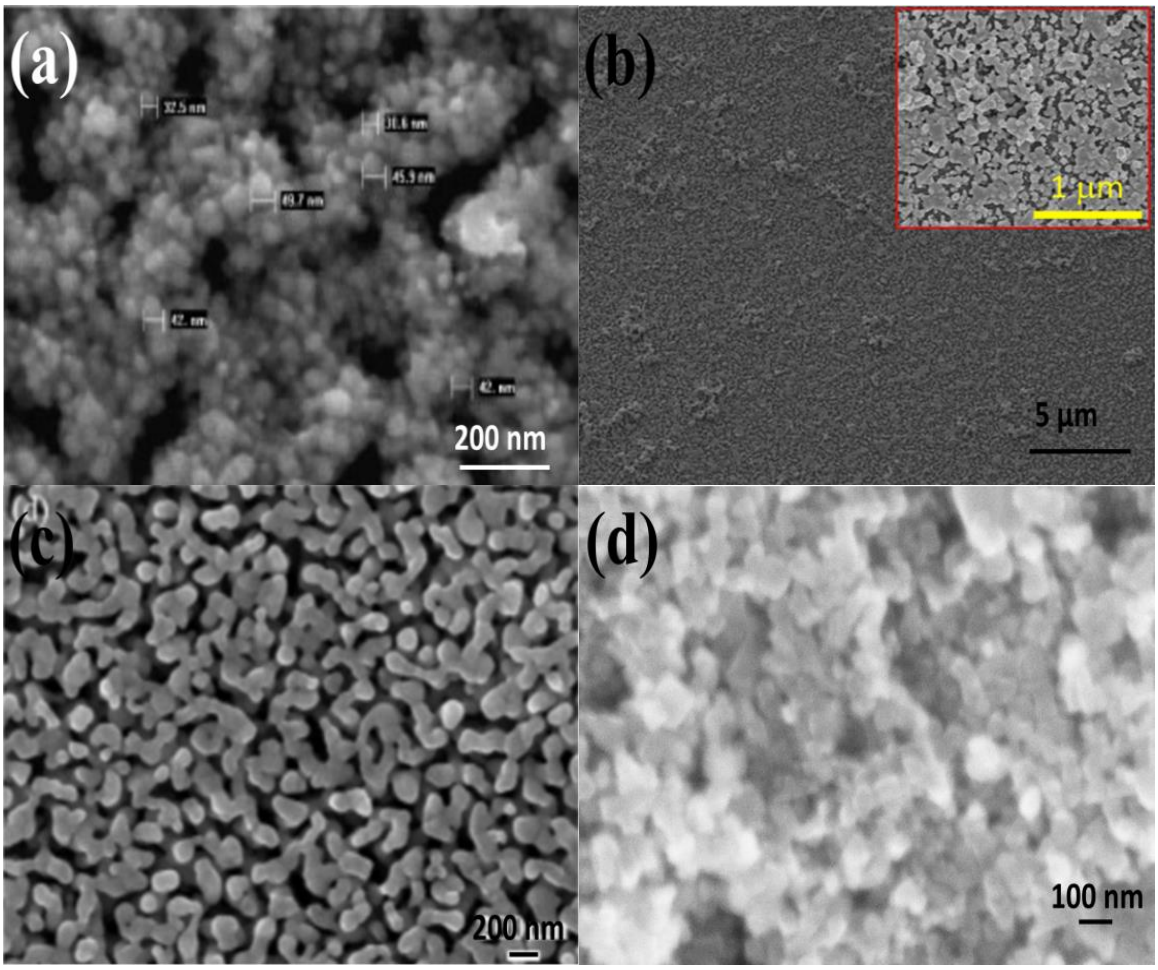

Figure 2.7 Surface morphology of (a) reference; (b) reference; (c) reference; (d) silver patterns synthesized in this work.

Source: (a) (Dearden et al., 2005); (b) (S.-P. Chen et al., 2012); (c) (Dong et al., 2015).

2.3.4 Application of silver ink

Figure 2.8 (a) shows the photograph of synthesized chemical reductive particle-free silver ink kept for 3 days at room temperature. The ink remains colorless and transparent without any precipitation suggests good stability. “NJIT” metallic shiny patterns are made by inkjet printing on flexible Kapton substrate as shown in Figure 2.8 (b). The mean width of patterns is 1 mm. No peeling off or cracking occurs while bending the patterns, which indicates a good flexibility of the printed patterns for circuits and sensors.

A tape test is performed to inspect the adhesion of synthesized silver patterns on Kapton substrate in Figure 2.8 (c) and (d). The printed patterns stay completely and smoothly after removal the tape suggests very strong adhesion between the patterns and Kapton substrate. Figure 2.8 (e) illustrates that the resolution of patterns made by silver ink is 40 μm. A small circuit board is also printed and shown in Figure 2.8 (f), the printed circuit board exhibits fine appearance and can be used in microelectronics, sensors and smart cards.

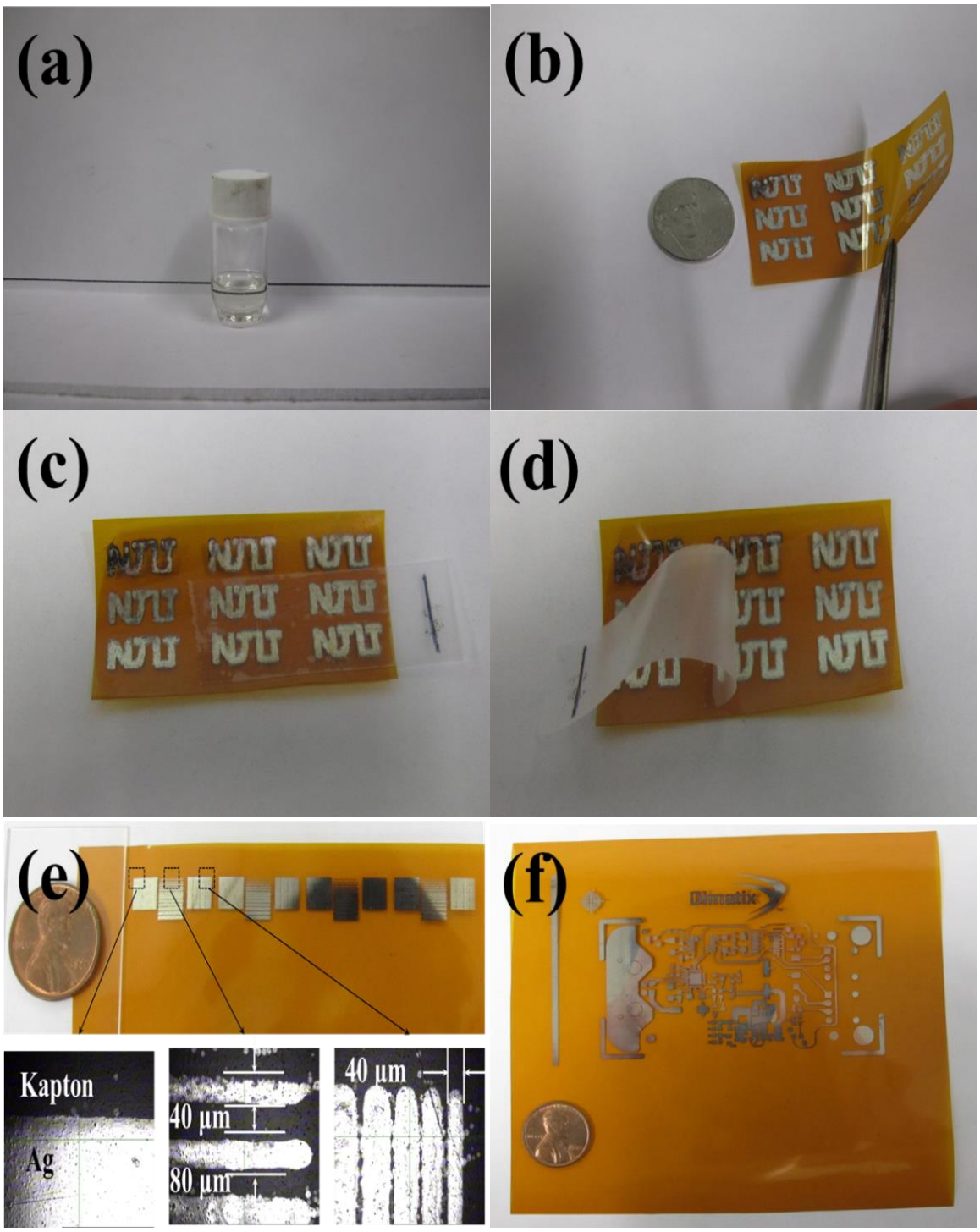

Figure 2.8 Images for (a) particle-free silver ink (chemical reduction with NaCMC) kept at room temperature for 3 days; (b) NJIT patterned silver thin flexible film made by inkjet printing; (c)-(d) tape test for printed silver thin film; (e) resolution of patterns; (f) circuit board made by silver ink.

2.4 Summary and Conclusion

In summary, colorless particle-free silver ink for printing is synthesized and compared by two major processes: thermal decomposition of silver salts and chemical reduction of silver complex. Both of them can produce pure silver without impurity. Examination of SEM images of silver films made by chemical reduction exhibit denser and more continuous structures than those made by thermal decomposition. The porous structure is caused by the volume shrinkage during silver precursor disproportionation reaction. Also, chemical reduction can make silver films at relative lower temperature compared to the thermal decomposition of silver citrate. The synthesized silver film has excellent electronic conductivity and adhesion compared to other reported research. Our research also indicates that NaCMC plays crucial role in the final particle size and uniformity. No peeling off and cracking of the printed silver patterns occurred when the film is bended with a large radius. This suggests that the ink made by chemical reduction is an attractive possibility for the flexible electronics fabrication in future.

CHAPTER 3

FABRICATION OF CONSTANTAN INK

3.1 Introduction

Interest in printed circuits, sensors, electronics and radio frequency identification tags which are fabricated via liquid based "ink" have grown considerably in recent years (Calvert, 2001; Crone et al., 2001; Daniel & Astruc, 2004; Herrmann et al., 2007; Jang et al., 2010; Yuning Li, Wu, & Ong, 2005; Shipway et al., 2000; Subramanian et al., 2005; A. Wu, Gu, Beck, Iqbal, & Federici, 2014; Y. Wu, Li, & Ong, 2006, 2007). Generally, the functional ink is made of metallic nanoparticles (NPs) dispersed in organic/inorganic solvents. By using the functional fluid, inkjet printing technology is a promising method to deposit metallic nanoparticles on polymer substrate with designed patterns. Then the printed patterns could be annealed via thermal, microwave, plasma and photonic sintering (Dong et al., 2015; Norita et al., 2015; Perelaer et al., 2006; Wunscher et al., 2014) methods to fabricate crack-free films. The patterns must be annealed at low temperature in order to protect flexible polymer substrates. The most widely used inks are made of silver and gold noble NPs due to the low melting temperature and chemical stability in air.

Constantan ($Cu_{55}Ni_{45}$) nickel-copper alloy is known for its excellent thermoelectrical properties. To be specific, constantan is used for precision resistors, thermocouples and strain gauges with low temperature coefficient of resistivity (TCR). However, this material suffers surface oxidation (Brückner, Baunack, Reiss, Leitner, & Knuth, 1995) which has been a serious impediment to the development and application of constantan in inkjet printing technology. Also, its high melting temperature of constantan

(1221~1300 ℃) makes it hard to sinter especially at low temperatures. Moreover, the high melting temperature oxidation layers further complicate the sintering of constantan. The sintering process of constantan usually requires a reducing atmosphere which is flammable gas, for instance hydrogen and methane. Reducing gas with high temperature dangerous and expensive to achieve and maintain in industry. We report here a novel and safe chemical process to anneal the inkjet printed constantan patterns at low temperature without using a flammable reducing gas.

3.2 Experimental Section

3.2.1 Materials

The constantan powder used in the ink formulation is commercially available with particle size around 100 nm purchased from American Elements, USA. The ammonia chloride (NH_4Cl), glycerol, Polyvinylpyrrolidone (PVP), potassium hydroxide and thiourea dioxide are all obtained from Sigma-Aldrich, USA. All chemicals are analytical grade and used as received without further purification.

3.2.2 Characterization

X-Ray Diffraction (XRD)

XRD measurements were carried out on a Philips PW3040 X-Ray Diffractometer, 2θ ranges from 10 °to 80 ° with CuK_α radiation (λ= 15.4 nm) with a step size of 0.02 °and a time per step of 15 s.

Scanning Electron Microscope (SEM)

LEO 1530VP Field Emission SEM instrument was used to observe the surface morphology of raw materials and printed patterns.

Resistivity Measurement

The resistivity of the patterns was measure by fore point probe (Jandel CYL-HM21, USA). The thickness of the patterns is confirmed by SEM to calculate the resistivity.

Thermal Analysis

Thermogravimetric analysis (TGA) and Differential thermal analysis (DTA), STA 449 F1 Jupiter from Netzsch, Inc. USA, were used to study the the thermal behavior of different inks and chemical reaction processes. Measurement was carried out in air with temperature rise 5 K/min.

Laser Particle Size Analyzer

The particle size was measured by Beckman Coulter N4 Plus laser particle size analyzer, Beckman, USA. Water was used as media and ultra-sonication was carried during measurement.

3.2.3 Ink formulation

The constantan ink is made by water, glycerol, PVP and constantan nano powder. Water is the solvent which is cheap and safe; PVP is used as binder and surfactant; glycerol is used to adjust the final viscosity. Different constantan, PVP and water weight ratio are studied (Table 1) labeled as 1, 2, 3, 4, 5, 6 and 7. All the inks are ultra-sonicated for 30 min to disperse constantan into the water.

Table 3.1 Ink Formulation

label	Constantan (wt. %)	Water (wt. %)	PVP (wt. %)
1	10 %	85 %	5 %
2	15 %	80 %	5 %
3	20 %	75 %	5 %
4	25 %	70 %	5 %
5	30 %	65 %	5 %
6	35 %	60 %	5 %
7	40 %	55 %	5 %

Figure 3.1 (a)-(g) show the particle size after ultra-sonication. Particle size increases with increasing solid fraction. The suitable particle size for DMP-2800 inkjet printer is below 450 nm. So ink 6 is chosen to be the final formulation.

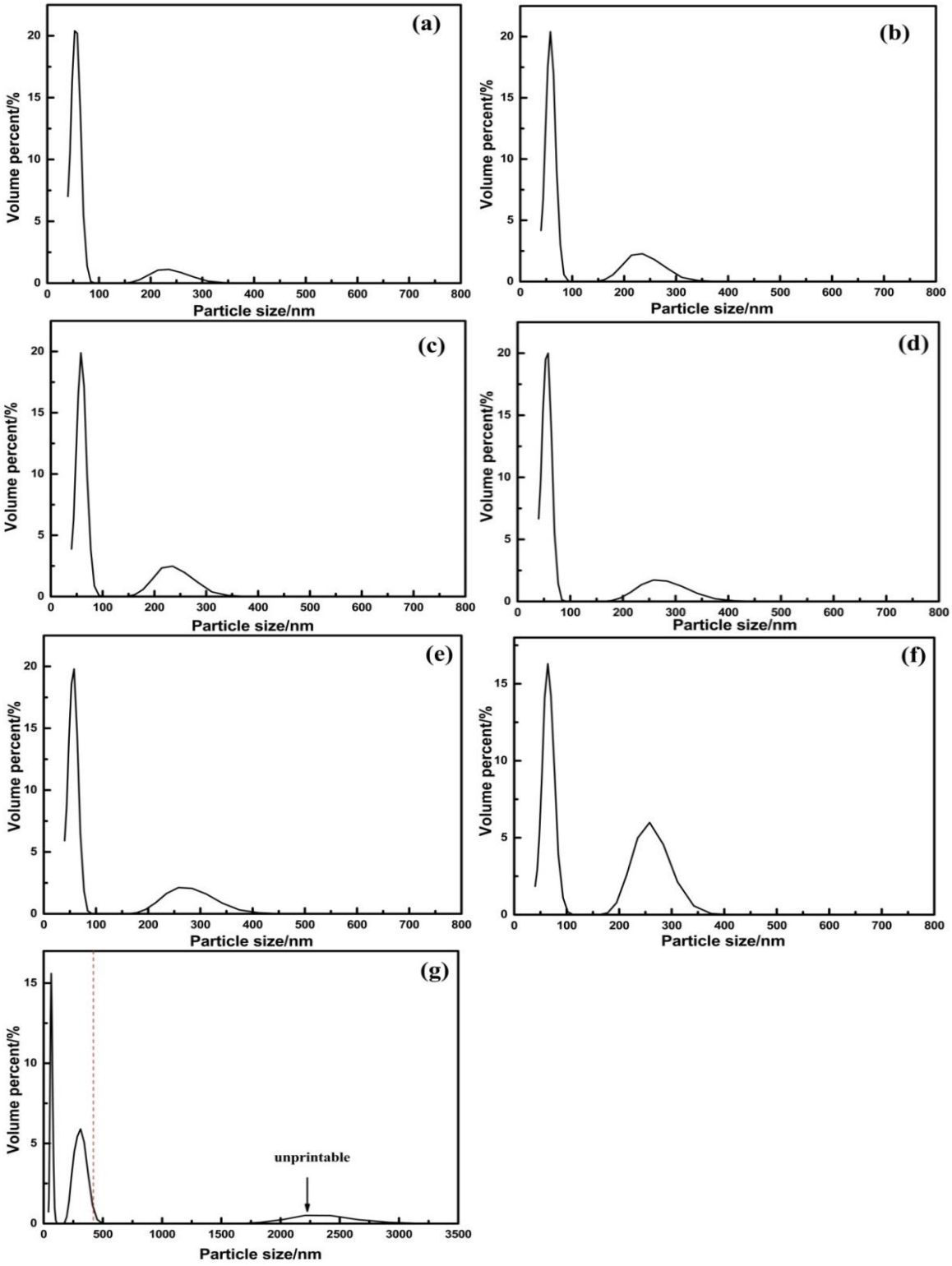

Figure 3.1 (a)-(g) Particle size of ink # 1-7.

Viscosity of those inks is checked by viscometer as shown in Figure 3.2. Viscosity

increases with increasing solid fraction, but none of them meets the requirement of DMP-2800 inkjet printer (12-14 cp). So glycerol is added to the ink to make it printable (only 6th ink is studied). Final ink formulation is:

Constantan suspension: water: glycerol: constantan: PVP=12: 5: 7: 1 by weight.

3.2.4 Preparation of constantan conductive films

Patterns are printed by a DMP-2800 inkjet printer (Fujifilm, Japan) on Kapton film at room temperature. The printed patterns are first dried at 180 ℃ in vacuum and then sintered in vacuum furnace at 350 ℃ in vacuum.

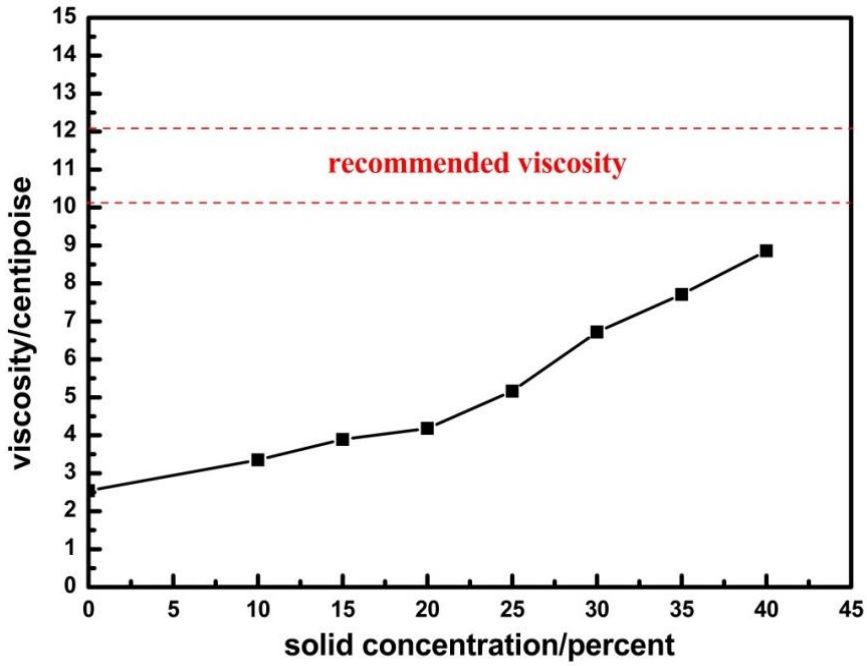

Figure 3.2 Viscosity of ink with different solid fraction.

Figure 3.3 shows XRD pattern of the final printed samples sintered in vacuum. Cu_2O and more CuO are found in sample. Considering samples are dried and sintered in vacuum environment, the impurities are introduced in ink fabrication and even printing process.

The resistivity of sample is tested and it is found to be infinite, which indicates oxidation invalidated the constantan sample.

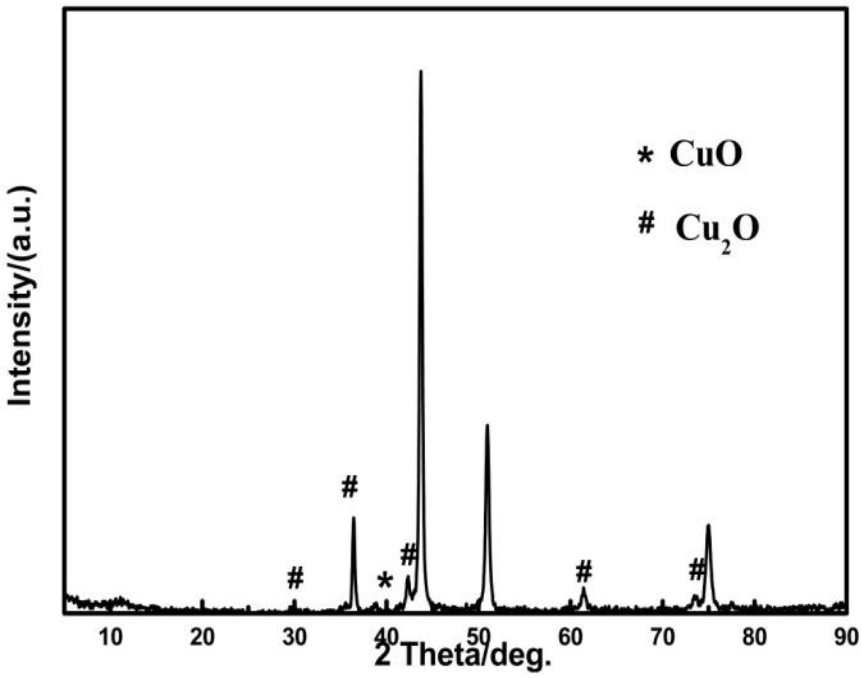

Figure 3.3 XRD patterns of constantan patterns after sintering in vacuum.

The above results indicate regular constantan ink cannot be sintered due to the oxidation layers which are introduced during ink preparation and the inkjet printing process. The popular method used to sinter metallic inks which have oxidation layers is forming gas sintering (Qin, Watanabe, Tsukamoto, & Yonezawa, 2014). However, forming gas is quite dangerous especially for massive production. A novel chemical method is introduced to make conductive constantan ink on plastic substrate which can be sintered in vacuum without using forming gas.

3.2.5 Preparation of functional ink

Figure 3.1 (a) shows the scheme of fabrication process. 4 g Constantan NPs and 0.3 g

PVP are dispersed in 4 g water by ultra-sonication for 30 min as shown in Figure 3.4 (a). Large particles are separated by centrifuge 5000 RPM for 5 min. NH_4Cl is added into the suspension to etch away surface oxidation (CuO and NiO), the suspension is magnetically stirred for 12 h to dissolve the oxidation completely; a copper/nickel ammonia complex is formed in the meanwhile in Figure 3.4 (b). Thiourea dioxide (TD) and KOH solution (1 mol/L) is added into that suspension as the reductant in Figure 3.4 (c). Viscosity is adjusted to 10 cp using glycerol as the thickener. The suspension then is magnetically stirred for 30 min to make uniform ink. As a control comparison, a separate batch of ink is formulated: constantan NPs and PVP are dispersed in glycerol/water solvent by ultra-sonication for 30 min, which contains: 40 wt. % constantan powders, 40 wt. % water, 20 wt. % glycerol and 3 wt. % PVP binder.

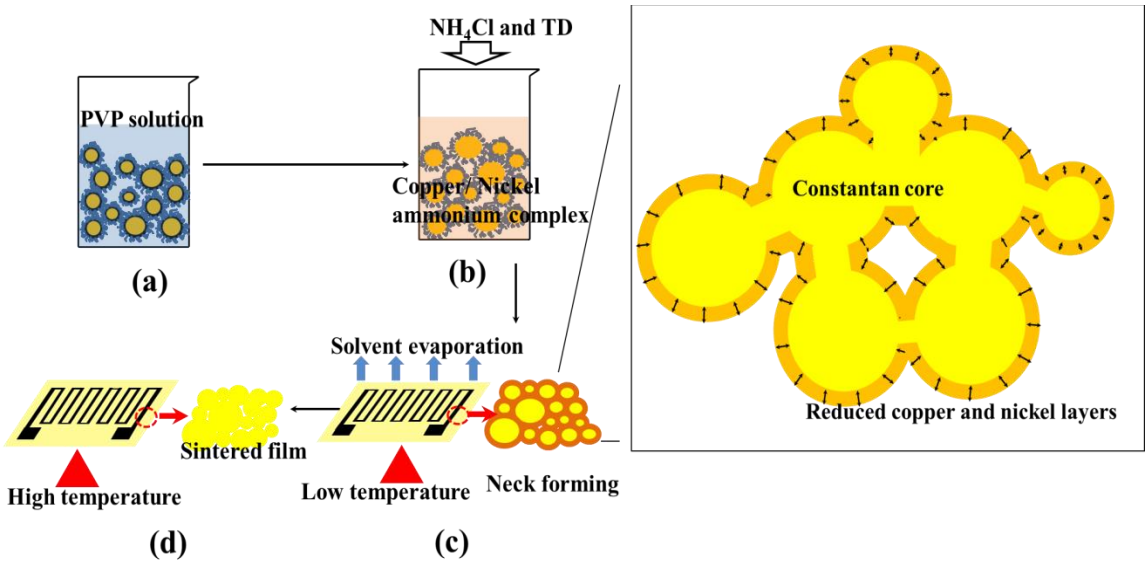

Figure 3.4 Schematics of sensor fabrication: (a) Constantan suspension in PVP-water solution; (b) Eating away surface oxidation by NH_4Cl; (c) Evaporation of solvents and thickener at low temperature in vacuum, at this time thiourea dioxide can reduce metal ions into nano-sized pure metal layers on constantan surface; (d) Solid diffusion among reduced nano-sized copper and nickel which causes activated sintering among constantan particles.

3.2.6 Preparation of constantan conductive films

Patterns are printed by a DMP-2800 inkjet printer (Fujifilm, Japan) on Kapton film at room temperature. The printed patterns are first dried at 180 ℃ in vacuum as shown in Figure 3.4 (c) to evaporate water and thickener. Thiourea dioxide can reduce most Cu^{2+} and Ni^{2+} with presence of OH^- around 80 ℃ according to a previous report (Haoyang Wang, Li, & Gao, 2014). Constantan particles are then surrounded by the reduced copper and nickel due to the wettability. Samples are then sintered at 350 ℃ in vacuum. The reduced copper and nickel have high surface energy and tend to merge to each other to form "necks". With the growth of necks, the solid diffusion among constantan particles is activated by the reduced copper and nickel (C.-J. Wu, Cheng, Sheng, & Tsao, 2015). Finally, annealed constantan film is obtained in Figure 3.4 (d) named sample with chemical reduction sintering (CRS) process. Also, the control ink without TD and KOH (i.e. without the chemical reduction sintering (CRS) process) is sintered under the same conditions as the sample containing TD/KOH.

3.3 Results and Discussion

3.3.1 CRS process research

The measured pH value change of the ink during fabrication is shown in Figure 3.4. The pH value of constantan/water/PVP dispersed is around 7.60 in process 1. In process 2, there is no significant pH change after adding ammonia chloride (NH_4Cl) into the constantan suspension. This confirms the formation of copper/nickel ammonia complex, because NH_4Cl solution is acidic if no copper/nickel ammonia complex is formed. The pH value drops down a little after adding TD into the suspension in process 3. The

interesting thing is the pH value remains the same after adding KOH into the suspension which suggests chemical reaction between TD and KOH at room temperature is:

$$(NH_2)_2CSO_2 + 2KOH = (NH_2)_2CO + K_2SO_2 + H_2O \quad (3.1)$$

Adding KOH has no effect on pH value according to Equation (3.1). The high chemical active SO_2^{2-} released from Equation (3.1) (marked red in Figure 3.5) can reduce copper/nickel ammonia complex at high temperature in basic environment as in Equation (3.2):

$$2K_2SO_2 + [Cu(NH_3)_4]^{2+} + [Ni(NH_3)_6]^{2+} + 4OH^- = Cu\downarrow + Ni\downarrow + 2H_2O + 2K_2SO_3 + 10NH_3 \quad (3.2)$$

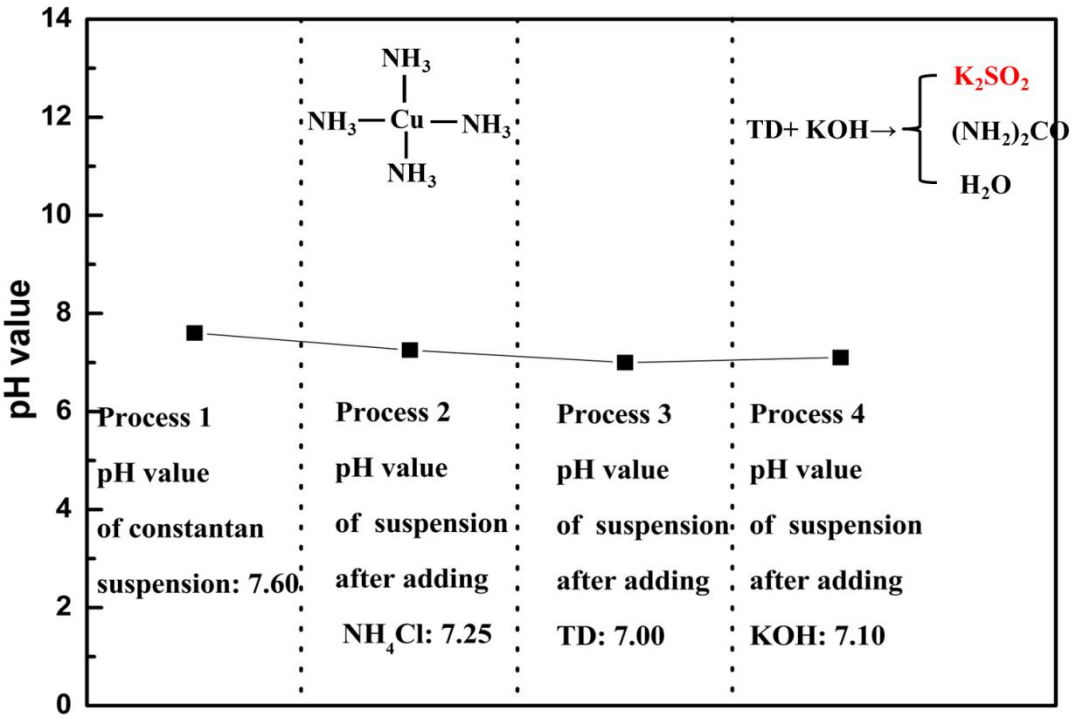

Figure 3.5 pH value changes during the ink fabrication.

Thermogravimetric analysis (TGA) and Differential thermal analysis (DTA) are carried out to study the sintering process of two constantan inks. All samples are tested in

inert atmosphere; “exo” is an abbreviation for exothermic reaction. TGA in Figure 3.6 (a) has three main mass losses: (a) before 150 ℃: is due to the evaporation of water which is around 40 wt. %, this process is corresponding to endothermic peak (1) in DTA curve; (b) between 150 and 250 ℃: is the evaporation of glycerol which is 20 wt. % and corresponding to endothermic peak (2) in DTA; (c) between 300 ℃ and 450 ℃: is the thermal decomposition of PVP binder, however, there is no obvious signal detected from DTA, this might be caused by the small quality of binder. A weak endothermic peak is detected in DTA around 600 ℃ without any mass loss in TGA curve; this weak endothermic peak might be the sintering process of constantan powder. 600 ℃ is above the melting temperature of most polymers. In contrast, a DTA peak shoulder in area (1) in Figure 3.6 (b) indicates a possible chemical reaction happens below 110 ℃. TD in basic environment has high reducing ability which can reduce Ni^{2+} in aqueous which has been reported (H. Wang et al., 2014). In this case, TD can also reduce Ni^{2+} and Cu^{2+} which are produced from NH_4Cl etching. Also, the slope changes around 110 ℃ in TGA curve (marked with black dash line) suggests a light mass change, this is caused by the H_2O and NH_3 produced from copper and nickel reduction as shown in Equation (3.2). Endothermic peaks (2) and (3) in Figure 3.6 (b) are representing water and glycerol evaporation as discussed above. A wide Endothermic peak (4) is detected between 350~400 ℃. This might be caused by solid diffusion between copper, nickel and constantan particles. DSC and TGA results suggest chemical reduction can lower the sintering temperature effectively and sinter constantan without damaging the polymer substrate.

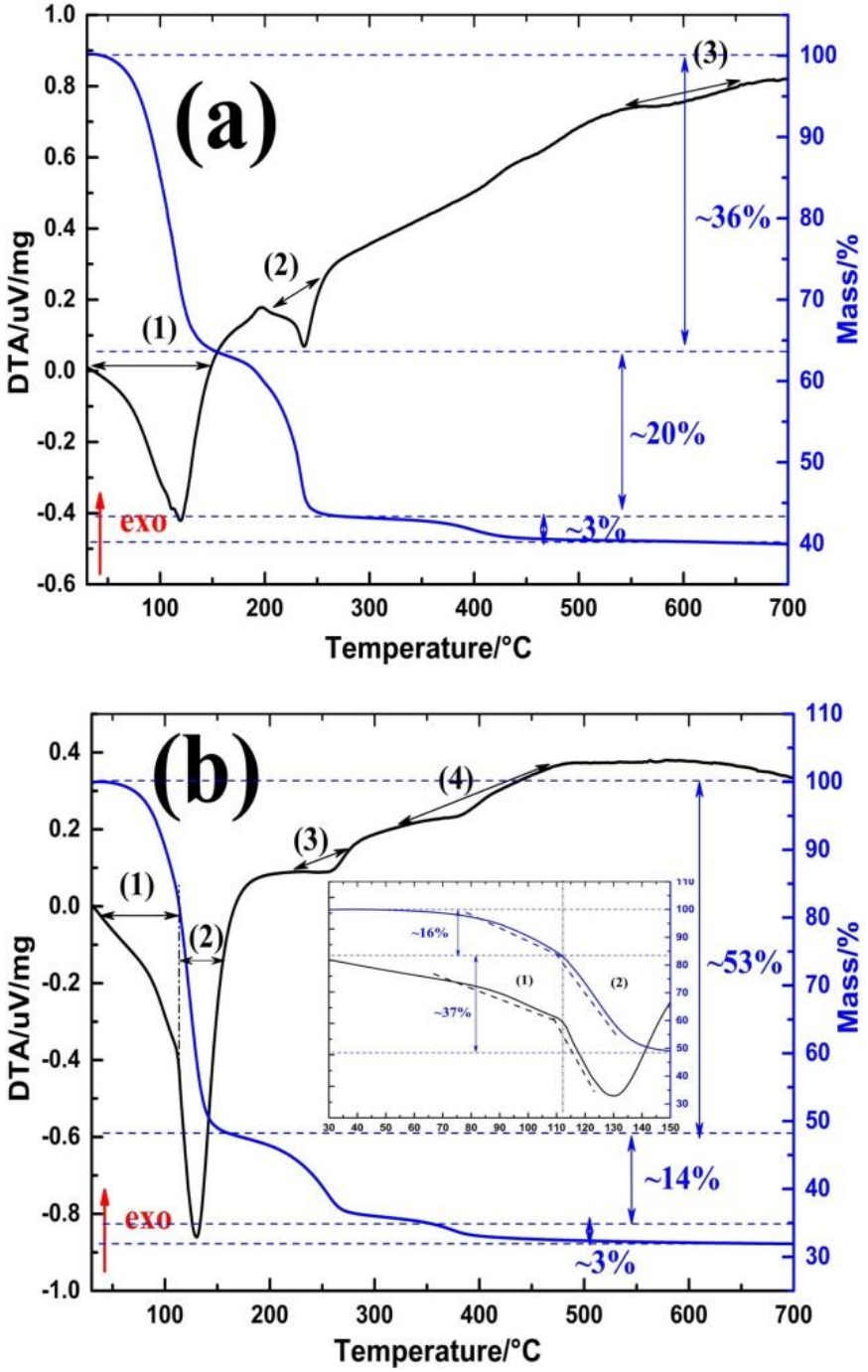

Figure 3.6 Thermogravimetric analysis (TGA) and Differential thermal analysis (DTA) of (a) constantan ink without CRS; (b) constantan ink without CRS, insert in (b) is the details between 30~150 ℃. All samples are tested in Ar with temperature rise rate: 5K/min.

Figure 3.7 shows the XRD patterns of different samples. The oxidation is

inevitable during constantan synthesis process in Figure 3.7 (a). The oxidation has low thermal and electronic conductivity which would prevent solid diffusion during thermal sintering process of constantan. Dispersing constantan particles in water during ink fabrication can make it worse as shown in Figure 3.7 (a), where most of the impurities are CuO and Cu_2O. In contrast, the CRS process can remove most of the oxidation at low temperature in Figure 3.7 (b). Weak pure nickel and copper signals are observed as we predicted before and some NH_4Cl is left in the sample. After high temperature sintering at vacuum, no NH_4Cl could be found in XRD patterns due to the chemical decomposition. The sharp XRD peaks of final constantan patterns after CRS process suggests fine and larger crystal structure (Patterson, 1939).

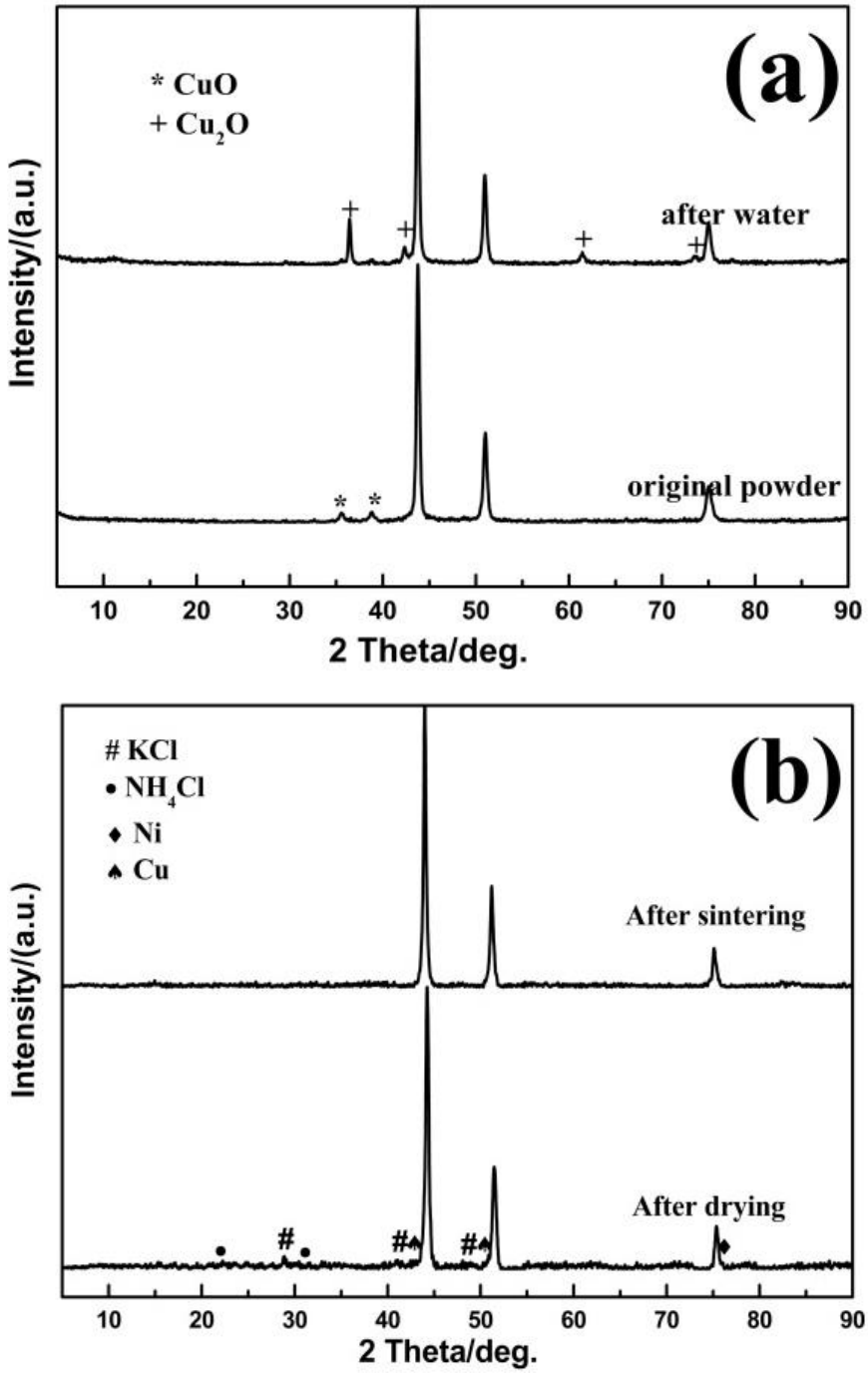

Figure 3.7 XRD patterns of (a) purchased constantan particles with oxidation and dried ink without CRS; (b) ink with CRS dried at 180 ℃ and sintered at 250 ℃ in vacuum.

To have a good understanding of TD reducing process during the designed chemical process, XPS is used to analyze the surface of synthesized constantan film

synthesized with/without CRS process (Figure 3.8). Cu 2p 3/2 can be deconvoluted into two peaks: low binding energy peak which originates from metallic copper atom, while high binding energy is bonding with oxygen ion in Figure 3.8 (a) and (b). The peak area ratio of copper to copper oxide obtained from constantan film without/with CRS process is 0.17 and 1.26, respectively. Also, Cu 2p 3/2 signal with CRS process constantan film shifts toward lower binding energy significantly compared to the samples without CRS process. XPS of Cu 2p 3/2 indicates less oxidation after CRS process. The same phenomenon can be seen from Ni 2p3/2: Ni^{2+} peak shifts to lower binding energy and decreases significantly with CRS process in Figure 3.8 (c) and (d). O 1s can also be deconvoluted into two peaks: a low binding energy peak which originates from the adsorbed oxygen on the sample, while high binding energy is from oxidation status (CuO and NiO) in Figure 3.8 (e) and (f). The peak area ratio of oxygen to oxidation obtained from constantan film without/with CRS process is 0.20 and 1.53, respectively. XPS results can be explained by two reasons: (a) the CRS process can remove/reduce oxidation effectively; (b) The CRS process is an efficacious method to sinter constantan because sintered constantan is more resistant to oxidation (no nano size effect) compared to nano sized constantan.

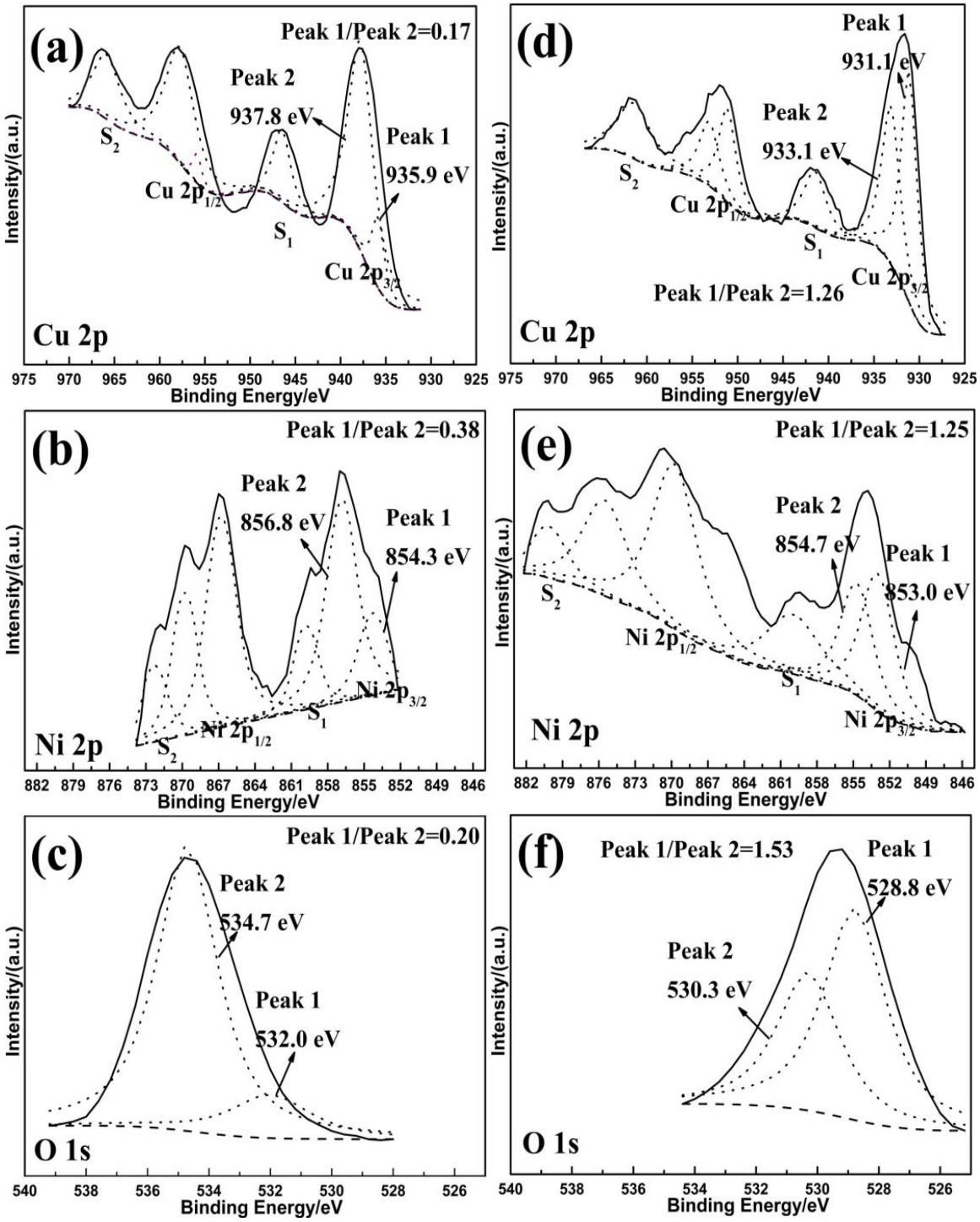

Figure 3.8 XPS spectra of sintered constantan film: (a) Cu 2p; (b) Ni 2p; (c) O 1s of sintered constantan film without CRS process and (d) Cu 2p; (e) Ni 2p; (f) O 1s of sintered constantan film without CRS process.

Figure 3.9 (a)-(f) show samples without CRS process and printed samples with

CRS process sintered at different temperature in vacuum. Figure 3.9 (a) shows a sample for which the CRS process is not sintered. The original particle size of constantan particles is around 100 nm which is not a very small number compared to prior research (Grouchko, Kamyshny, & Magdassi, 2009; Tang, Yang, & Wang, 2010). It is also the smallest size commercial constantan particle. Small particles are preferred because the melting temperature is reduced due to Nano size effect, so the smaller particle the easier to be sintered. The commercial available constantan size is around 100 nm which has almost the same melting temperature as the bulk constantan metal. As mentioned before, this is one of the main reasons limit the application of constantan in inkjet printing technology: it cannot be sintered without damaging the flexible polymer substrate. On the other hand, densification and grain growth start when sintering constantan samples at 250 ℃ for 15 min. as shown in Figure 3.9 (b). The surface becomes uniform and smooth and particles contact to each other to an increases extent after 30 min sintering in Figure 3.9 (c). Grain rearrangement and neck formations among particles are found. In this stage, the particles are penetrated by softened copper and nickel; different microstructure evolution pathways are formed. We believe solid diffusion happens after 30 min sintering from Figure 3.9 (d). Particles start merging together and grain boundaries start disappearing. With an increase of sintering time, particles continue disappearing and a smooth surface can be detected in Figure 3.9 (d). The grains merge more and more after being sintering for 90 min which is displayed in Figure 3.9 (e). No particles are left and pore shrinkage can been seen after 2 h sintering as shown in Figure 3.9 (f). Theoretically, constantan cannot be sintered at low temperature due to its high melting point. However, solid diffusion among constantan particles can be “activated” by the merging of reduced

copper and nickel from dissolved oxidation. In other words, the reduced copper and nickel transport results into particles bonding of constantan.

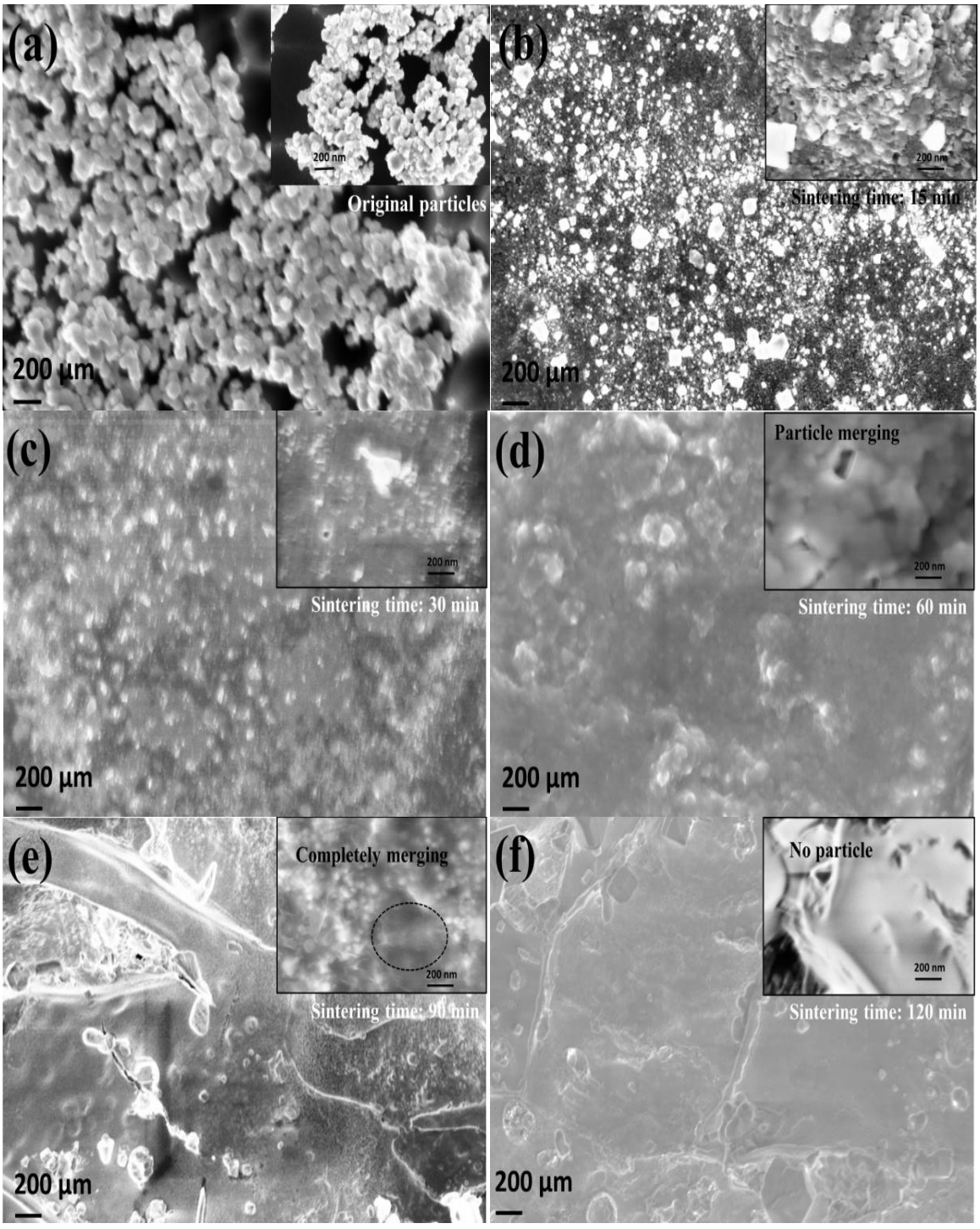

Figure 3.9 SEM imagines of (a) sample without CRS process; samples with CRS process sintered (b) 15 min; (c) 30 min; (d) 60 min; (e) 90 min; (f) 120 min at 250 ℃ in vacuum environment.

3.3.2 Electronical properties of constantan patterns

The resistivity and temperature coefficients of samples without/with the CRS process are measured in Figure 3.10. Samples without CRS process have almost infinity resistivity (not show). The resistivity of samples with CRS process decreases with increase sintering time. Resistivity becomes stable after being sintered 60 min, but the final resistivity is still ten times large than constantan bulk metal (Figure 3.10 (a)). The high resistivity relative to bulk is caused by interspace and pores among sintering constantan particles. In this research, the porous cannot be eliminated due to the low temperature. The temperature coefficient is also measured in Figure 3.10 (b). The slope of three black solid lines represent temperature coefficient of constantan, copper and nickel bulk metal, which are 4×10^{-5} K^{-1}, 4.29×10^{-3} K^{-1} and 6.41×10^{-3} K^{-1} respectively. The temperature coefficient of constantan samples becomes closer to the theoretical value of constantan bulk metal with increasing sintering time from the Figure 3.10 (b). This suggests solid diffusion of sintering takes time to finish. Though the sintered constantan has relative high electronical resistivity compared to bulk, it still has good and stable temperature coefficient.

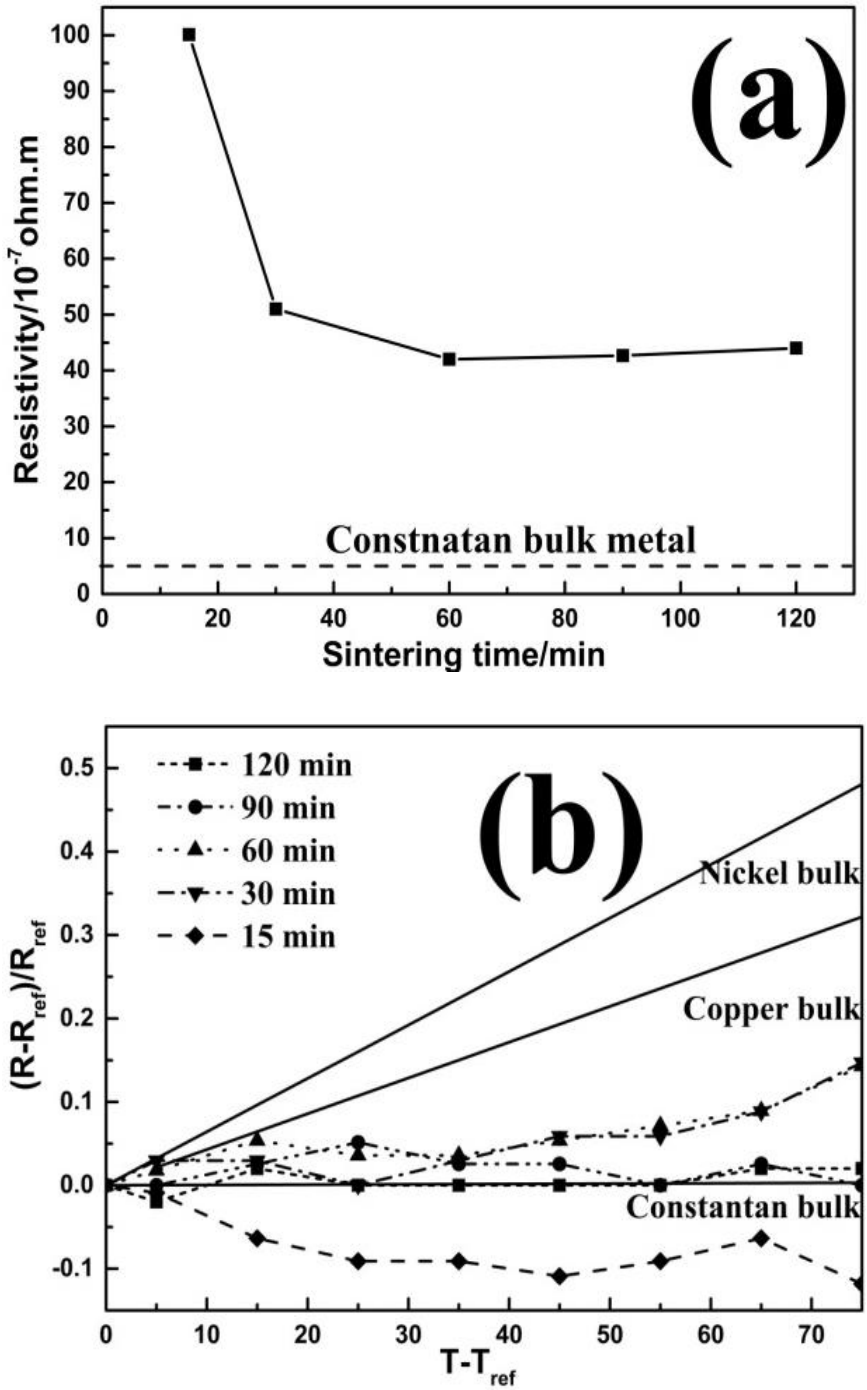

Figure 3.10 (a) Resistivity change with increasing sintering temperature; (b) Relative resistance change versus temperature change, testing temperature 25~100 ℃.

Figure 3.11 (a) displays the constantan samples prepared with chemical reducing process dried at 180 ℃ in vacuum. Thickener (glycerol) and water solvent are evaporated

during this process. In this process, copper and nickel ions in water solvent are reduced by TD in basic condition; reduced copper and nickel tend to stick on constantan nano particles to reduce surface energy. In the meantime, constantan particles are joined by the reduced copper and nickel to form a net structure. The dried samples are then transferred to a vacuum oven and sintered at 250 ℃ in vacuum for 2 h. The structure becomes denser and most inter porous structures disappear in Figure 3.11 (b). The reduced copper and nickel enhance solid diffusion of constantan at relative low temperatures during this process. Figure 3.11 (c) shows the cross-side of printed samples. The printed samples are sintered very well not only on the surface but also in depth. Inter porousity is also detected from the cross-side which explains the high resistivity of the printed samples compared with constantan bulk. Figure 3.11 (d) shows the flexibility of printed constantan strain gauges prepared from CRS process, No peeling off or cracking occurs while bending the patterns. Adhesion of constantan on Kapton substrate is performed by tape testing (not show). The constantan can stay on substrate completely and smoothly after removing the tape.

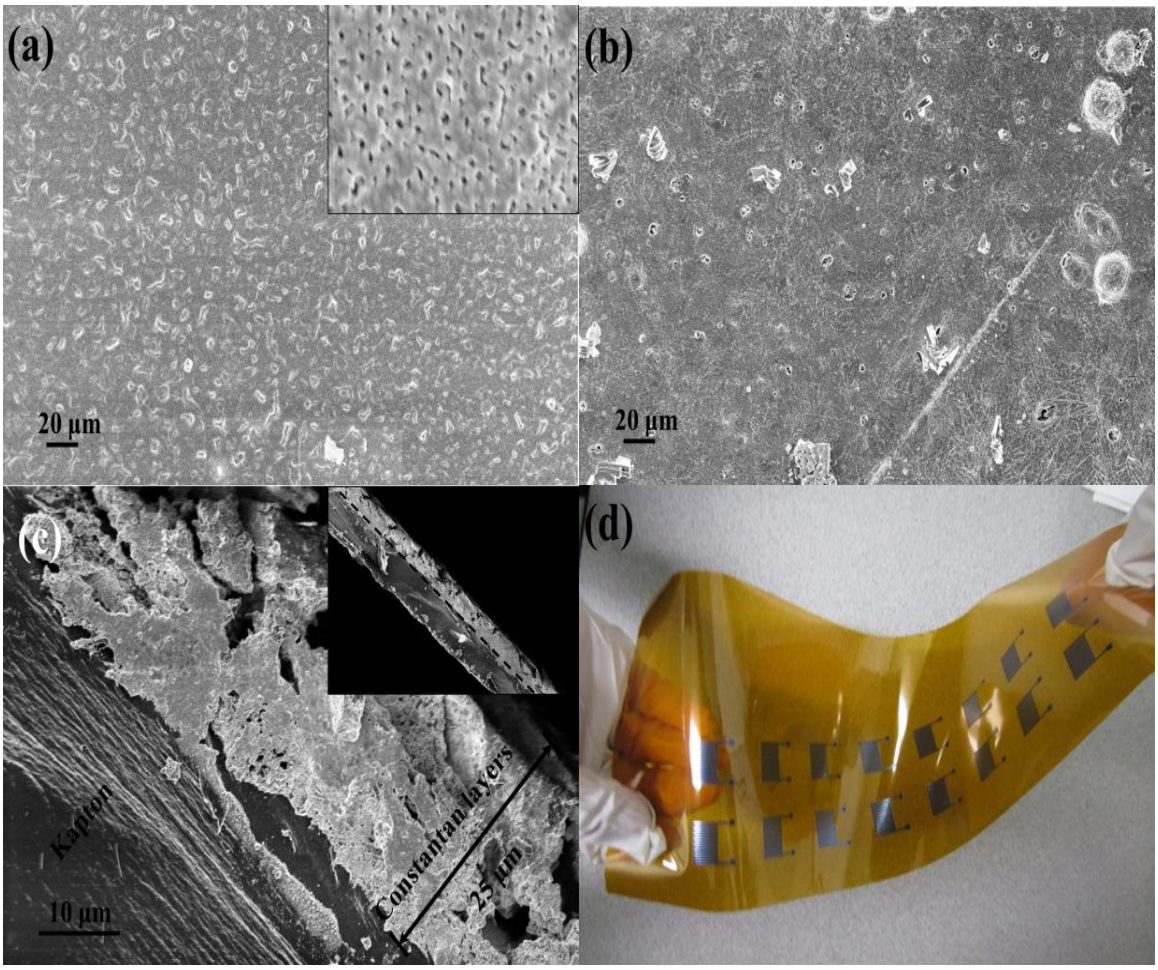

Figure 3.11 (a) Printed constantan samples with CRS process dried at 180 ℃ in vacuum; (b) Sintered at 250 ℃ for 2 h after drying; (c) Cross-side of printed constantan samples after sintering; (d) Optic photos of constantan strain gauges after sintering. The insert is the SEM with different magnification.

3.3.3 Ink stability

Stability of this chemical process is evaluated in the practical application. Three samples are made as shown in Figure 3.12: constantan, PVP, glycerol, TD and NH_4Cl are mixed in DI water, KOH is added to the suspension after 72 h, this ink is marked as #1. Using the same procedure, constantan, PVP, glycerol, KOH and NH_4Cl are mixed in DI water; TD is added to the suspension after 72 h marked as #2. Constantan, PVP, glycerol, KOH, TD and NH_4Cl are mixed in DI water and age 72 h marked as #3.

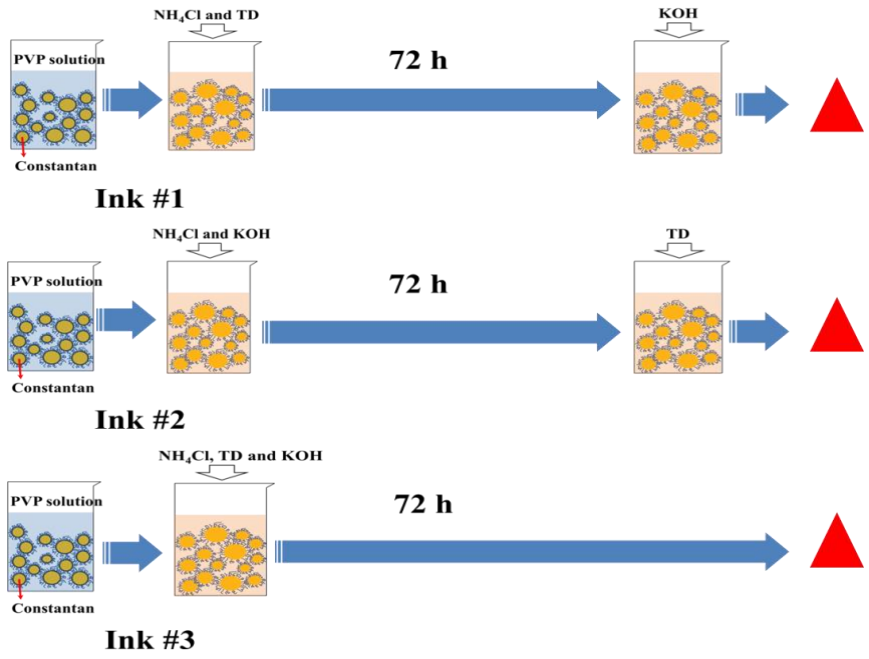

Figure 3.12 Three inks with different store methods.

Three inks are dried and sintered 2 h in vacuum following the same process mentioned above. Figure 3.13 shows XRD patterns of sintered samples by the ink with CRS process aged for 0 h (Figure 3.13 (a)), #1, #2 and #3 inks (Figure 3.13 (b), (c) and (d)). No significant impurity detected in Figure 3.13 (b) which shows the same space structure as the ink kept for 0 h (Figure 3.13 (a)). However, nantokite and nickel oxide have been found in the sample from the #2 ink in Figure 3.13 (c). Copper/nickel ammonia complexes are not very stable with the presence of OH^- according to the following chemical Equation (3.3)-(3.6); CuO and NiO precipitation may consume OH^-. After 72 h, adding TD may not reduce the precipitated solid CuO, NiO and corresponding salts. Also TD cannot release active SO_2^{2-} due to lack of OH^- according to Equation (3.1). Figure 3.13 (d) shows pure nickel has been detected in sample from #3 ink which suggests TD still can exhibit reducing capability in neutral condition, although the

reducing rate is slow at room temperature. It can still reduce a significant amount of nickel and copper ions. Reduced copper and nickel would merge together and form big particles. Those big particles cannot be sintered at relative low temperature due to losing the nano effect. XRD results suggest that ink can be stored in room temperature for a long time without alkaline. Alkaline is needed to activate the chemical process before using the ink.

$$Cu^{2+} + 4NH_3 = [Cu(NH_3)_4]^{2+} \quad (3.3)$$

$$K = \frac{\alpha_{[Cu(NH_3)_4]^{2+}}}{\alpha_{Cu^{2+}} P_{NH_3}^4} = 1.2 \times 10^{13}$$

$$Ni^{2+} + 6NH_3 = [Ni(NH_3)_6]^{2+} \quad (3.4)$$

$$K = \frac{\alpha_{[Ni(NH_3)_6]^{2+}}}{\alpha_{Ni^{2+}} P_{NH_3}^6} = 2.0 \times 10^{8}$$

$$Cu^{2+} + 2OH^- = Cu(OH)_2 \downarrow \quad (3.5)$$

$$K = \frac{1}{\alpha_{Cu^{2+}} \alpha_{OH^-}^2} = 1.7 \times 10^{19}$$

$$Ni^{2+} + 2OH^- = Ni(OH)_2 \downarrow \quad (3.6)$$

$$K = \frac{1}{\alpha_{Ni^{2+}} \alpha_{OH^-}^2} = 1.8 \times 10^{15}$$

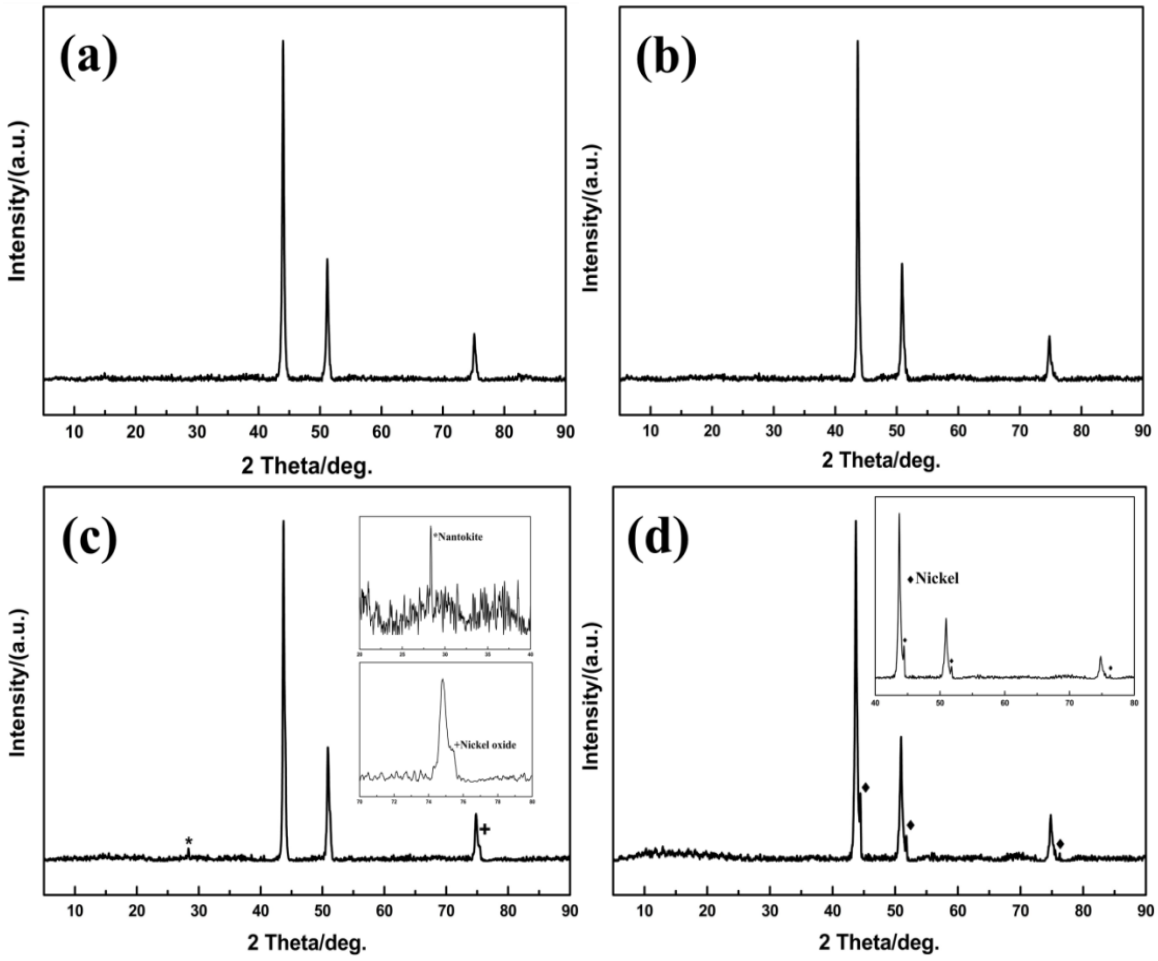

Figure 3.13 XRD patterns of sintered samples of (a) ink aged for 0 h; (b) #1 ink; (c) #2 ink; (d) #3 ink.

Figure 3.14 (a) is the sample sintered from the ink stored for 0 h. Similar morphology can be seen from sample sintered from the #1 ink in Figure 3.14 (b). Figure 3.14 (c) shows sample sintered from the #2 ink which is not sintered very well in the high magnification SEM: particles are barely merged. This is attributed to the oxidation formation during storage in basic condition; precipitated oxidation cannot be sintered due to the high melting temperature. For sample sintered from the ink #3, copper deposition can be seen from the bottle in Figure 3.14 (d); this is because of the slow reducing process of copper and nickel ions by TD at room temperature. Reduced copper and nickel

agglomerate and settles on the bottle. The agglomerated copper and nickel effectively are wasted: large particles cannot be sintered together at low temperature as discussed before. The aged experiment indicates that ink can be stored for a long time without KOH; KOH should be added into the ink right before printing.

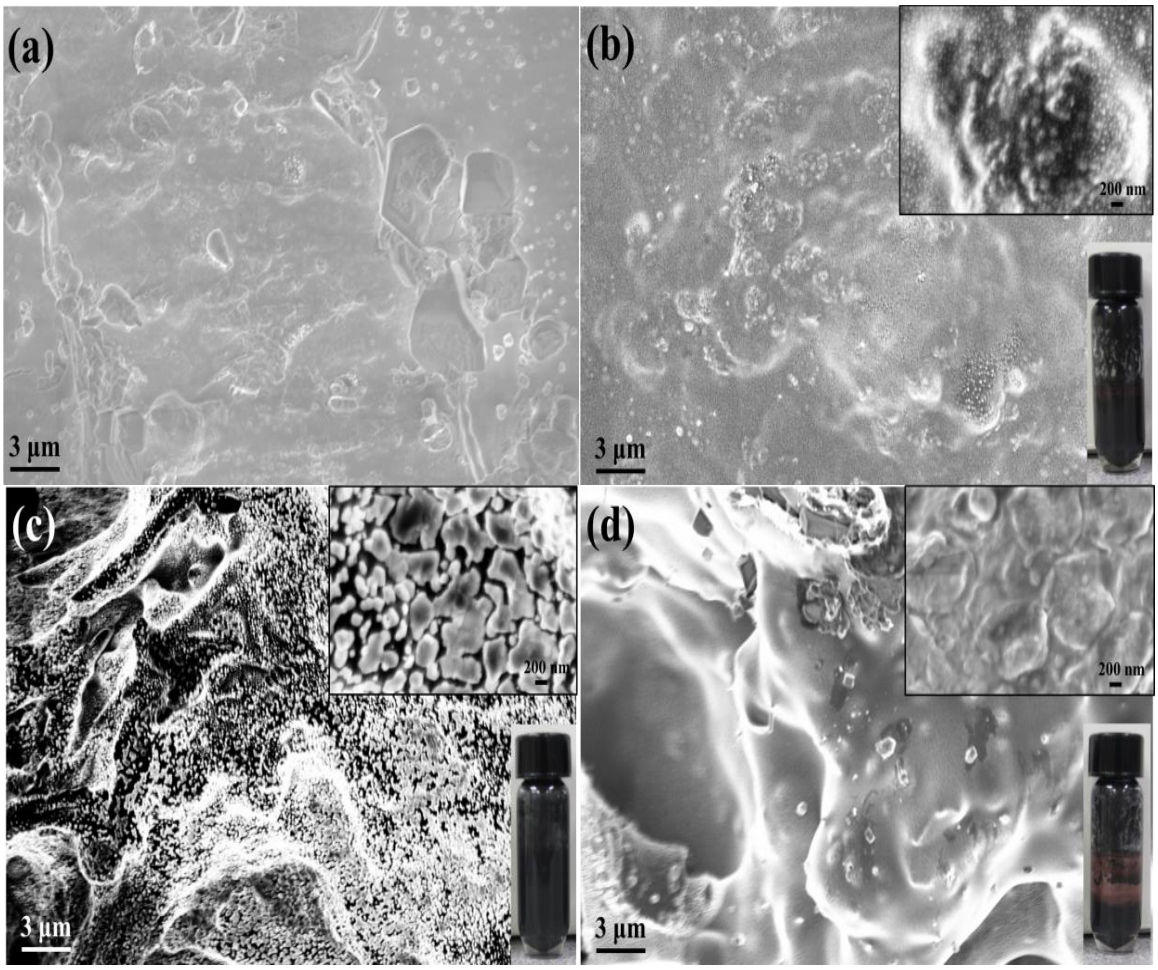

Figure 3.14 SEM imagines of sintered samples of (a) ink kept for 0 h; (b) #1 ink kept with TD for 72 h, KOH added before sintering; (c) #2 ink with KOH kept for 72 h, TD added into ink before sintering; (d) #3 ink with TD and KOH kept for 72 h.

3.4 Summery and Conclusion

Using a CRS process, stable constantan ink is formulated and constantan patterns are fabricated by inkjet printing. This simple process can remove/reduce surface oxidation and sinter high melting temperature constantan alloy NPs at relative low temperature without flammable reducing gas, this has been confirmed by TGA and DTA. The composition of sintered constantan film is confirmed by XRD and XPS. SEM shows the CRS process can anneal constantan NPs effectively after sintering for 2 h at 250 ℃ in vacuum. The solid diffusion of constantan NPs is activated by merging of reduced copper and nickel. The printed constantan patterns electronical resistivity values within a factor of 10 and temperature coefficients comparable to constantan bulk. The fabricated constantan patterns on Kapton have excellent mechanical flexibility. In addition, we also propose a way of storage of functional constantan ink during application. This CRS process can make printed constantan resistor and strain gauge possible in future.

CHAPTER 4

FABRICATION OF NICKEL AND COPPER INK

4.1 Introduction

An increasing number of research groups have focussed on the development of conductive inks such as silver ink and gold for the fabrication of flexible electronics. The most important motivations are the good electrical conductivity and chemical stability of noble metals. For instance, intense interest and many research attempts have been focused on the development of highly conductive and inexpensive material Al due to its cheap cost and excellent electrical conductivity. However, attempts to complete the deposition of Al have failed because of the sensitive activity of Al with oxygen and moisture (H. M. Lee, Choi, & Jung, 2013; H. M. Lee et al., 2012; H. M. Lee et al., 2014). The chemical reactive makes it hard to fabricate printable aluminum ink for flexible electronics. The other reason for interest in metallic inks is the acceptable melting temperature which allows low temperature sintering without damaging the flexible polymer substrate. For instance the melting temperature of gold is 1063 ℃ and silver is 961 ℃, so those metallic inks can be sintered as low as 400 ℃. Aluminum also has low melting temperature which is 660 ℃, but aluminum is surrounded by a very dense oxidation layers which can prevent sintering. Commercial aluminum ink needs to be sintered as high as 560 ℃ with the help of hydrogen in order to break the oxidation. While silver and gold nanoparticle inks have excellent conductivity, the materials and production process for the nanoparticles makes the inks very expensive. Printed copper and nickel is an alternative way to replace noble metallic inks. There are many

advantages of copper and nickel electronics: (a) copper have excellent electrical conductivity which is even better than gold (conductivity of copper is 58.5×106 S/m, gold is 44.2×106 S/m) with cheap raw materials (b) nickel is used as a barrier against oxidation, which could greatly help in the production of printable circuit boards (PCBs), (c) also nickel has a special usage in the energy storage. However, those two metals suffer serious problems as jettable inks: copper nanoparticles are rapidly oxidized in air which can prevent copper sintering. On the other hand, nickel particles are surrounded by a thin dense oxidation layers like aluminum. Sintering would probably have to be done in the forming atmosphere (mixture of hydrogen and nitrogen). What is worse, the melting point of nickel is 1440 ℃ which makes it impossible to sinter with normal thermal curing. There is report in order to conquer this problem (D. Li et al., 2009). In Li et. al.'s research, a multi printing method has been adopted to avoid thermal sintering which is shown in Figure 4.1. The nickel precursor ($NiSO_4$) solution is printed on polymer substrate with suitable viscosity and surface tension as shown is Figure 4.1 (a). Following nickel precursor deposition, reducing agent ($NaBH_4$) solution is printed on the top of nickel precursor solution as displayed in Figure 4.1 (b). The $NaBH_4$ can reduce Ni^{2+} into nickel particles at room temperature and then settled down on the polymer substrate. The reduced nickel particles will aggregate together to form a nickel layer due to a reduction in high surface energy in Figure 4.1 (c). This method can also be applied to copper, silver and gold. The drawback of multi-printing method is it is hard to control the reducing agents to nickel precursor ratio which means this method may produce lots of chemical remains due to its uncontrollable chemical reaction; chemical remains can lower the conductivity of printed nickel film. To our knowledge, no other report on the printable

nickel conductive ink.

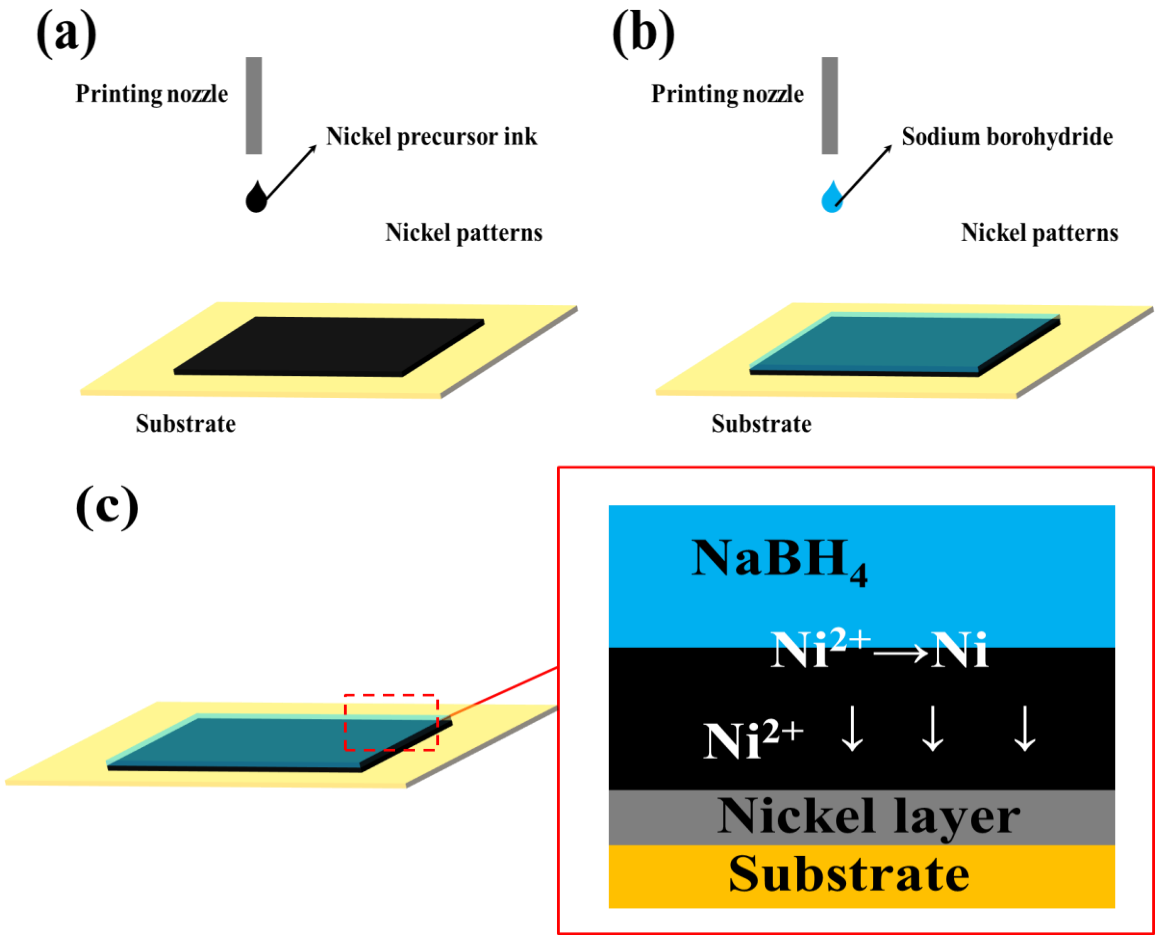

Figure 4.1 Schematics of nickel printing: (a) Nickel precursor printing; (b) Reducing agent printing on the nickel precursor layers; (c) Details of the chemical reducing process in the solution and nickel layer formation.

In the previous chapter, a CRS method is used to make flexible electronics by using high melting point metals. In this chapter, a modified CRS method is used to make printable nickel and copper inks.

4.2 Experimental Section

4.2.1 Materials

The nickel and copper powders used in the ink formulation are commercially available from American Elements, USA with particle sizes around 80 nm purchased. The ammonia chloride (NH_4Cl), glycerol, Polyvinylpyrrolidone (PVP), potassium hydroxide, nickel chloride ($NiCl_2$) and thiourea dioxide are all obtained from Sigma-Aldrich, USA. All chemicals are analytical grade and used as received without further purification.

4.2.2 Preparation of nickel and copper inks

Figure 4.2 shows the scheme of fabrication process. 4 g nickel NPs and 0.3 g PVP are dispersed in 4 g water by ultra-sonication for 30 min as shown in Figure 4.2 (a). Large particles are separated by centrifuge 5000 RPM for 5 min. NH_4Cl is added into the suspension to etch away nickel oxide, and the suspension is magnetically stirred for 12 h to dissolve the oxidation completely; a nickel ammonia complex is formed in the meanwhile in Figure 4.2 (b). However, unlike nickel which is surrounded by a thin dense oxidation which can prevent nickel particles from further oxidized, the key of CRS method is usinga reduced metal from etched oxidations to join metallic particles; the reduced metal acts like bridge while thermal sintering. The thin oxidation nickel oxide layer cannot provide enough nickel ions to join nickel particles. Nickel chloride is added to the nickel suspension to provide enough nickel ions as shown in Figure 4.2 (c), in the meantime, thiourea dioxide (TD) and KOH solution (1 mol/L) is added into that suspension as the reductant. Viscosity is adjusted to 10 cp using glycerol as the thickener. The suspension then is magnetically stirred for 30 min to make a uniform ink. As a

control comparison, a separate batch of ink is formulated: constantan NPs and PVP are dispersed in glycerol/water solvent by ultra-sonication for 30 min, which contains: 40 wt. % nickel powders, 40 wt. % water, 20 wt. % glycerol and 3 wt. % PVP binder. The final ink is printed and sintered as descripted previous in Figure 4.2 (d). The preparation of the copper ink is followed the same procedure as constantan ink as descripted previously.

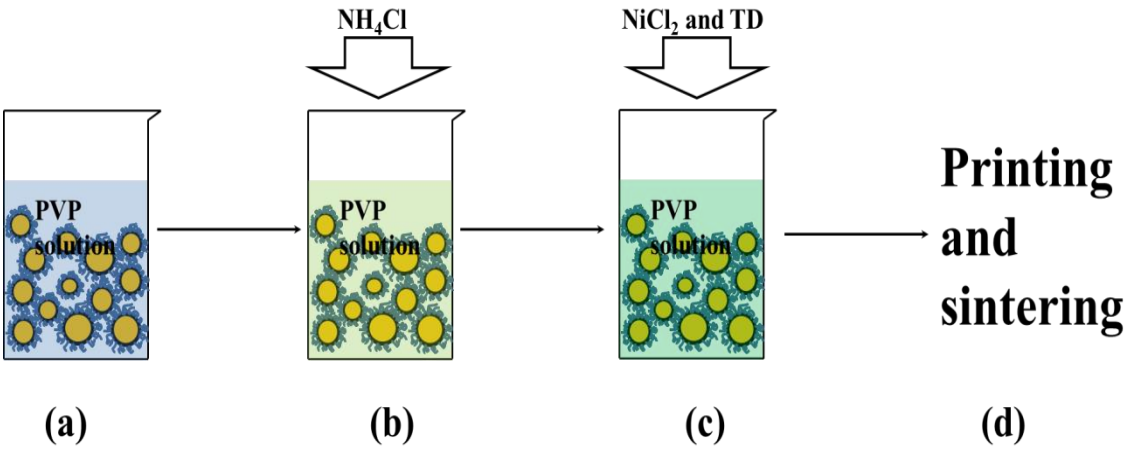

Figure 4.2 Schematics of nickel ink: (a) Nickel suspension in PVP-water solution; (b) Eating away surface oxidation by NH_4Cl; (c) $NiCl_2$ is added into the suspension to increase the nickel ions concentration; (d) Printing and sintering process.

4.2.3 Preparation of nickel conductive film

Patterns are printed by a DMP-2800 inkjet printer (Fujifilm, Japan) on Kapton film at room temperature. The printed patterns are first dried at 180 ℃ in vacuum and then sintered at high temperature in vacuum. The copper patterns are sintered at 250 ℃ while the nickel patterns are sintered at 400 ℃.

4.2.4 Characterization

X-Ray Diffraction (XRD)

XRD measurements were carried out on a Philips PW3040 X-Ray Diffractometer, 2θ ranges from 10 °to 80 ° with CuK_α radiation (λ= 15.4 nm) with a step size of 0.02 °and a time per step of 15 s.

Scanning Electron Microscope (SEM)

LEO 1530VP Field Emission SEM instrument was used to observe the surface morphology of raw materials and printed patterns.

Resistivity Measurement

The resistivity of the patterns was measure by fore point probe (Jandel CYL-HM21, USA). The thickness of the patterns is confirmed by SEM to calculate the resistivity.

Thermal Analysis

Thermogravimetric analysis (TGA) and Differential thermal analysis (DTA), STA 449 F1 Jupiter from Netzsch, Inc. USA, were used to study the thermal behavior of different inks and chemical reaction processes. Measurements were carried out in air with temperature increasing at a rate of 5 K/min.

4.3 Results and Discussion

4.3.1 Nickel part

Figure 4.3 (a) shows the XRD patterns of nickel powder before and after sintering. All of them show at 2θ of 44.5 º, 51.8 ºand 76.4 ºindex as (111), (200) and (220) (JCPDS file No. 04-0783) reflections of the Fm-3m space group without any significant impurities. Usually, nickel is oxidized in air and surrounded by a thin and dense oxidation. This phenomenon is similar with aluminum. However, no oxidation is detected from XRD results indicating that this oxidation layer is too thin to be detected. This oxidation layer is very dense and has very tight chemical connect with the nickel bulk to prevent further

oxidation, which would be a barrier among the particles during sintering. The thin oxidation layer cannot provide enough nickel ions which play an important role during CRS process; additional external nickel ions are needed. After the CRS process, no impurities remains in the nickel patterns, with extra chloride and ammonia ions completely evaporated. The position of XRD signals is compared in order to study the crystal lattice change after CRS as shown in Figure 4.3 (b). The XRD patterns shift to lower angles after CRS suggesting a grain growth (Patterson, 1939) which confirms the sintering process. Also, the peaks become sharper indicating larger crystals after RCS process.

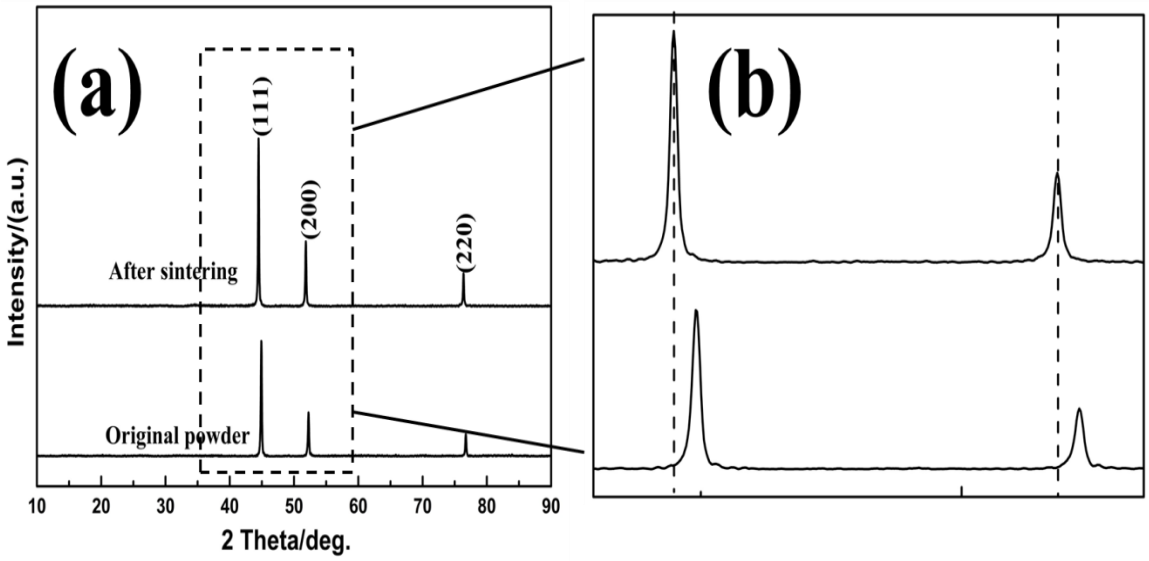

Figure 4.3 (a) XRD patterns of nickel before and after sintering; (b) Details of the top two strongest XRD signals.

Figure 4.4 shows the surface morphology of nickel powders before and after CRS process. The original particle size of nickel particles is below 100 nm with spherical shape in Figure 4.4 (a) and (b). Primary particles aggregate together and form secondary

micro-sized bundles to reduce the high surface energy. Large particles can cause serious nozzle clogging. In this research, PVP is used to separate nickel nanoparticles with the help of ultra-sonication. After CRS process, the particles are joined together very well. Surfaces becomes much smoother as shown in Figure 4.4 (c); Neck formation is found among particles which suggest grain growth occurs during sintering in Figure 4.4 (d) marked with black arrows. The reduced nickel nucleates and grows on the original nickel particles (etched without oxidation), which acts like bridge to enhance the solid diffusion under certain temperature. However, due to the high melting temperature of nickel bulk, nickel cannot be sintered completely. The porous structure can lower the conductivity of the final products.

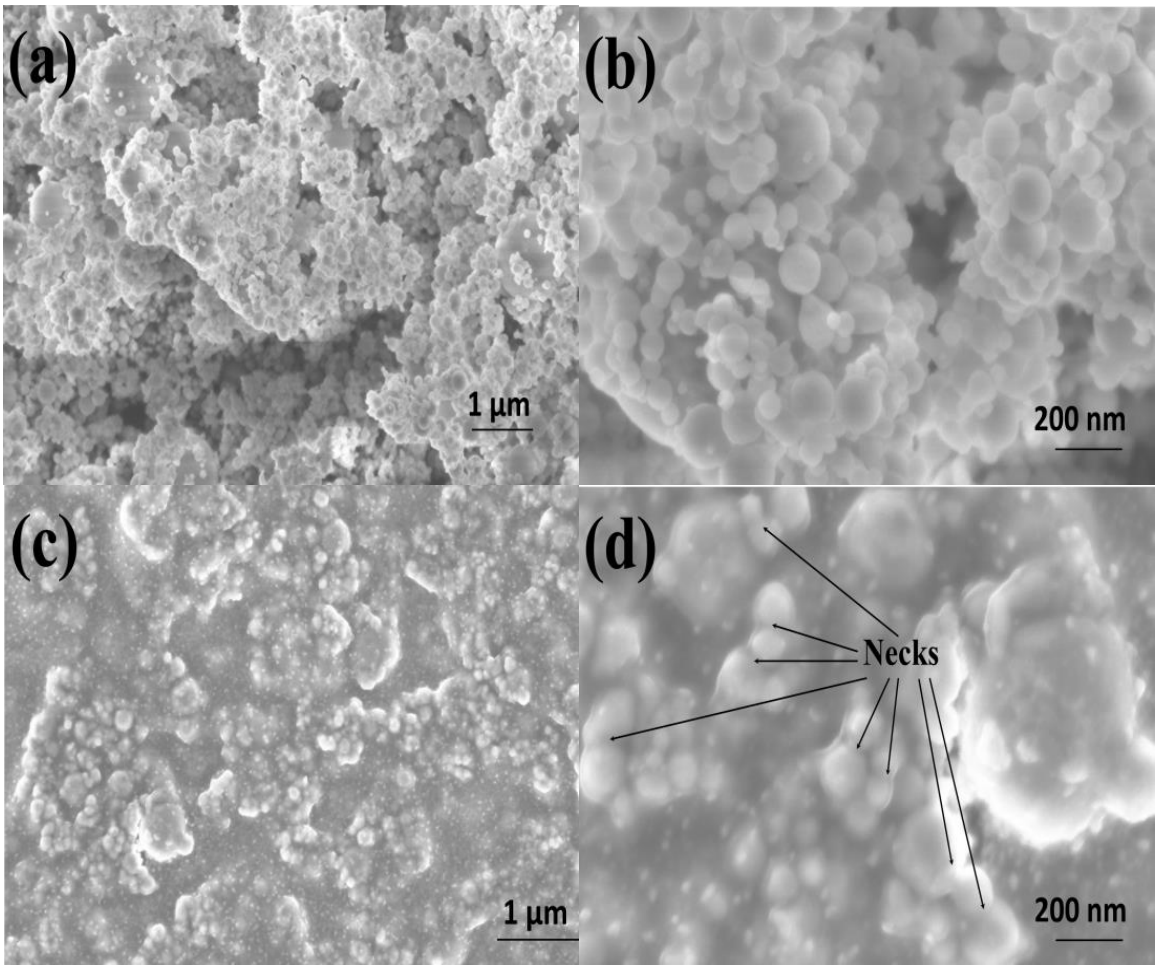

Figure 4.4 SEM images of (a)-(b) nickel nano powders; (c)-(d) nickel patterns after CRS process with different magnifications. The neck formation is marked by black arrows.

Figure 4.5 displays the resistance of the printed patterns. The thickness is around 20 μm measured by micrometer. The insert graph is the sintered patterns on Kapton, which shows good mechanical flexibility; this suggests CRS can make conductive nickel patterns without damaging the polymer substrate. The resistance of the printed patterns is still higher than the nickel bulk film, which is caused by the porous structure as discussed before. The resistivity is calculated by the Equation (4.1):

$$\rho = R\frac{S}{L} \tag{4.1}$$

In Equation (4.1): R is the resistance of the pattern, S and L are the cross-side area of the pattern and length of the pattern, respectively.

The resistivity of the printed pattern is around 500 μΩ·cm which means the conductivity is 1.4 % of the nickel bulk. This result is ten times lower than the multi-printing method reported (D. Li et al., 2009) because of the more complete sintering.

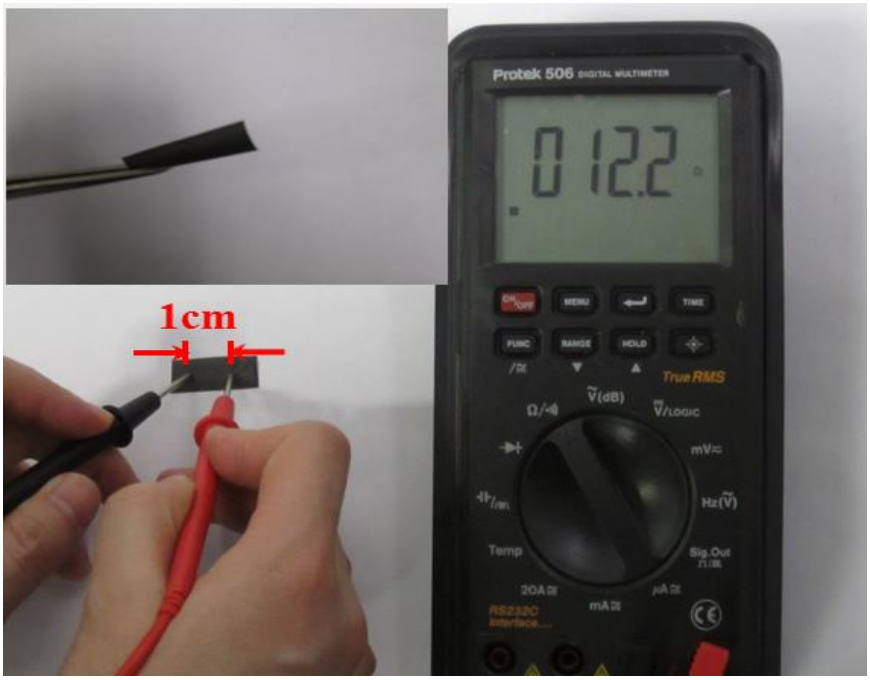

Figure 4.5 Conductive testing of the printed nickel patterns after CRS process, the insert is the flexibility of patterns on the Kapton substrate.

4.3.2 Copper part

Figure 4.6 (a) shows the XRD patterns of copper powder before and after sintering. All of them show at 2θ of 43.6 º, 50.8 ºand 74.4 ºindex as (111), (200) and (220) (JCPDS file No. 04-0783) reflections of the Fm-3m space. Unlike nickel nanoparticles, copper nanoparticles have significant oxidation as shown in Figure 4.6 (a) marked by a star. In normal conditions, copper cannot form dense oxidation layers to prevent further

oxidation, which means oxidation keeps advancing until no pure metal copper is left. This is even worse for copper nanoparticles due to the high surface area in nano size. This is the main challenge in copper ink; most of the time, copper nanoparticles or inks are kept in a glovebox to prevent oxidation. However, no oxidation is detected from XRD results after the CRS process indicating that the CRS method can eliminate oxidation effectively: NH_4Cl can etch away and convert oxidation into copper ions. Copper ions are reduced into copper and bridge the original copper particles. The solid diffusion and neck formation are triggered among copper particles through the copper "bridge" and low temperature sintering is achieved. Crystal lattice change is compared by the position of XRD signals after CRS as shown in Figure 4.6 (b). Similar with nickel, the XRD patterns shift to lower angles after CRS indicates a grain growth which confirms the sintering process. Also, after RCS process, the peaks become sharper indicates a larger copper crystal lattice because of the particle merge.

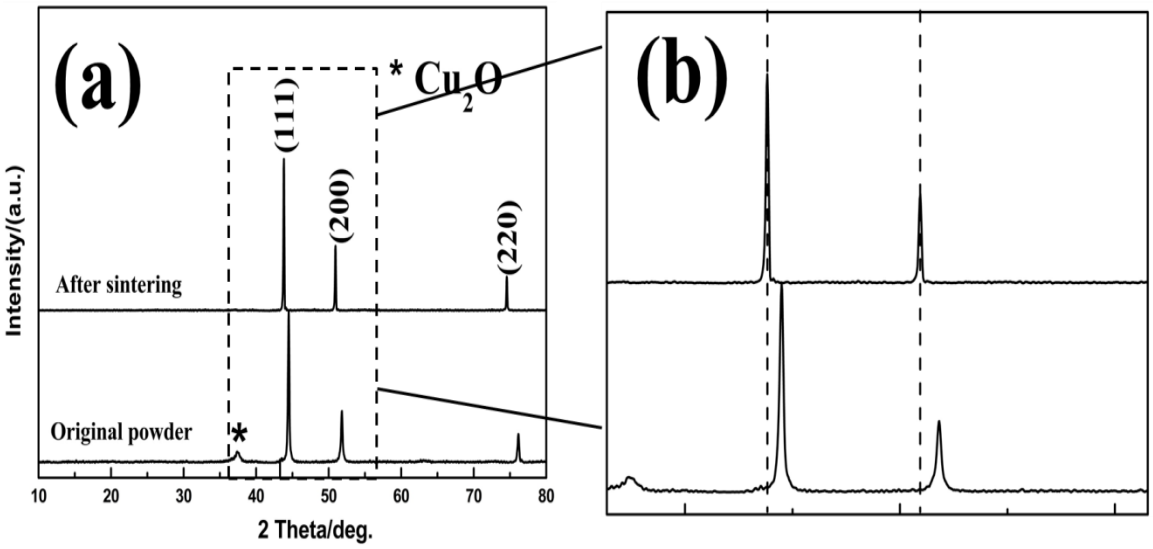

Figure 4.6 (a) XRD patterns of copper before and after sintering; (b) Details of the top two strongest XRD signals.

The morphology of copper nanoparticles before and after CRS is studied by SEM displayed in Figure 4.7. Original copper particle size is around 200 nm with sphere shape as shown in Figure 4.7 (a). The primary copper particles aggregate together due to the high surface energy in Figure 4.7 (b). The stable copper suspension can be achieved by the steric repulsion from the adsorbed PVP. An obvious particle union is discovered in Figure 4.7 (b): original copper particles and reduced copper marked by the black and red, respectively. The copper film is quite different from the nickel film after CRS process: more smooth areas (Figure 4.7 (c)) are detected representing the reduced copper. This can be explained by the much more oxidation in copper than nickel. The copper oxidation is converted into copper and sticks on the original copper nanoparticles and functions as a bridge for the solid diffusion which is proven in Figure 4.7 (d).

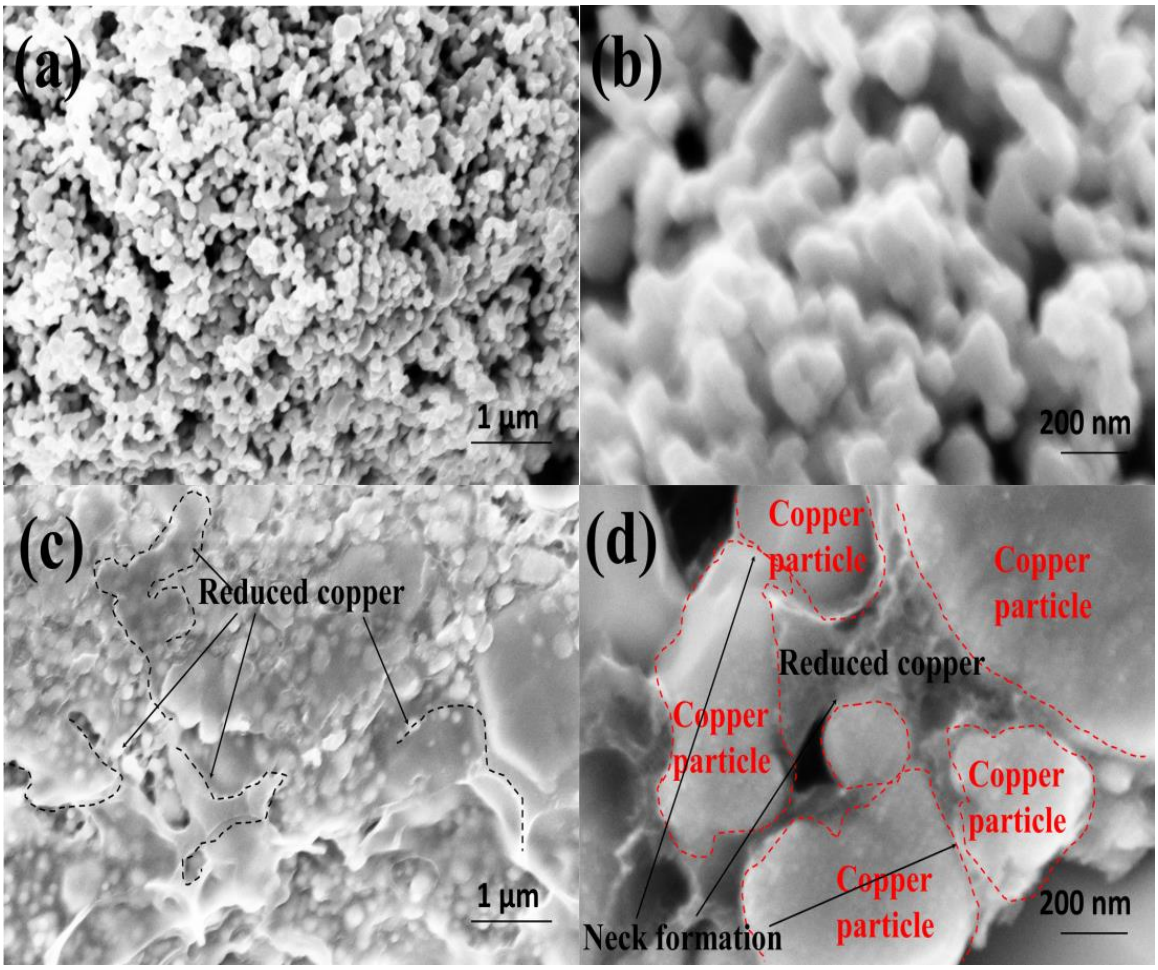

Figure 4.7 SEM images of (a)-(b) copper nano powders; (c)-(d) copper patterns after CRS process with different magnifications. The neck formation and reduced copper are marked by black arrows and original copper particles are marked by red dash line.

The conductivity testing is performed in Figure 4.8. The thickness is around 20 µm measured by micrometer. The sintering temperature of copper is much lower than nickel, so copper films also shows good mechanical flexibility as displayed in the insert graph in Figure 4.8. The resistivity of copper film made by CRS is around 125 µΩ·cm, so the conductivity is 1.3 % of the copper bulk. Although this result is lower than other researchers' reports, CRS provides a simple, safe and economic method to make conductive copper ink. Copper has more promising market than silver in the fabrication

of electronics and circuit boards due to the low cost and acceptable conductivity.

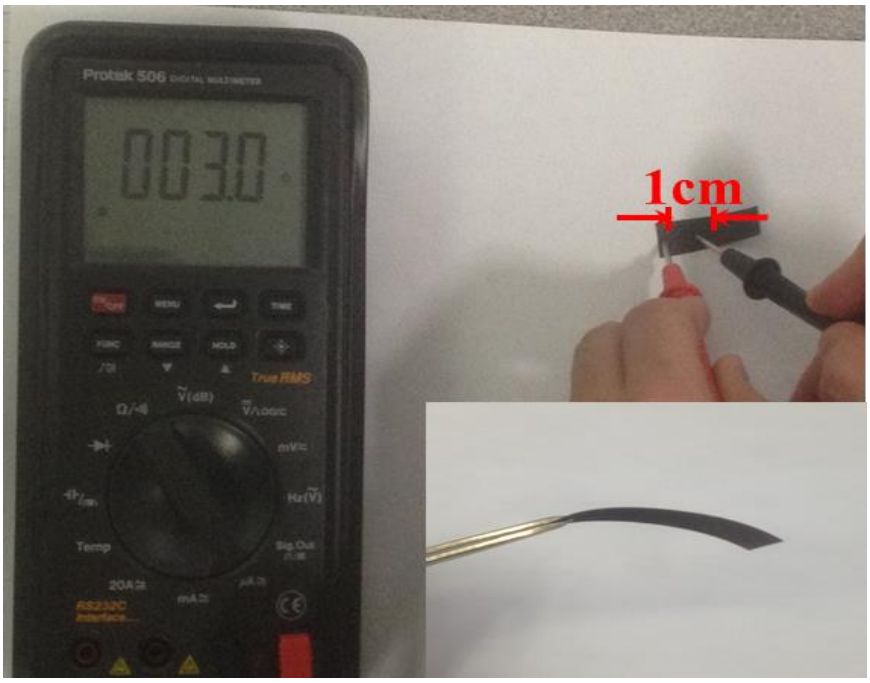

Figure 4.8 Conductive testing of the printed copper patterns after CRS process, the insert is the flexibility of patterns on the Kapton substrate.

4.4 Summery and Conclusion

In this chapter, copper and nickel inks are developed to make conductive films. Usually, nickel cannot be sintered very easily due to the high melting point of the bulk; what is more, nickel nanoparticles are covered by dense and isolated oxidation with poor thermal conductivity. High sintering temperature is required to break the oxidation and initiate nickel particles to sinter. Most prior art requires forming gas to help the sintering. The CRS process is evaluated to make conductive nickel film in vacuum environment at 400 ℃ without using forming gas. Compared to its formulation for constantan ink, the CRS process is modified a little bit to make nickel ink: external nickel source are added to the suspension in order to provide enough nickel ions to be reduced to pre-connect nickel particles. The composition of sintered nickel film is confirmed by XRD which indicates CRS does not change the composition of nickel or introduce any impurities. The sintering phenomenon is confirmed by SEM: neck formation and particle merge are found. The conductivity of the nickel film is tested by multi-meter and the resistivity is estimated to be 1.4 % of the bulk metal. Nickel ink has potential application on the energy storage devices due to its high stability at relative high voltage, which can be used to replace expensive gold and poor performance carbon serious materials.

The other research described in this chapter focusses on copper ink. It indicates that copper conductive film can be made at 250 ℃ by the same CRS process as constantan. The composition and morphology are characterized by XRD and SEM: no impurity is found and copper particles merge together. Copper ink is very useful in the electronical devices and circuit board fabrication due to its high conductivity and low cost.

CRS process is an ideal method to make metallic conductive ink based this chapter on the previous one. This method does not require complex sintering machines like photonic, plasma and microwave sintering methods. Also no dangerous forming gas is needed to eliminate or break the oxidation. It has “built in” reducing ability to remove oxidation during the ink fabrication and sintering process.

Conductive metallic films have very wide application on many areas. The possibility of using nickel and silver conductive film to make flexible and rechargeable lithium-ion batteries is discussed in next chapter.

CHAPTER 5

FABRICATION OF LITHIUM-ION BATTERIES BY INKJET PRINTING

5.1 Introduction

In recent years, there has been more and more attention devoted to the fabrication of energy storage devices like printable supercapacitors and solar cells (Kaempgen, Chan, Ma, Cui, & Gruner, 2009; E. Lee et al., 2011; Mei et al., 2014; Wee, Salim, Lam, Mhaisalkar, & Srinivasan, 2011; Y. Xu et al., 2013). Among chemical energy storage devices, the lithium-ion battery has outstanding performance such as: high energy density, high capacity, easy fabrication process and high working voltage. So lithium-ion batteries are the most widely used portable energy devices in the last decades. The popular fabrication of lithium-ion batteries is tape casting which can achieve roll-to-roll production. The drawback of this method is difficult to fabricate ultra-thin film and shape control of electrodes.

Inkjet printing is one of the most promising manufactory methods to make thin films with computer controllable shape as mentioned before. To the best of our knowledge, there is no report on the fully printed lithium-ion batteries. The main barrier preventing a fully printed lithium-ion battery is the current collector. The current collector materials must meet two requirements: (a) It must not facilitate an electrochemical reaction with cathode and anode; (b) It must remain stable at high voltage in the presence of electrolyte. Potential materials which could be used in lithium-ion batteries view are exhibited in Figure 5.1. All potentials mentioned in this paper refer to the potential versus Li^+. Material potentials lower than 1.55 V cannot be used either as

cathode or anode due to dissolution in the electrolyte. Potentials between 1.55 V and 4.2 V have possible use in anode current collector. Potential above 4.2 V can be applied for both cathode and anode current collectors. Based on this point, carbon materials should be the ideal current collector material, however, carbon materials suffer great contact resistance after printing which is caused by its high sintering temperature. Moreover, carbon materials have poor adhesion on polymer substrates which is caused by the same reason. From the potential scale, silver is very close to the minimum limitation of cathode current collector. So in this paper, silver is used as the comparison current collector. In the previous research gold is used for the fabrication of both cathode and anode current collectors for lithium-ion batteries. The main disadvantage of gold current collector is the high cost: it is not an economic material for batteries.

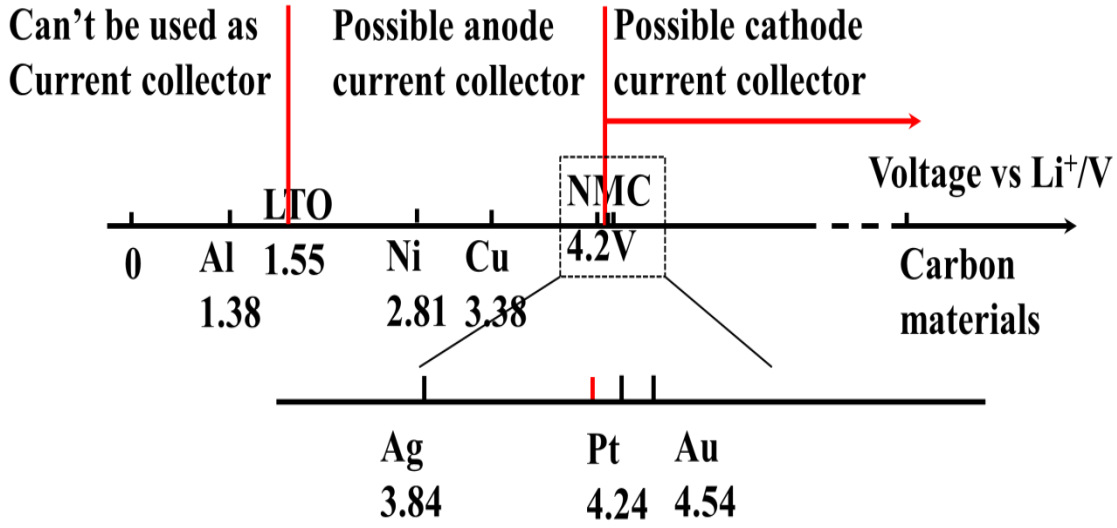

Figure 5.1 Voltage scale for materials versus Li/Li^+.

The commercial available current collector for cathode and anode for lithium-ion battery are aluminum and copper, respectively. The potential of aluminum is 1.38 V

which is even lower than the requirements of anode current collector. However, aluminum is usually covered by a passive oxidation layers which can prevent aluminum from further oxidized. This passivation is very thin and doesn't affect the conductivity of aluminum bulk, which is the reason aluminum can be used as cathode current collector. But aluminum is a very reactive material which makes it hard to print under normal environments; also, aluminum can only be used in cathode structure because it can react with lithium ions to form aluminum-lithium alloy at low voltage. On the other hand, copper is not stable at high voltage which makes it can only be used as anode current collector. There is no common material in industrial which can act as both cathode and anode current collectors. From the potential scale bar in Figure 5.1, not many metals are qualified to be used as cathode and anode current collectors except for gold, platinum and carbon materials. None of them has commercial value due to the disadvantages discussed before.

James H. Pikul reports a method to fabricate lithium-ion battery with nickel as both cathode and anode current collectors (Pikul, Gang Zhang, Cho, Braun, & King, 2013). Nickel is an excellent material for the application of batteries due to its high electrochemical stability; it is protected by the passivated layer which prevents nickel reacting with lithium ions and further oxidation. However, the melting temperature of nickel bulk (1440 ℃) is too high for printing on the polymer substrate. Also, the protection oxidation passivation layer prevents nickel from sintering at low temperature. There have been previous methods of fabricating nickel conductive film on flexible substrate as mentioned before (D. Li et al., 2009).

5.2 Experimental Section

5.2.1 Fabrication of current collectors for lithium-ion batteries

Figure 5.2 displays the structure of multi-layers electrodes for lithium-ion batteries fabricated by conductive silver and nickel current collectors printed onto plastic substrates.

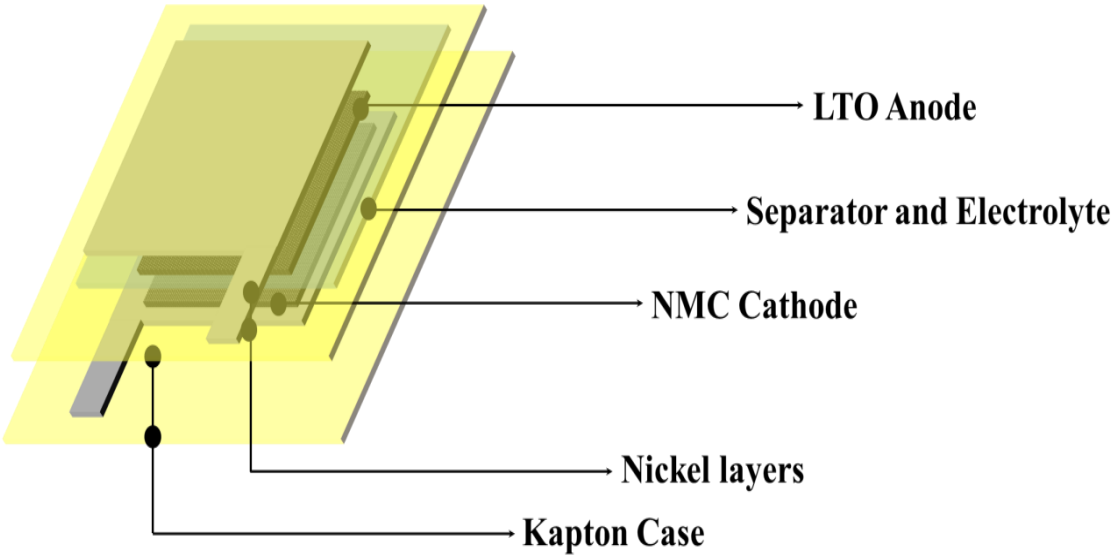

Figure 5.2 Structure of multi-layers flexible electrode made by plastic conductive film.

5.2.2 Fabrication of flexible lithium-ion batteries

Figure 5.3 shows the process of fabrication of flexible lithium-ion batteries. The battery inks (cathode and anode inks) contains: water, Triton X and battery materials. The ratio of Triton X to battery materials is fixed at 1:9 by weight. The battery materials contain 80 wt. % wt. active material (NMC for cathode and LTO for anode), 10 wt. % carbon black as conductive agent and 10 wt. %. PVP as binder. The viscosity is adjusted at 10 cp to meet the requirements of DMP 2800 printer. The inks are first mixed by a rotating mixer overnight and then ultra-sonicated for 30 min, then centrifuged at 5000 rpm to eliminate

large particles. The inks are then printed on the conductive film and dried in vacuum at 100 ℃ to evaporate the solvent. Flexible batteries are assembled in an argon filled glove box in the form of punch cell to make sure the seal. The electrolyte is made of $LiPF_6$ (1 M) in a 1:1 (V/V) mixture of dimethyl carbonate (DMC) and ethylene carbonate (EC) is used as electrolyte. The separator is Celgard2400. The batteries are assembled in nitrogen protective glovebox.

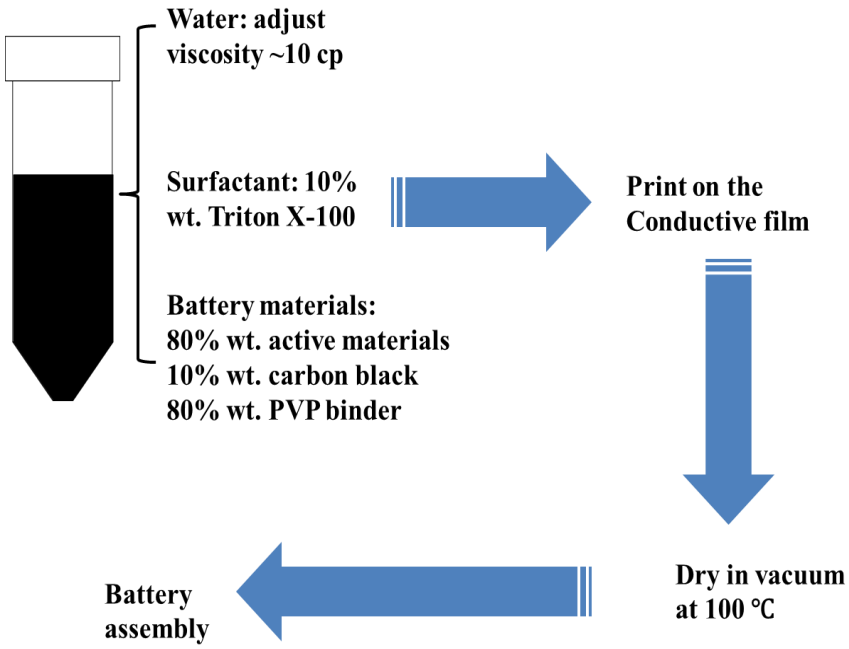

Figure 5.3 Process of fabrication of flexible lithium-ion batteries.

5.2.3 Characterization

X-Ray Diffraction (XRD)

XRD measurements were carried out on a Philips PW3040 X-Ray Diffractometer, 2θ ranges from 10 °to 80 ° with CuK_α radiation (λ= 15.4 nm) with a step size of 0.02 ° and a time per step of 15 s.

Scanning Electron Microscope (SEM)

LEO 1530VP Field Emission SEM instrument was used to observe the surface morphology of raw materials and printed patterns.

Electrochemical Testing

Punch cells were cycled at a rate of 0.1 C (1 C = 150 mAh/g) between 0.5 and 2.5 V at 25 ℃, using a Battery Analyzer (BST8-MA, MTI Inc.). The cyclic voltammetry (CV) measurements were carried out on CHI832C (CH Instruments, Inc.) at 25 ℃. The cyclic voltammetry (CV) measurements were carried out on CHI832C (CH Instruments, Inc.) at 25 ℃. The counter electrode is Li metal and the scanning rate is 1 mV/s.

5.3 Results and Discussion

5.3.1 Performance of battery inks

In order to characterize the performance of the battery inks, the conventional battery is assembled with traditional aluminum cathode current collector and copper anode current collector. The performance of the battery is shown in Figure 5.4. The working voltage and current strength of the LED are 2.0 V and 20 mA, respectively. The battery can work with flatted and bended shape suggests the stability of the battery inks and inkjet printing process. The water solvent, surfactant, dispersing process and printing process have no significant effect on the composition of NMC and LTO materials. On the other side, PVP is excellent water based binder which provides strong adhesion between battery materials and current collector and prevents battery material peeling off. The flexible battery can be fold to fit into any shapes of flexible electronics in the future. Traditional battery slurry uses chemical toxical organic solvent such as N-Methyl-2-pyrrolidone (NMP) or

Dimethylformamide (DMF) as solvent. Environmental friendly water is used in this method to replace those organic solvent.

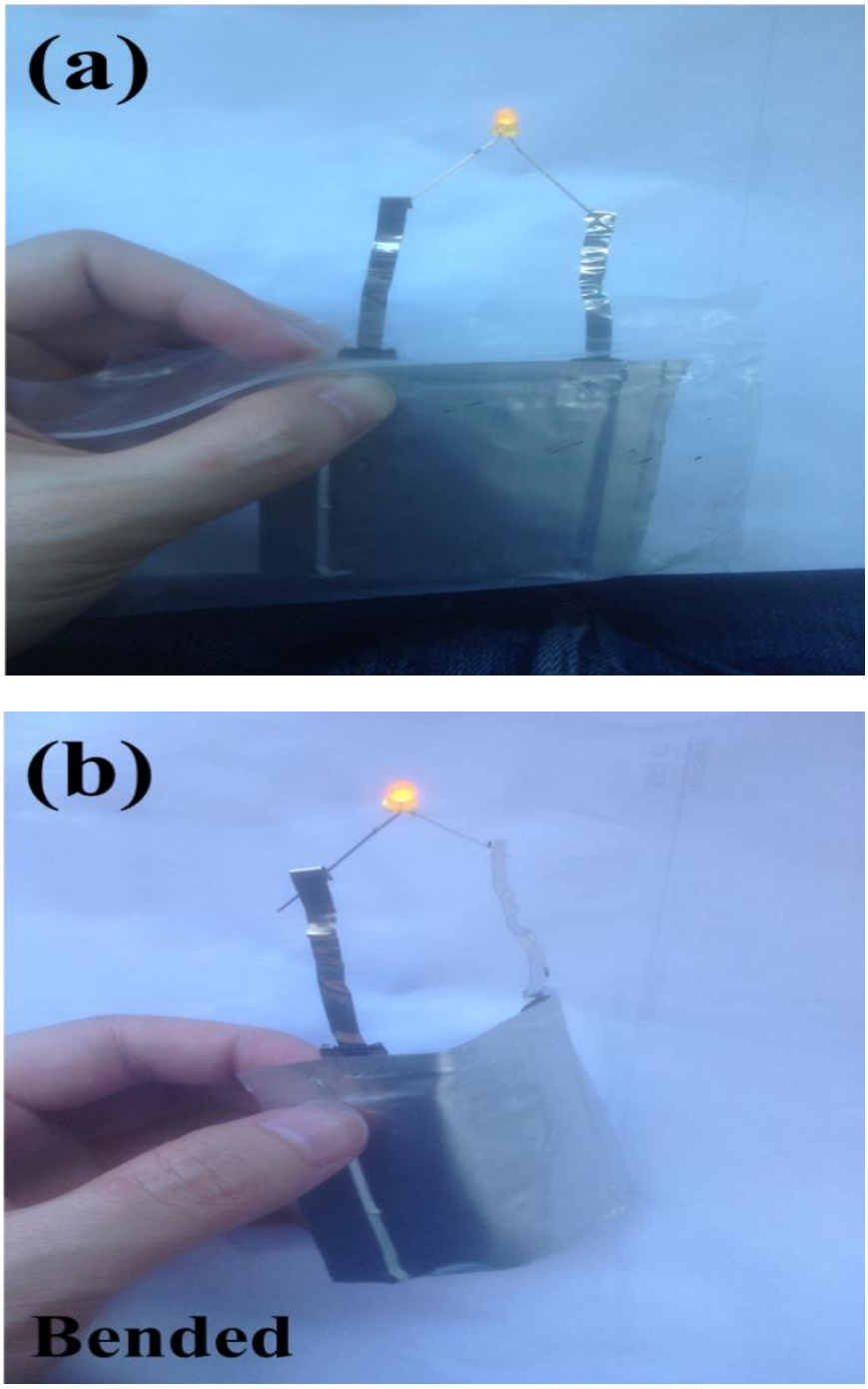

Figure 5.4 (a) Flat; (b) Bended performance of the printed batteries with traditional aluminum and copper current collectors.

5.3.2 Silver and nickel current collectors for flexible batteries

The lithium-ion batteries with silver current collectors fail at 0.8-1.0 V. The batteries are disassembled to study the mechanism. Figure 5.5 (a) and (b) displays the optical images cathode and anode of flexible batteries with silver current collectors after charging. A serious peeling off is detected from the cathode and anode which is the main reason for the failure of battery. The peeling cathode and anode is caused by different mechanisms: silver can react with lithium ions and to form silver-lithium alloy; there is report use GITT technology study the silver in lithium-ion batteries, which indicates silver can form different lithium-silver alloy at vary potential (Taillades & Sarradin, 2004). On this point, silver is a possible anode material for lithium-ion battery. The internal short circuit happens while charging the battery. Another reason of peeling off is caused by silver oxidation in electrolyte above 0.8-1.0 V during battery charging which is shown in Equation (5.1), the Ag^+ dissolved into electrolyte and cause active materials to peel off. Silver ink is not suitable for the fabrication of lithium-ion batteries.

$$Ag \xrightarrow{0.8\,V} Ag^+(aq) + e^- \tag{5.1}$$

In contrast, Figure 5.5 (c) and (d) displays the images of cathode and anode of flexible battery made by nickel current collector. The battery is disassembled after first charge and recharge. No peeling off (the slight peeling off is caused by battery assembly) is detected suggests nickel is very stable inside the battery during the electrochemical reaction. Nickel does not react with lithium ion to form alloy or get oxidized at high operating voltage.

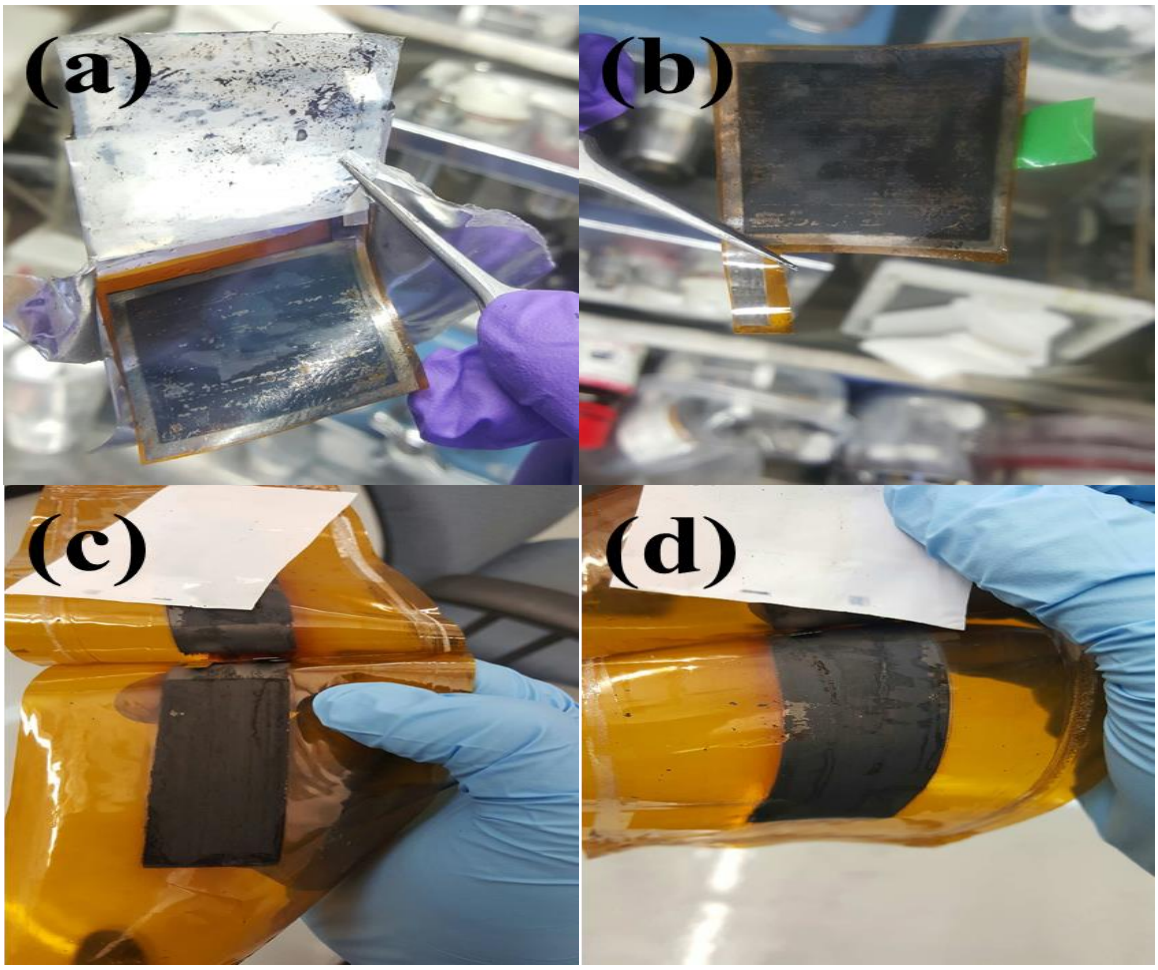

Figure 5.5 Optical images of the flexible batteries made by silver current collector: (a) Anode electrode; (b) Cathode electrode; Images of the flexible batteries made by nickel current collector (c) Anode electrode; (d) Cathode electrode. All are disassembled after first cycling.

5.3.3 Performance of flexible batteries

The printed nickel ink has potential application on the lithium-ion batteries due to the easy manufactory and sintering process. The resistivity of thin films made by different materials is summarized on table 5.1 including the nickel film, all these materials have potential application on the battery current collector (aluminum and silver are not included). From Table 5.1, gold (K. Sun et al., 2013) (other noble metals like platinum is also good current collector for lithium-ion batteries, but no printable platinum conductive ink has been reported yet) is obvious the most outstanding material for the fabrication of

printable batteries. However, gold is expensive which can limit the application of printable batteries. Carbon is an ideal material for the batteries (Chew et al., 2009; Hu, Wu, La Mantia, Yang, & Cui, 2010) which has been applied on the battery as conductive agent, but carbon suffers high resistance as current collector due to the contact resistance. High inert resistance may affect the energy output of batteries caused by thermal runaway. Indium Tin Oxide (ITO) is a new conductive material which already shows excellent stability and conductivity in solar cell (Frederik C. Krebs, 2009a, 2009c; Schmidt et al., 2009). The application of ITO in lithium-ion batteries has not been evaluated, but the market price of ITO is not as cheap as nickel nanoparticles. On the other hand, nickel film has even lower surface resistance than ITO film.

Table 5.1 Properties of Conductive Inks for Batteries

Materials	Types	Surface resistance/$\Omega \cdot sq^{-1}$
Carbon Nanotubes	Inkjet printable	Above 10000 (Beecher et al., 2007; Fan, Wei, Luo, & Wei, 2005; Vaillancourt et al., 2008)
Graphene	Inkjet printable	Around 6000 (Blake et al., 2008; Grande et al., 2012; Lemme, Echtermeyer, Baus, & Kurz, 2007; Tan et al., 2007)
ITO	Gravure printing	500~1000 (Ederth et al., 2003; Heusing et al., 2009)
Gold ink	Inkjet printable	0.02 (Redinger, Molesa, Shong, Farschi, & Subramanian, 2004)
Nickel thin film	Inkjet printable	Below 50

Figure 5.6 demonstrates the structure of printed electrodes for lithium-ion

batteries. Basically, the electrodes are fabricated layer by layer (Kapton-nickel layers-battery materials). In this research, commercial available LTO and NMC nanopowders are used as active materials for lithium-ion batteries due to the high stability in water. The sintered nickel electrode is conductive enough to act as current collectors as discussed before. The multi-layers electrodes after printing are shown in Figure 5.6 (a), which has excellent flexibility bended with 1cm radius of curvature without any obvious peeling off. The electrodes then assembled into a full cell and cycled from 0~2.5 V. The cycled positive electrode is shown in Figure 5.6 (b), which indicates nickel is very stable in $LiPF_6$ electrolyte with high working potential. The corrosion resistance of nickel is better than silver. The outstanding corrosion resistance is contributed to the thin dense oxidation layer on the nickel surface; oxidation has low electronical and thermal conductivities which prevent thermal sintering. However, the oxidation layer is the key prevent nickel bulk from oxidation furtherly at high operation potential without affecting the electronical conductivity significantly. The same positive protection mechanism is also shown on aluminum, but nickel is much more stable than aluminum at low operation potential because nickel does not form alloy structure with lithium like aluminum.

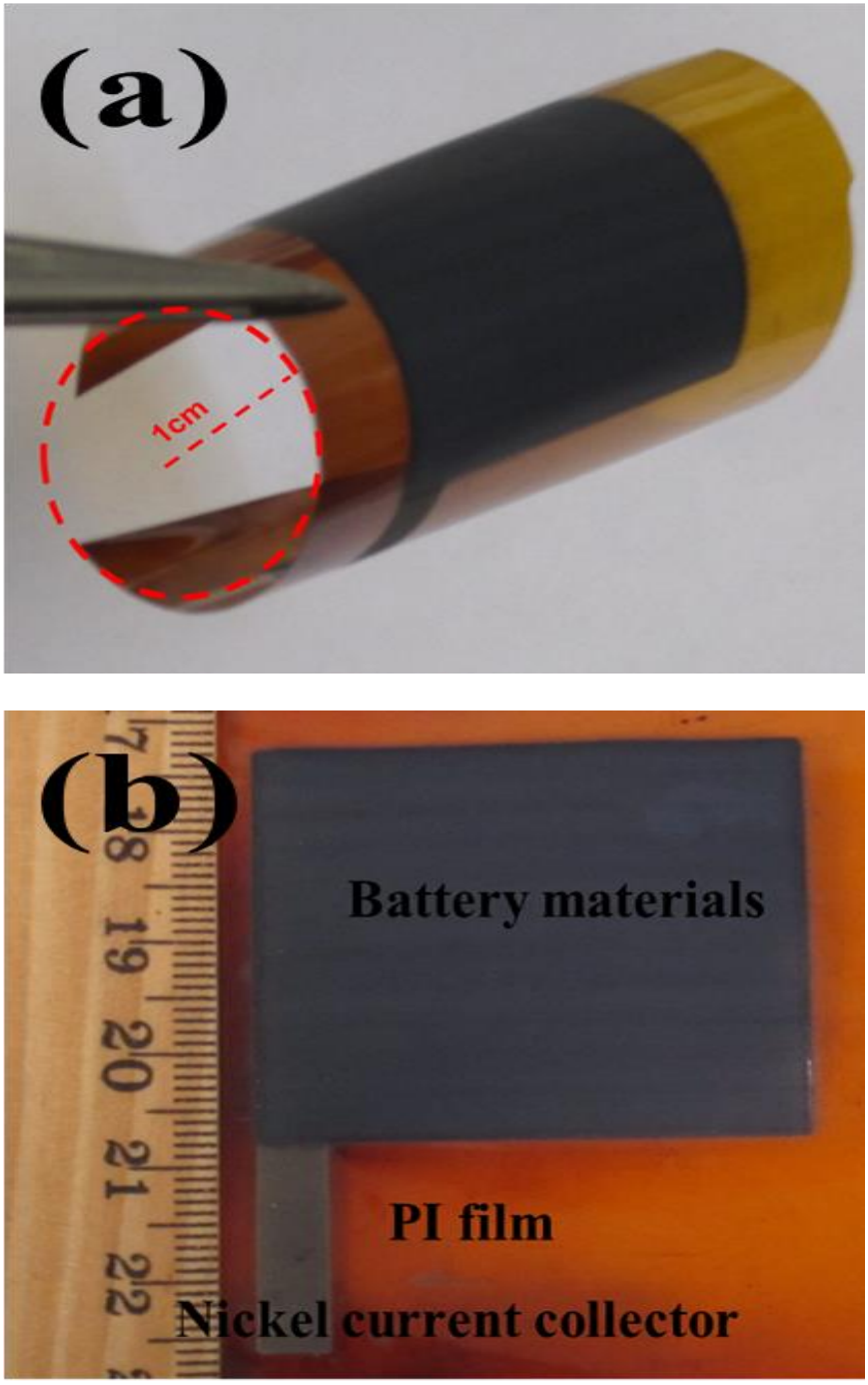

Figure 5.6 (a) Flexibility of printed electrodes with nickel conductive current collectors, the radius of curvature is around 1 cm; (b) Structure of flexible electrodes made by inkjet printing.

After nickel current collector deposition and thermal sintering, the cathode and anode mixture suspensions are printed on the nickel film. The cathode and anode then

dried at 100 ℃ to evaporate water solvents. Figure 5.7 (a) and (b) shows the XRD patterns of printed cathode and anode electrodes. The sintered nickel film is covered by a passivation layers which can protect further oxidation, also it can prevent potential corrosion from the cathode and anode inks which is confirmed by XRD: no obvious impurity is discovered. Nickel current collector has better corrosion resistance than the traditional aluminum and copper materials. This is crucial when water is used as solvent because aluminum and copper are very sensitive to the pH with the oxygen presents. XRD results also indicate the stability of NMC and LTO water suspension. NMC has better stability than LFP in water: a Li_3PO_4 layer of a few nanometers thick was observed and reported at the $LiFePO_4$ grains' surface after immersion in water. Li_3PO_4 accompanied by an increase of Fe^{III} percentage in the grains, which can cause loss of active materials. There is no similar phenomenon happens on NMC and LTO materials.

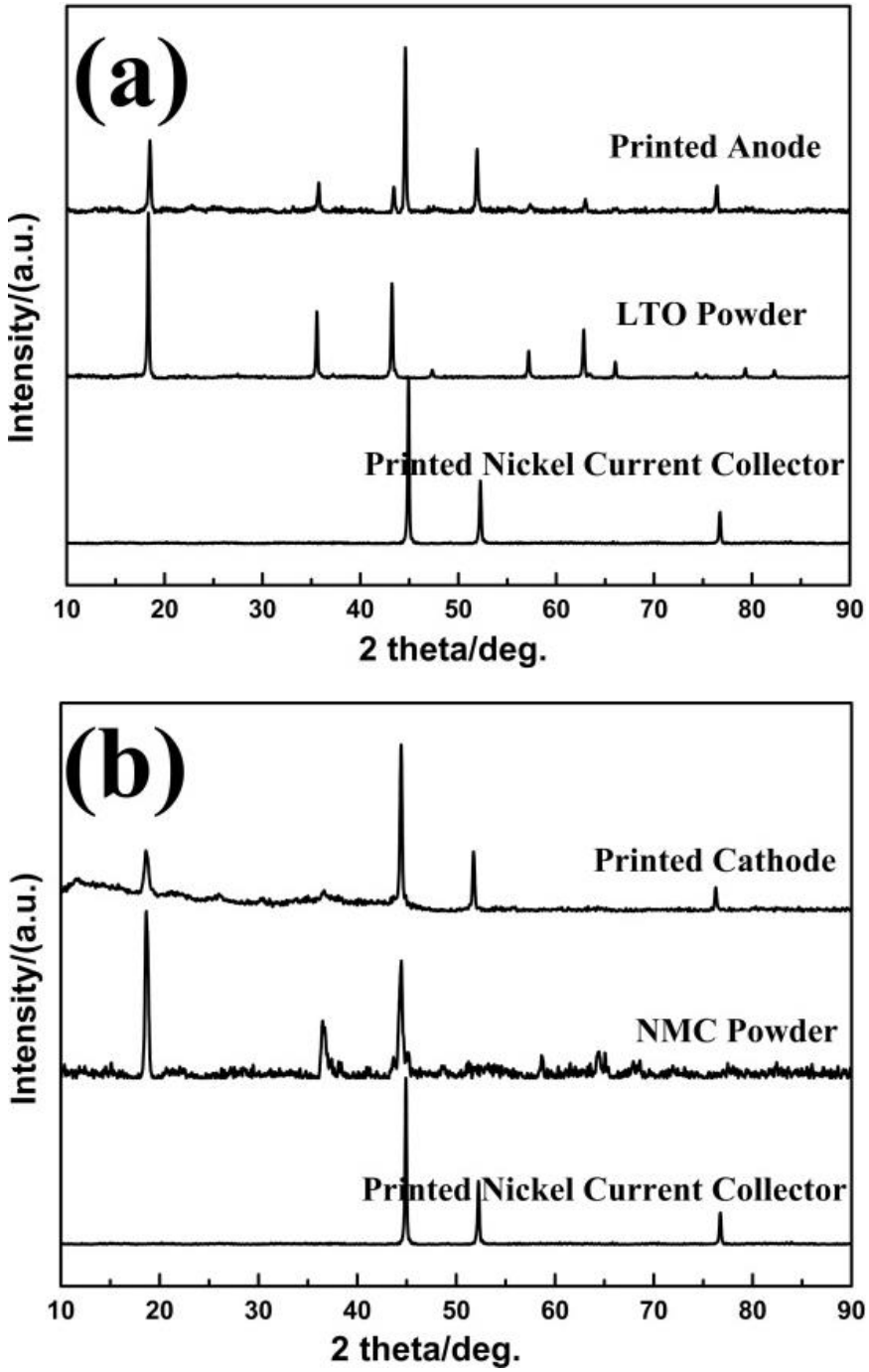

Figure 5.7 XRD patterns of printed (a) anode; (b) cathode electrodes.

The electrochemical cyclic voltammogram (CV) technology is used to test the corrosion resistance of the printed nickel film in the electrolyte (1M $LiPF_6$ in EC/EMC (3:7)) shown in Figure 5.8. The stainless steel is used as the comparison because stainless

steel is very stable as the current collector for lithium-ion batteries. A small chemical reactive signal is detected at ~3.8 V in the first cycle which represents the anode passivation process of nickel film. As talked before, nickel is covered with thin and dense oxidation passivation in air which prevents nickel from further oxidation. This oxidation passivation also protects nickel inside lithium-ion batteries below 3.8 V. The anodic current at a voltage of 3.8 V disappears with CV cycle number, indicating that the tolerance for corrosion is improved by the irreversible anodic reaction which produces more stable passivation layers. The second and the third cycles of nickel are closer to the stainless steel. Other research points out it could be Ni-P alloy (T. Liu et al., 2013) which has superior tolerance against electrolyte even the operating voltage is polarized up to 4.5 V. Pre-Phosphating treatments would benefits the stability of nickel film inside the batteries. CV characterization confirms nickel has potential usage for current collector in lithium-ion batteries.

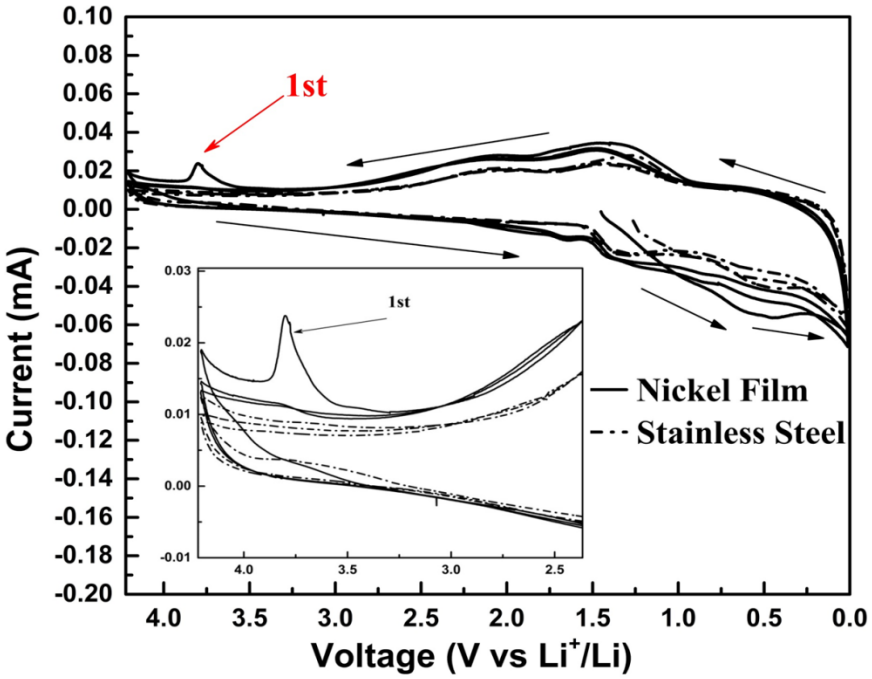

Figure 5.8 CV characterizations of nickel and stainless steel inside lithium-ion batteries.

Figure 5.9 (a) and (b) displays the surface morphology of printed LTO and NMC electrodes. The printed electrodes have smooth and uniform surface with no cracks. This is contributed by the layer by layer process of inkjet printing, which can control the deposition more precisely than tape-casting. The insert shows the thickness of the printed active layers which is around 2 μm. After battery assembly, the whole thickness of the battery is below 150 μm (50 μm for each Kapton substrate, 10 μm for the nickel conductive layer). Inkjet printing or other printing provide a much easier method to fabricate thin film batteries.

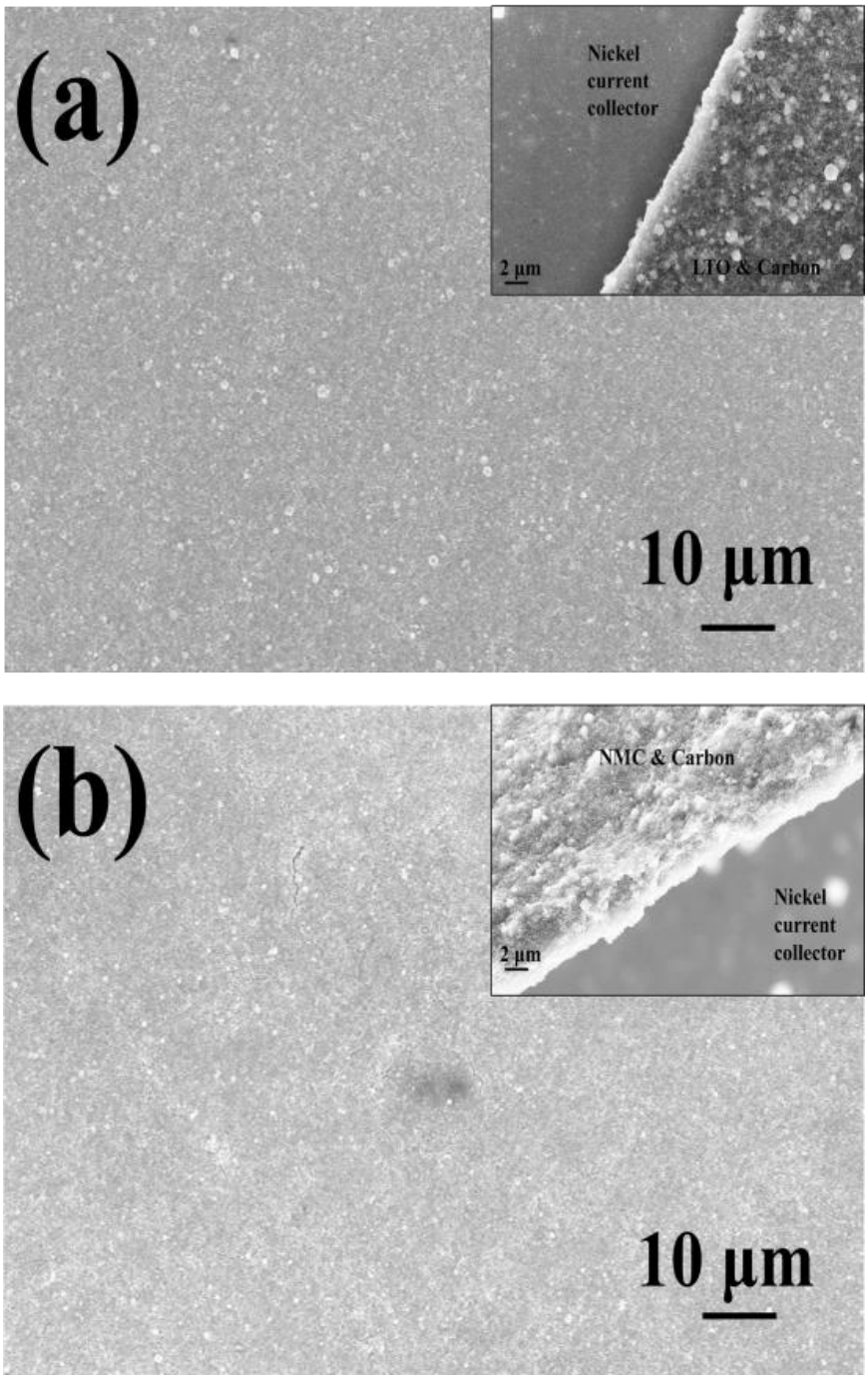

Figure 5.9 SEM images of printed (a) anode; (b) cathode electrodes. The inserts are the lay structure at the edge of the printed electrodes.

Figure 5.10 show first cycling of the flexible batteries. The first charge and discharge capacity of the battery is 106 mAh/g and 96 mAh/g. The capacity is calculated

by the cathode. The theoretical specific capacity of the NMC-LTO battery is around 160-170 mAh/g. The relative low capacity of the flexible battery is caused by unequal capacity between the cathode and anode. Usually full cells should have extra anode material to hold the lithium ions from the cathode material. The cut off voltage is set at 0.5-2.5 V, no obvious disturbance during charging and discharging curve means the good stability of nickel current collector inside the batteries. The polarization voltage between charging and discharging curve is around 250 mV which is very close to the traditional batteries; this indicates that low conductivity of printed nickel current collector does not have significant influence on the battery performance.

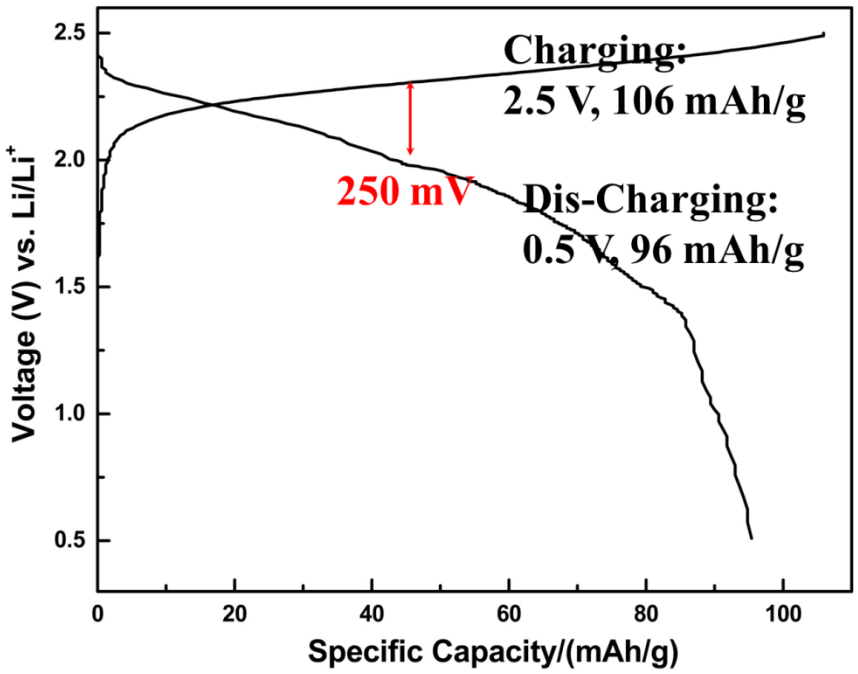

Figure 5.10 The first charge/discharge curves of flexible battery tested at 0.1 C current rates between 0.5-2.5 V at 25 ℃.

5.4 Summary and Conclusion

In summary, water based battery inks (cathode and anode) are synthesized, the inks are stable at room temperature and very suitable for inkjet printing. Water is used to replace chemically toxic organic solvent. The ink fabrication process and inkjet have no effect on the composition and performance of the active materials. Conventional batteries with traditional aluminum and copper current collectors are made by inkjet printing. The battery work very well with good mechanical flexibility. In order to make full printable lithium-ion batteries, two kinds of printed conductive films (silver and nickel) are synthesized and compared as current collector for printed batteries. Nickel shows more stable performance inside the battery during charging and discharging than silver. The silver current collector fails at 0.8 V which are caused by anodic dissolution (cathode part) and formation of silver-lithium alloy (anode part). This research indicate silver is not suitable for the fabrication of printable lithium-ion batteries. While nickel has outstanding chemical and physical stability during battery fabrication and battery charging and discharging, it has good corrosion resistance to the battery inks and stability at high potential. The stability of nickel is contributed by the passivate nickel oxidation layer which is very similar to the aluminum. Moreover, on nickel and lithium cannot form alloy during charging and discharging. The printed nickel has higher conductivity than the widely used carbon materials and does not affect the battery polarization very much. This research indicates inkjet printing is a good method to deposit material and fabricate thin film as electrodes for lithium-ion batteries.

CHAPTER 6

SUMMARY

The printable conductive inks and battery inks are synthesized and studied in this thesis. The biggest challenge of inkjet printing or digital printing is nozzle clogging which severely affects the final printing resolution and printing cost (cartridge and nozzle consumption). Water based particle free silver ink is a perfect solution to this problem. The resolution of printed conductive silver film is 40 μm which is the limitation of the DMP 2800 inkjet printer. Polymer and organic reductant are used to modify the properties of the silver ink which can uniform and smaller the silver particles which benefits to thermal sintering and conductivity. The conductivity of printed silver is about 50 % of the bulk.

Constantan nano particles ink is formulated by a novel Chemical Reducing Sintering (CRS process) which etches the oxidation layer and pre-join the constantan nano particles before thermal sintering. The plastic flow or solid diffusion can be triggered through the "bridge" among constantan nano particles which achieve sintering at relative low temperature. This is the first time to make constantan film by inkjet printing. The CRS process is then modified to make copper and nickel nano inks. The conductivity printed copper and nickel is 1.3 % and 1.4 % of the copper and nickel bulk.

The flexible lithium-ion battery is made by inkjet printing. Nickel ink is used to fabricate the current collectors inside the battery to replace the carbon or gold current collectors. The printed battery shows a good charge and discharge capacity and stability. More work is needed to replace the polymer separator using printable ceramics ink (like

Al_2O_3) to achieve 100 % printable lithium-ion batteries.

REFERENCES

Akamatsu, K., Ikeda, S., & Nawafune, H. (2003). Site-selective direct Silver metallization on surface-modified polyimide layers. *Langmuir, 19*(24), 10366-10371. doi:10.1021/la034888r

Akamatsu, K., Ikeda, S., & Nawafune, H. et al. (2004). Direct patterning of copper on polyimide using ion exchangeable surface templates generated by site-selective surface modification. *Journal of the American Chemical Society, 126*(35), 10822-10823. doi:10.1021/ja047700e

Akamatsu, K., Nakahashi, K., & Ikeda, S. et al. (2003). Fabrication and structural characterization of nanocomposites consisting of Ni nanoparticles dispersed in polyimide films. *The European Physical Journal D - Atomic, Molecular, Optical and Plasma Physics, 24*(1), 377-380. doi:10.1140/epjd/e2003-00116-7

Akamatsu, K., Shinkai, H., & Ikeda, S. et al. (2005). Controlling interparticle spacing among metal nanoparticles through metal-catalyzed decomposition of surrounding polymer matrix. *Journal of the American Chemical Society, 127*(22), 7980-7981. doi:10.1021/ja050735+

Amatucci, G. G., Badway, F., & Du Pasquier et al. (2001). An asymmetric hybrid nonaqueous energy storage cell. *Journal of The Electrochemical Society, 148*(8), A930-A939. doi:10.1149/1.1383553

Ammundsen, B., Jones, D. J., & Rozière, J. et al. (1996). Effect of chemical extraction of lithium on the local structure of spinel lithium manganese oxides determined by X-ray absorption spectroscopy. *Chemistry of Materials, 8*(12), 2799-2808. doi:10.1021/cm960287s

Arora, P., & Zhang, Z. (2004). Battery Separators. *Chemical Reviews, 104*(10), 4419-4462. doi:10.1021/cr020738u

Beecher, P., Servati, P., & Rozhin, A. et al. (2007). Ink-jet printing of carbon nanotube thin film transistors. *Journal of Applied Physics, 102*(4), 043710. doi:http://dx.doi.org/10.1063/1.2770835

Bishop, P., Ashfield, L., & Berzins, A. et al. (2010). Printed gold for electronic applications. *Gold Bulletin, 43*(3), 181-188.

Blake, P., Brimicombe, P. D., & Nair, R. R. et al. (2008). Graphene-based liquid crystal device. *nano letters, 8*(6), 1704-1708. doi:10.1021/nl080649i

Boulineau, A., Simonin, L., & Colin, J.-F. et al. (2013). First evidence of manganese–nickel segregation and densification upon cycling in Li-Rrich layered oxides for lithium batteries. *Nano Letters, 13*(8), 3857-3863. doi:10.1021/nl4019275

Brückner, W., Baunack, S., & Reiss, G. et al. (1995). Oxidation behaviour of Cu-Ni(Mn) (constantan) films. *Thin Solid Films, 258*(1–2), 252-259. doi:http://dx.doi.org/10.1016/0040-6090(94)06358-3

Calvert, P. (2001). Inkjet printing for materials and devices. *Chemistry of Materials, 13*(10), 3299-3305. doi:10.1021/cm0101632

Carlé, J. E., Andersen, T. R., & Helgesen, M. et al. (2013). A laboratory scale approach to polymer solar cells using one coating/printing machine, flexible substrates, no ITO, no vacuum and no spincoating. *Solar Energy Materials and Solar Cells*, *108*, 126-128. doi:http://dx.doi.org/10.1016/j.solmat.2012.09.008

Chen, J., Wang, S., & Cai, D. et al. (2014). Porous SiO2 as a separator to improve the electrochemical performance of spinel $LiMn2O_4$ cathode. *Journal of Membrane Science, 449*, 169-175. doi:http://dx.doi.org/10.1016/j.memsci.2013.08.028

Chen, J., Wang, S., & Ding, L. et al. (2014). Performance of through-hole anodic aluminum oxide membrane as a separator for lithium-ion battery. *Journal of Membrane Science, 461*, 22-27. doi:http://dx.doi.org/10.1016/j.memsci.2014.03.005

Chen, S.-P., Kao, Z.-K., & Lin, J.-L. et al. (2012). Silver conductive features on flexible substrates from a thermally accelerated chain reaction at low sintering temperatures. *ACS Applied Materials & Interfaces, 4*(12), 7064-7068. doi:10.1021/am302505j

Chew, S. Y., Ng, S. H., & Wang, J. et al. (2009). Flexible free-standing carbon nanotube films for model lithium-ion batteries. *Carbon, 47*(13), 2976-2983. doi:http://dx.doi.org/10.1016/j.carbon.2009.06.045

Cho, C.-K., Hwang, W.-J., & Eun, K. et al. (2011). Mechanical flexibility of transparent PEDOT:PSS electrodes prepared by gravure printing for flexible organic solar cells. *Solar Energy Materials and Solar Cells, 95*(12), 3269-3275. doi:http://dx.doi.org/10.1016/j.solmat.2011.07.009

Chong, J., Xun, S., & Zheng, H. et al. (2011). A comparative study of polyacrylic acid and poly(vinylidene difluoride) binders for spherical natural graphite/$LiFePO_4$ electrodes and cells. *Journal of Power Sources, 196*(18), 7707-7714.

Chung, J., Ko, S., & Bieri, N. R. et al. (2004). Conductor microstructures by laser curing of printed gold nanoparticle ink. *Applied Physics Letters, 84*(5), 801-803. doi:http://dx.doi.org/10.1063/1.1644907

Crone, B. K., Dodabalapur, A., & Sarpeshkar, R. et al. (2001). Design and fabrication of organic complementary circuits. *Journal of Applied Physics, 89*(9), 5125-5132. doi:10.1063/1.1362635

Dam, H. F., Andersen, T. R., & Madsen, M. V. et al. (2015). Roll and roll-to-roll process scaling through development of a compact flexo unit for printing of back electrodes. *Solar Energy Materials and Solar Cells, 140*, 187-192. doi:http://dx.doi.org/10.1016/j.solmat.2015.04.007

Daniel, M.-C., & Astruc, D. (2004). Gold nanoparticles: assembly, supramolecular chemistry, quantum-size-related properties, and applications toward biology, catalysis, and nanotechnology. *Chemical Reviews, 104*(1), 293-346. doi:10.1021/cr030698+

de las Casas, C., & Li, W. (2012). A review of application of carbon nanotubes for lithium ion battery anode material. *Journal of Power Sources, 208*, 74-85. doi:http://dx.doi.org/10.1016/j.jpowsour.2012.02.013

Dearden, A. L., Smith, P. J., & Shin, D.-Y. et al. (2005). A low curing temperature silver ink for use in ink-jet printing and subsequent production of conductive tracks. *Macromolecular Rapid Communications, 26*(4), 315-318. doi:10.1002/marc.200400445

Dong, Y., Li, X., & Liu, S. et al. (2015). Facile synthesis of high silver content MOD ink by using silver oxalate precursor for inkjet printing applications. *Thin Solid Films, 589*, 381-387. doi:http://dx.doi.org/10.1016/j.tsf.2015.06.001

Ederth, J., Johnsson, P., & Niklasson, G. A. et al. (2003). Electrical and optical properties of thin films consisting of tin-doped indium oxide nanoparticles. *Physical Review B, 68*(15), 155410.

Ervin, M. H., Le, L. T., & Lee, W. Y. (2014). Inkjet-printed flexible graphene-based supercapacitor. *Electrochimica Acta, 147*, 610-616. doi:http://dx.doi.org/10.1016/j.electacta.2014.10.006

Fan, Z., Wei, T., & Luo, G. et al. (2005). Fabrication and characterization of multi-walled carbon nanotubes-based ink. *Journal of Materials Science, 40*(18), 5075-5077. doi:10.1007/s10853-005-1622-7

Fjelstad, J. (2008). Flexible circuit materials. *Circuit World, 34*(4), 19-24. doi:10.1108/03056120810918088

Flexion Batteries. (2013). Retrieved from http://www.solicore.com/ (accessed on August 26,2016)

Fuller, S. B., Wilhelm, E. J., & Jacobson, J. M. (2002). Ink-jet printed nanoparticle microelectromechanical systems. *Microelectromechanical Systems, Journal of, 11*(1), 54-60. doi:10.1109/84.982863

Gao, Y., & Dahn, J. R. (1996). Correlation between the growth of the 3.3 V discharge plateau and capacity fading in $Li_{1+x}Mn_{2-x}O_4$ materials. *Solid State Ionics, 84*(1–2), 33-40. doi:http://dx.doi.org/10.1016/S0167-2738(96)83003-7

Global Battery Markets. (2011). Retrieved from http://batteryuniversity.com/learn/article/global_battery_markets (accessed on August 26,2016)

Goodenough, J. B. (1994). Design considerations. *Solid State Ionics, 69*(3), 184-198. doi:http://dx.doi.org/10.1016/0167-2738(94)90409-X

Grande, L., Chundi, V. T., & Wei, D. et al. (2012). Graphene for energy harvesting/storage devices and printed electronics. *Particuology, 10*(1), 1-8. doi:http://dx.doi.org/10.1016/j.partic.2011.12.001

Greer, J. R., & Street, R. A. (2007). Thermal cure effects on electrical performance of nanoparticle silver inks. *Acta Materialia, 55*(18), 6345-6349.

Grouchko, M., Kamyshny, A., & Magdassi, S. (2009). Formation of air-stable copper-silver core-shell nanoparticles for inkjet printing. *Journal of Materials Chemistry, 19*(19), 3057-3062. doi:10.1039/b821327e

Guerfi, A., Kaneko, M., & Petitclerc, M. et al. (2007). $LiFePO_4$ water-soluble binder electrode for Li-ion batteries. *Journal of Power Sources, 163*(2), 1047-1052. doi:http://dx.doi.org/10.1016/j.jpowsour.2006.09.067

Hahne, P., Hirth, E., & Reis, I. E. et al. (2001). Progress in thick-film pad printing technique for solar cells. *Solar Energy Materials and Solar Cells, 65*(1–4), 399-407. doi:http://dx.doi.org/10.1016/S0927-0248(00)00119-7

Harrey, P. M., Ramsey, B. J., & Evans, P. S. A. et al. (2002). Capacitive-type humidity sensors fabricated using the offset lithographic printing process. *Sensors and Actuators B: Chemical, 87*(2), 226-232. doi:http://dx.doi.org/10.1016/S0925-4005(02)00240-X

He, M., Zhang, X., & Jiang, K. et al. (2015). Pure inorganic separator for lithium ion batteries. *ACS Applied Materials & Interfaces, 7*(1), 738-742. doi:10.1021/am507145h

He, X., & Zervos, H. (2014). Flexible, printed and thin film batteries 2015-2025. Retrieved from http://www.idtechex.com/research/reports/flexible-printed-and-thin-film-batteries-2015-2025-000410.asp (accessed on August 26,2016) (accessed on August 26,2016)

Herrmann, J., Müller, K.-H., & Reda, T. et al. (2007). Nanoparticle films as sensitive strain gauges. *Applied Physics Letters, 91*(18), 183105. doi:http://dx.doi.org/10.1063/1.2805026

Heusing, S., de Oliveira, P. W., & Kraker, E. et al. (2009). Wet chemical deposited ITO coatings on flexible substrates for organic photodiodes. *Thin Solid Films, 518*(4), 1164-1169. doi:http://dx.doi.org/10.1016/j.tsf.2009.06.056

Hilder, M., Winther-Jensen, B., & Clark, N. B. (2009). Paper-based, printed zinc–air battery. *Journal of Power Sources, 194*(2), 1135-1141. doi:http://dx.doi.org/10.1016/j.jpowsour.2009.06.054

Hsien-Hsueh, L., Kan-Sen, C., & Kuo-Cheng, H. (2005). Inkjet printing of nanosized silver colloids. *Nanotechnology, 16*(10), 2436.

Hu, L., Wu, H., & La Mantia, F. et al. (2010). Thin, flexible secondary Li-ion paper batteries. *ACS Nano, 4*(10), 5843-5848. doi:10.1021/nn1018158

Huang, H., Yin, S.-C., & Nazar, L. F. (2001). Approaching theoretical capacity of $LiFePO_4$ at room temperature at high rates. *Electrochemical and Solid-State Letters, 4*(10), A170-A172. doi:10.1149/1.1396695

Huang, X., & Hitt, J. (2013). Lithium ion battery separators: Development and performance characterization of a composite membrane. *Journal of Membrane Science, 425–426*, 163-168. doi:http://dx.doi.org/10.1016/j.memsci.2012.09.027

Huggins, R. A., & Nix, W. D. (2000). Decrepitation model for capacity loss during cycling of alloys in rechargeable electrochemical systems. *Ionics (Kiel), 6*(1-2), 57-63.

Hunter, J. C. (1981). Preparation of a new crystal form of manganese dioxide: λ-MnO_2. *Journal of Solid State Chemistry, 39*(2), 142-147. doi:http://dx.doi.org/10.1016/0022-4596(81)90323-6

Hwang, S. S., Cho, C. G., & Park, K.-S. (2011). Stabilizing $LiCoO_2$ electrode with an overlayer of LiNi0.5Mn1.5O4 by using a Gravure printing method. *Electrochemistry Communications, 13*(3), 279-283. doi:http://dx.doi.org/10.1016/j.elecom.2011.01.003

Hyun-Jun, H., Wan-Ho, C., & Hak-Sung, K. (2012). In situ monitoring of flash-light sintering of copper nanoparticle ink for printed electronics. *Nanotechnology, 23*(48), 485205.

Jacoby, M. (2013). Batteries Get Flexible. *Chemical & Engineering News, 91*(18), 13-18.

Jahn, S. F., Blaudeck, T., & Baumann, R. R. et al. (2010). Inkjet printing of conductive silver patterns by using the first aqueous particle-free MOD ink without additional stabilizing ligands. *Chemistry of Materials, 22*(10), 3067-3071. doi:10.1021/cm9036428

Jang, S., Seo, Y., & Choi, J. et al. (2010). Sintering of inkjet printed copper nanoparticles for flexible electronics. *Scripta Materialia, 62*(5), 258-261. doi:http://dx.doi.org/10.1016/j.scriptamat.2009.11.011

Jarvis, K. A., Deng, Z., & Allard, L. F. et al. (2011). Atomic structure of a lithium-rich layered oxide material for lithium-ion batteries: evidence of a solid solution. *Chemistry of Materials, 23*(16), 3614-3621. doi:10.1021/cm200831c

Joshi, N., & Banerjee, S. (2015). PVP coated copper–iron oxide nanocomposite as an efficient catalyst for click reactions. *Tetrahedron Letters, 56*(28), 4163-4169. doi:http://dx.doi.org/10.1016/j.tetlet.2015.05.011

Julien, C. M., Mauger, A., & Groult, H. et al. (2010). $LiCo_{1-y}B_yO_2$ as cathode materials for rechargeable lithium batteries. *Chemistry of Materials, 23*(2), 208-218. doi:10.1021/cm1026865

Julien, C. M., Mauger, A., & Zaghib, K. et al. (2014). Comparative issues of cathode materials for Li-ion batteries. *Inorganics, 2*(1), 132-154.

Kaempgen, M., Chan, C. K., & Ma, J. et al. (2009). Printable thin film supercapacitors using single-walled carbon nanotubes. *nano letters, 9*(5), 1872-1876. doi:10.1021/nl8038579

Kamyshny, A., Steinke, J., & Magdassi, S. (2011). Metal-based inkjet inks for printed electronics. *The Open Applied Physics Journal, 4*(1).

Kang, J. S., Kim, H. S., & Ryu, J. et al. (2010). Inkjet printed electronics using copper nanoparticle ink. *Journal of Materials Science: Materials in Electronics, 21*(11), 1213-1220. doi:10.1007/s10854-009-0049-3

Kang, J. S., Ryu, J., & Kim, H. S. et al. (2011). Sintering of inkjet-printed silver nanoparticles at room temperature using intense pulsed light. *Journal of Electronic Materials, 40*(11), 2268-2277. doi:10.1007/s11664-011-1711-0

Kim, D., Jeong, S., & Lee, S. et al. (2007). Organic thin film transistor using silver electrodes by the ink-jet printing technology. *Thin Solid Films, 515*(19), 7692-7696. doi:http://dx.doi.org/10.1016/j.tsf.2006.11.141

Kim, H.-S., Dhage, S. R., & Shim, D.-E. et al. (2009). Intense pulsed light sintering of copper nanoink for printed electronics. *Applied Physics A, 97*(4), 791-798. doi:10.1007/s00339-009-5360-6

Kim, M., Han, G. Y., & Yoon, K. J. et al. (2010). Preparation of a trilayer separator and its application to lithium-ion batteries. *Journal of Power Sources, 195*(24), 8302-8305. doi:http://dx.doi.org/10.1016/j.jpowsour.2010.07.016

Kim, S.-P., Datta, D., & Shenoy, V. B. (2014). Atomistic mechanisms of phase boundary evolution during initial lithiation of crystalline silicon. *Meeting Abstracts, MA2014-02*(5), 276.

Kim, Y., Lee, B., & Yang, S. et al. (2012). Use of copper ink for fabricating conductive electrodes and RFID antenna tags by screen printing. *Current Applied Physics, 12*(2), 473-478. doi:http://dx.doi.org/10.1016/j.cap.2011.08.003

Koo, M., Park, K.-I., & Lee, S. H. et al. (2012). Bendable inorganic thin-film battery for fully flexible electronic systems. *Nano Letters, 12*, 4810-4816.

Kopola, P., Aernouts, T., & Sliz, R. et al. (2011). Gravure printed flexible organic photovoltaic modules. *Solar Energy Materials and Solar Cells, 95*(5), 1344-1347. doi:http://dx.doi.org/10.1016/j.solmat.2010.12.020

Kraus, T., Malaquin, L., & Schmid, H. et al. (2007). Nanoparticle printing with single-particle resolution. *Nat Nano, 2*(9), 570-576. doi:http://www.nature.com/nnano/journal/v2/n9/suppinfo/nnano.2007.262_S1.html

Krebs, F. C. (2009a). All solution roll-to-roll processed polymer solar cells free from indium-tin-oxide and vacuum coating steps. *Organic Electronics, 10*(5), 761-768. doi:http://dx.doi.org/10.1016/j.orgel.2009.03.009

Krebs, F. C. (2009b). Pad printing as a film forming technique for polymer solar cells. *Solar Energy Materials and Solar Cells, 93*(4), 484-490. doi:http://dx.doi.org/10.1016/j.solmat.2008.09.003

Krebs, F. C. (2009). Polymer solar cell modules prepared using roll-to-roll methods: knife-over-edge coating, slot-die coating and screen printing. *Solar Energy Materials and Solar Cells, 93*(4), 465-475.

Krebs, F. C. (2009c). Roll-to-roll fabrication of monolithic large-area polymer solar cells free from indium-tin-oxide. *Solar Energy Materials and Solar Cells, 93*(9), 1636-1641. doi:http://dx.doi.org/10.1016/j.solmat.2009.04.020

Lee, B., Kim, Y., & Yang, S. et al. (2009). A low-cure-temperature copper nano ink for highly conductive printed electrodes. *Current Applied Physics, 9*(2), e157-e160.

Lee, E., Park, S. J., & Cho, J. W. et al. (2011). Nearly carbon-free printable CIGS thin films for solar cell applications. *Solar Energy Materials and Solar Cells, 95*(10), 2928-2932.

Lee, H., Yanilmaz, M., & Toprakci, O. et al. (2014). A review of recent developments in membrane separators for rechargeable lithium-ion batteries. *Energy & Environmental Science, 7*(12), 3857-3886. doi:10.1039/c4ee01432d

Lee, H. M., Choi, S.-Y., & Jung, A. (2013). Direct deposition of highly conductive aluminum thin film on substrate by solution-dipping process. *ACS Applied Materials & Interfaces, 5*(11), 4581-4585. doi:10.1021/am400812e

Lee, H. M., Lee, H. B., & Jung, D. S. et al. (2012). Solution processed aluminum paper for flexible electronics. *Langmuir, 28*(36), 13127-13135. doi:10.1021/la302479x

Lee, H. M., Seo, J. Y., & Jung, A. et al. (2014). Long-term sustainable aluminum precursor solution for highly conductive thin films on rigid and flexible substrates. *ACS Applied Materials & Interfaces, 6*(17), 15480-15487. doi:10.1021/am504134f

Lee, J., Lee, C.-L., & Park, K. et al. (2014). Synthesis of an Al_2O_3-coated polyimide nanofiber mat and its electrochemical characteristics as a separator for lithium ion batteries. *Journal of Power Sources, 248*, 1211-1217. doi:http://dx.doi.org/10.1016/j.jpowsour.2013.10.056

Lemme, M. C., Echtermeyer, T. J., & Baus, M. et al. (2007). A graphene field-effect device. *IEEE Electron Device Letters, 28*(4), 282-284. doi:10.1109/led.2007.891668

Leung, S. Y. Y., & Lam, D. C. C. (2008). Geometric and compaction dependence of printed polymer-based RFID tag antenna performance. *Electronics Packaging Manufacturing, IEEE Transactions on, 31*(2), 120-125. doi:10.1109/tepm.2008.919334

Leyland, N. S., Evans, J. R., & Harrison, D. J. (2002). Lithographic printing of force-sensitive resistors. *Journal of Materials Science: Materials in Electronics, 13*(7), 387-390.

Li, D., Sutton, D., & Burgess, A. et al. (2009). Conductive copper and nickel lines via reactive inkjet printing. *Journal of Materials Chemistry, 19*(22), 3719-3724.

Li, Y., Lu, Q., & Qian, X. et al. (2004). Preparation of surface bound silver nanoparticles on polyimide by surface modification method and its application on electroless metal deposition. *Applied Surface Science, 233*(1–4), 299-306. doi:http://dx.doi.org/10.1016/j.apsusc.2004.03.235

Li, Y., Wu, Y., & Ong, B. S. (2005). Facile synthesis of silver nanoparticles useful for fabrication of high-conductivity elements for printed electronics. *Journal of the American Chemical Society, 127*(10), 3266-3267. doi:10.1021/ja043425k

Liu, Q., Wang, S., & Tan, H. et al. (2013). Preparation and doping mode of doped $LiMn_2O_4$ for Li-Ion batteries. *Energies, 6*(3), 1718-1730.

Liu, T., Zhao, L., & Wang, D. et al. (2013). Corrosion resistance of nickel foam modified with electroless Ni-P alloy as positive current collector in a lithium ion battery. *RSC Advances, 3*(48), 25648-25651. doi:10.1039/c3ra43568g

Ma, S., Bromberg, V., & Egitto, F. D. et al. (2013). Low temperature plasma sintering of silver nanoparticles for potential flexible electronics applications. *MRS Online Proceedings Library Archive, 1529*, mrsf12-1529-ww1506-1514 (1526 pages). doi:10.1557/opl.2012.1718

Ma, S., Bromberg, V., & Liu, L. et al. (2014). Low temperature plasma sintering of silver nanoparticles. *Applied Surface Science, 293*, 207-215. doi:http://dx.doi.org/10.1016/j.apsusc.2013.12.135

Magdassi, S., Bassa, A., & Vinetsky, Y. et al. (2003). Silver nanoparticles as pigments for water-based ink-jet inks. *Chemistry of Materials, 15*(11), 2208-2217. doi:10.1021/cm021804b

Maideen, N., Sahudin, S., & Yahya, N. M., et al. (2016). *Practical Framework: Implementing OEE Method in Manufacturing Process Environment.* Paper presented at the IOP Conference Series: Materials Science and Engineering.

Maleki, H., Deng, G., & Kerzhner-Haller, I. et al. (2000). Thermal stability studies of binder materials in anodes for lithium-ion batteries. *Journal of The Electrochemical Society, 147*(12), 4470-4475.

Mark, L. A., Mikko, A., & Tomi, M. et al. (2008). Electrical sintering of nanoparticle structures. *Nanotechnology, 19*(17), 175201.

Mei, A., Li, X., & Liu, L. et al. (2014). A hole-conductor–free, fully printable mesoscopic perovskite solar cell with high stability. *Science, 345*(6194), 295-298. doi:10.1126/science.1254763

Merilampi, S., Laine-Ma, T., & Ruuskanen, P. (2009). The characterization of electrically conductive silver ink patterns on flexible substrates. *Microelectronics Reliability, 49*(7), 782-790. doi:http://dx.doi.org/10.1016/j.microrel.2009.04.004

Mooring, L., Karousos, N. G., & Livingstone, C. et al. (2005). Evaluation of a novel pad printing technique for the fabrication of disposable electrode assemblies. *Sensors and Actuators B: Chemical, 107*(2), 491-496. doi:http://dx.doi.org/10.1016/j.snb.2004.11.005

Mukhopadhyay, A., & Sheldon, B. W. (2014). Deformation and stress in electrode materials for Li-ion batteries. *Progress in Materials Science, 63*, 58-116.

Myung, S.-T., Kumagai, N., & Komaba, S. et al. (2001). Effects of Al doping on the microstructure of LiCoO2 cathode materials. *Solid State Ionics, 139*(1–2), 47-56. doi:http://dx.doi.org/10.1016/S0167-2738(00)00828-6

Nanda, K., Sahu, S., & Behera, S. (2002). Liquid-drop model for the size-dependent melting of low-dimensional systems. *Physical Review A, 66*(1), 013208.

Ng, J. H. G., Desmulliez, M. P. Y., & Lamponi, M. et al. (2009). A direct-writing approach to the micro-patterning of copper onto polyimide. *Circuit World, 35*(2), 3-17. doi:10.1108/03056120910953268

Nie, X., Wang, H., & Zou, J. (2012). Inkjet printing of silver citrate conductive ink on PET substrate. *Applied Surface Science, 261*, 554-560. doi:http://dx.doi.org/10.1016/j.apsusc.2012.08.054

Nir, M. M., Zamir, D., & Haymov, I. et al. (2010). Electrically conductive inks for inkjet printing. *The chemistry of inkjet inks. New Jersey-London-Singapore: World Scientific*, 225-254.

Nishide, H., & Oyaizu, K. (2008). Toward flexible batteries. *Science, 319*(5864), 737-738.

Norita, S., Kumaki, D., & Kobayashi, Y. et al. (2015). Inkjet-printed copper electrodes using photonic sintering and their application to organic thin-film transistors. *Organic Electronics, 25*, 131-134. doi:http://dx.doi.org/10.1016/j.orgel.2015.06.026

Oishi, M., Fujimoto, T., & Takanashi, Y. et al. (2013). Charge compensation mechanisms in $Li_{1.16}Ni_{0.15}Co_{0.19}Mn_{0.50}O_2$ positive electrode material for Li-ion batteries analyzed by a combination of hard and soft X-ray absorption near edge structure. *Journal of Power Sources, 222*, 45-51.

Park, B. K., Kim, D., & Jeong, S. et al. (2007). Direct writing of copper conductive patterns by ink-jet printing. *Thin Solid Films, 515*(19), 7706-7711. doi:http://dx.doi.org/10.1016/j.tsf.2006.11.142

Park, S.-H., Chung, W.-H., & Kim, H.-S. (2014). Temperature changes of copper nanoparticle ink during flash light sintering. *Journal of Materials Processing Technology, 214*(11), 2730-2738. doi:http://dx.doi.org/10.1016/j.jmatprotec.2014.06.007

Pastoriza-Santos, I., & Liz-Marzán, L. M. (2000). Reduction of silver nanoparticles in DMF Formation of monolayers and stable colloids. *Pure and Applied Chemistry, 72*, 83-90.

Patterson, A. L. (1939). The Scherrer formula for X-ray particle size determination. *Physical Review, 56*(10), 978-982.

Pech, D., Brunet, M., & Taberna, P.-L. et al. (2010). Elaboration of a microstructured inkjet-printed carbon electrochemical capacitor. *Journal of Power Sources, 195*(4), 1266-1269. doi:http://dx.doi.org/10.1016/j.jpowsour.2009.08.085

Peramunage, D., & Abraham, K. M. (1998). Preparation of micron-sized $Li_4Ti_5O_{12}$ and its electrochemistry in polyacrylonitrile electrolyte-based lithium cells. *Journal of The Electrochemical Society, 145*(8), 2609-2615. doi:10.1149/1.1838689

Perelaer, J., de Gans, B. J., & Schubert, U. S. (2006). Ink-jet printing and microwave sintering of conductive silver tracks. *Advanced Materials, 18*(16), 2101-2104. doi:10.1002/adma.200502422

Pikul, J. H., Gang Zhang, H., & Cho, J. et al. (2013). High-power lithium ion microbatteries from interdigitated three-dimensional bicontinuous nanoporous electrodes. *Nat Commun, 4*, 1732. doi:10.1038/ncomms2747

Pudas, M., Hagberg, J., & Leppävuori, S. (2004). Gravure offset printing of polymer inks for conductors. *Progress in Organic Coatings, 49*(4), 324-335. doi:http://dx.doi.org/10.1016/j.porgcoat.2003.09.013

Pudas, M., Halonen, N., & Granat, P. et al. (2005). Gravure printing of conductive particulate polymer inks on flexible substrates. *Progress in Organic Coatings, 54*(4), 310-316. doi:http://dx.doi.org/10.1016/j.porgcoat.2005.07.008

Qi, W. H. (2005). Size effect on melting temperature of nanosolids. *Physica B: Condensed Matter, 368*(1–4), 46-50. doi:http://dx.doi.org/10.1016/j.physb.2005.06.035

Qiao, Q. Q., Zhang, H. Z., & Li, G. R. et al. (2013). Surface modification of Li-rich layered $Li(Li_{0.17}Ni_{0.25}Mn_{0.58})O_2$ oxide with Li-Mn-PO_4 as the cathode for lithium-ion batteries. *Journal of Materials Chemistry A, 1*(17), 5262-5268. doi:10.1039/c3ta00028a

Qin, G., Watanabe, A., & Tsukamoto, H. et al. (2014). Copper film prepared from copper fine particle paste by laser sintering at room temperature: Influences of sintering atmosphere on the morphology and resistivity. *Japanese Journal of Applied Physics, 53*(9), 096501.

Redinger, D., Molesa, S., Shong, Y., & Farschi, R. et al. (2004). An ink-jet-deposited passive component process for RFID. *IEEE Transactions on Electron Devices, 51*(12), 1978-1983. doi:10.1109/ted.2004.838451

Reinhold, I., Hendriks, C. E., & Eckardt, R. et al. (2009). Argon plasma sintering of inkjet printed silver tracks on polymer substrates. *Journal of Materials Chemistry, 19*(21), 3384-3388. doi:10.1039/b823329b

Rivera, M. (2012). Current and next-generation energy storage devices for micro vehicle applications. *SAE International Journal of Materials and Manufacturing, 5*(1), 19-29.

Roy, R., Agrawal, D., & Cheng, J., et al. (1999). Full sintering of powdered-metal bodies in a microwave field. *Nature, 399*(6737), 668-670.

Ryu, J., Kim, H.-S., & Hahn, H. T. (2010). Reactive sintering of copper nanoparticles using intense pulsed light for printed electronics. *Journal of Electronic Materials, 40*(1), 42-50. doi:10.1007/s11664-010-1384-0

Sangoi, R., Smith, C. G., & Seymour, M. D. et al. (2005). Printing radio frequency identification (RFID) tag antennas using inks containing silver dispersions. *Journal of Dispersion Science and Technology, 25*(4), 513-521. doi:10.1081/dis-200025721

Sarkar, A., Mukherjee, T., & Kapoor, S. (2008). PVP-stabilized copper nanoparticles: A reusable catalyst for "click" reaction between terminal alkynes and azides in nonaqueous solvents. *The Journal of Physical Chemistry C, 112*(9), 3334-3340. doi:10.1021/jp077603i

Schmidt, H., Flügge, H., & Winkler, T. et al. (2009). Efficient semitransparent inverted organic solar cells with indium tin oxide top electrode. *Applied Physics Letters, 94*(24), 243302. doi:http://dx.doi.org/10.1063/1.3154556

Scrosati, B., & Garche, J. (2010). Lithium batteries: Status, prospects and future. *Journal of Power Sources, 195*(9), 2419-2430. doi:http://dx.doi.org/10.1016/j.jpowsour.2009.11.048

Shaheen, S. E., Radspinner, R., & Peyghambarian, N. et al. (2001). Fabrication of bulk heterojunction plastic solar cells by screen printing. *Applied Physics Letters, 79*(18), 2996-2998. doi:http://dx.doi.org/10.1063/1.1413501

Shin, K. Y., Hong, J. Y., & Jang, J. (2011). Micropatterning of graphene sheets by inkjet printing and its wideband dipole-antenna application. *Advanced Materials, 23*(18), 2113-2118.

Shipway, A. N., Katz, E., & Willner, I. (2000). Nanoparticle arrays on surfaces for electronic, optical, and sensor applications. *ChemPhysChem, 1*(1), 18-52. doi:10.1002/1439-7641(20000804)1:1<18::aid-cphc18>3.0.co;2-l

Silverbrook, K. (2002). Method of manufacture of a thermoelastic bend actuator using PTFE and corrugated copper ink jet printer: Google Patents (US 6416679 B1).

Skripov, V. P., Koverda, V. P., & Skokov, V. N. (1981). Size effect on melting of small particles. *physica status solidi (a), 66*(1), 109-118. doi:10.1002/pssa.2210660111

Slistan-Grijalva, A., Herrera-Urbina, R., & Rivas-Silva, J. F. et al. (2008). Synthesis of silver nanoparticles in a polyvinylpyrrolidone (PVP) paste, and their optical properties in a film and in ethylene glycol. *Materials Research Bulletin, 43*(1), 90-96. doi:http://dx.doi.org/10.1016/j.materresbull.2007.02.013

Sousa, R. E., Oliveira, J., & Gören, A. et al. (2016). High performance screen printable lithium-ion battery cathode ink based on C-LiFePO_4. *Electrochimica Acta, 196*, 92-100. doi:http://dx.doi.org/10.1016/j.electacta.2016.02.189

Southee, D., Hay, G. I., & Evans, P. S. et al. (2007). Lithographically printed voltaic cells-a feasibility study. *Circuit World, 33*(1), 31-35.

Stanciu, L. A., Raether, F., & Groza, J. (2016). In-situ sintering studies on nano-alumina. *une, 13*, 15.

Subramanian, V., Fréchet, J. M. J., & Chang, P. C. et al. (2005). Progress toward development of all-printed RFID tags: Materials, processes, and devices. *Proceedings of the IEEE, 93*(7), 1330-1338. doi:10.1109/jproc.2005.850305

Sun, K., Wei, T. S., & Ahn, B. Y. et al. (2013). 3D printing of interdigitated Li-ion microbattery architectures. *Advanced Materials, 25*(33), 4539-4543.

Sun, Y.-K., Lee, M.-J., & Yoon, C. S. et al. (2012). The role of AlF_3 coatings in improving electrochemical cycling of Li-enriched nickel-manganese oxide electrodes for Li-ion batteries. *Advanced Materials, 24*(9), 1192-1196. doi:10.1002/adma.201104106

Suren, S., & Kheawhom, S. (2016). Development of a high energy density flexible zinc-air battery. *Journal of The Electrochemical Society, 163*(6), A846-A850. doi:10.1149/2.0361606jes

Szczech, J. B., Megaridis, C. M., & Gamota, D. R. et al. (2002). Fine-line conductor manufacturing using drop-on demand PZT printing technology. *Electronics Packaging Manufacturing, IEEE Transactions on, 25*(1), 26-33. doi:10.1109/tepm.2002.1000480

Taillades, G., & Sarradin, J. (2004). Silver: High performance anode for thin film lithium ion batteries. *Journal of Power Sources, 125*(2), 199-205. doi:http://dx.doi.org/10.1016/j.jpowsour.2003.07.004

Tan, Y. W., Zhang, Y., & Bolotin, K. et al. (2007). Measurement of scattering rate and minimum conductivity in graphene. *Physical Review Letters, 99*(24), 246803.

Tang, X.-F., Yang, Z.-G., & Wang, W.-J. (2010). A simple way of preparing high-concentration and high-purity nano copper colloid for conductive ink in inkjet printing technology. *Colloids and Surfaces A: Physicochemical and Engineering Aspects, 360*(1–3), 99-104. doi:http://dx.doi.org/10.1016/j.colsurfa.2010.02.011

Tehrani, Z., Korochkina, T., & Govindarajan, S. et al. (2015). Ultra-thin flexible screen printed rechargeable polymer battery for wearable electronic applications. *Organic Electronics, 26*, 386-394. doi:http://dx.doi.org/10.1016/j.orgel.2015.08.007

Teki, R., Datta, M. K., & Krishnan, R. et al. (2009). Nanostructured silicon anodes for lithium ion rechargeable batteries. *Small, 5*(20), 2236-2242.

Tortorich, R. P., Song, E., & Choi, J.-W. (2014). Inkjet-printed carbon nanotube electrodes with low sheet resistance for electrochemical sensor applications. *Journal of The Electrochemical Society, 161*(2), B3044-B3048.

United States Environmental Protection Agency (2006). Retrieved from http://www.epa.gov/opprd001/inerts/methyl.pdf (accessed on August 26,2016)

Vaillancourt, J., Zhang, H., & Vasinajindakaw, P. et al. (2008). All ink-jet-printed carbon nanotube thin-film transistor on a polyimide substrate with an ultrahigh operating frequency of over 5 GHz. *Applied Physics Letters, 93*(24), 243301. doi:http://dx.doi.org/10.1063/1.3043682

Van Osch, T. H., Perelaer, J., & de Laat, A. W. et al. (2008). Inkjet printing of narrow conductive tracks on untreated polymeric substrates. *Advanced Materials, 20*(2), 343-345.

Volkman, S. K., Pei, Y., & Redinger, D. et al. (2004). *Ink-jetted silver/copper conductors for printed RFID applications.* Paper presented at the MRS Proceedings.

Wang, H., Li, Q., & Gao, C. (2014). Preparation of nanometer nickel powder from spent electroless nickel plating baths by using thiourea dioxide as a green reductant. *Journal of Cleaner Production, 84*, 701-706. doi:http://dx.doi.org/10.1016/j.jclepro.2014.03.091

Wang, H., Qiao, X., & Chen, J. et al. (2005). Mechanisms of PVP in the preparation of silver nanoparticles. *Materials Chemistry and Physics, 94*(2–3), 449-453. doi:http://dx.doi.org/10.1016/j.matchemphys.2005.05.005

Wang, Q., Ping, P., & Zhao, X. et al. (2012). Thermal runaway caused fire and explosion of lithium ion battery. *Journal of Power Sources, 208*, 210-224. doi:http://dx.doi.org/10.1016/j.jpowsour.2012.02.038

Wang, X., Lu, X., & Liu, B. et al. (2014). Flexible energy-storage devices: Design consideration and recent progress. *Advanced Materials, 26*(28), 4763-4782. doi:10.1002/adma.201400910

Wang, Z., Winslow, R., & Madan, D. et al. (2014). Development of MnO_2 cathode inks for flexographically printed rechargeable zinc-based battery. *Journal of Power Sources, 268*, 246-254. doi:http://dx.doi.org/10.1016/j.jpowsour.2014.06.032

Wee, G., Salim, T., & Lam, Y. M. et al. (2011). Printable photo-supercapacitor using single-walled carbon nanotubes. *Energy & Environmental Science, 4*(2), 413-416. doi:10.1039/c0ee00296h

Wen, Y., He, K., & Zhu, Y. et al. (2014). Expanded graphite as superior anode for sodium-ion batteries. *Nat Commun, 5*. doi:10.1038/ncomms5033

Wolfer, T., Bollgruen, P., & Mager, D. et al. (2014). Flexographic and inkjet printing of polymer optical waveguides for fully integrated sensor systems. *Procedia Technology, 15*, 521-529.

Wu, A., Gu, Y., & Beck, C. et al. (2014). Reversible chromatic sensor fabricated by inkjet printing TCDA-ZnO on a paper substrate. *Sensors and Actuators B: Chemical, 193*, 10-18. doi:http://dx.doi.org/10.1016/j.snb.2013.10.130

Wu, C.-J., Cheng, S.-L., & Sheng, Y.-J. et al. (2015). Reduction-assisted sintering of micron-sized copper powders at low temperature by ethanol vapor. *RSC Advances, 5*(66), 53275-53279. doi:10.1039/c5ra08167j

Wu, F., Li, N., & Su, Y. et al. (2013). Spinel/layered heterostructured cathode material for high-capacity and high-rate Li-ion batteries. *Advanced Materials, 25*(27), 3722-3726. doi:10.1002/adma.201300598

Wu, J.-T., Hsu, S. L.-C., & Tsai, M.-H. et al. (2009). Conductive silver patterns via ethylene glycol vapor reduction of ink-jet printed silver nitrate tracks on a polyimide substrate. *Thin Solid Films, 517*(20), 5913-5917. doi:http://dx.doi.org/10.1016/j.tsf.2009.04.049

Wu, J.-T., Hsu, S. L.-C., & Tsai, M.-H. et al. (2011). Inkjet printing of low-temperature cured silver patterns by using $AgNO_3$/1-dimethylamino-2-propanol inks on polymer substrates. *The Journal of Physical Chemistry C, 115*(22), 10940-10945. doi:10.1021/jp200972y

Wu, S.-H., & Chen, D.-H. (2004). Synthesis of high-concentration Cu nanoparticles in aqueous CTAB solutions. *Journal of Colloid and Interface Science, 273*(1), 165-169. doi:http://dx.doi.org/10.1016/j.jcis.2004.01.071

Wu, Y., Li, Y., & Ong, B. S. (2006). Printed silver ohmic contacts for high-mobility organic thin-film transistors. *Journal of the American Chemical Society, 128*(13), 4202-4203.

Wu, Y., Li, Y., & Ong, B. S. (2007). A simple and efficient approach to a printable silver conductor for printed electronics. *Journal of the American Chemical Society, 129*(7), 1862-1863.

Wunscher, S., Stumpf, S., & Perelaer, J. et al. (2014). Towards single-pass plasma sintering: temperature influence of atmospheric pressure plasma sintering of silver nanoparticle ink. *Journal of Materials Chemistry C, 2*(9), 1642-1649. doi:10.1039/c3tc32120g

Wünscher, S., Stumpf, S., & Perelaer, J. et al. (2014). Towards single-pass plasma sintering: temperature influence of atmospheric pressure plasma sintering of silver nanoparticle ink. *Journal of Materials Chemistry C, 2*(9), 1642-1649.

Xia, Y., Yang, P., & Sun, Y. et al. (2003). One-dimensional nanostructures: Synthesis, characterization, and applications. *Advanced Materials, 15*(5), 353-389.

Xia, Y., & Yoshio, M. (1996). Aninvestigation of lithium ion insertion into spinel structure Li-Mn-O compounds. *Journal of The Electrochemical Society, 143*(3), 825-833.

Xiang, H., Chen, J., Li, Z., & Wang, H. (2011). An inorganic membrane as a separator for lithium-ion battery. *Journal of Power Sources, 196*(20), 8651-8655. doi:http://dx.doi.org/10.1016/j.jpowsour.2011.06.055

Xiao, A. Y., Tong, Q. K., & Savoca, A. C. et al. (2001). Conductive ink for through hole application. *Components and Packaging Technologies, IEEE Transactions on, 24*(3), 445-449. doi:10.1109/6144.946492

Xie, H., & Zhou, Z. (2006). Physical and electrochemical properties of mix-doped lithium iron phosphate as cathode material for lithium ion battery. *Electrochimica Acta, 51*(10), 2063-2067. doi:http://dx.doi.org/10.1016/j.electacta.2005.07.014

Xu, J., & Chen, G. (2010). Effects of doping on the electronic properties of LiFePO4: A first-principles investigation. *Physica B: Condensed Matter, 405*(3), 803-807. doi:http://dx.doi.org/10.1016/j.physb.2009.05.035

Xu, Y., Schwab, M. G., & Strudwick, A. J. et al. (2013). Screen-printable thin film supercapacitor device utilizing graphene/polyaniline inks. *Advanced Energy Materials, 3*(8), 1035-1040. doi:10.1002/aenm.201300184

Yabuuchi, N., Yoshii, K., & Myung, S.-T. et al. (2011). Detailed studies of a high-capacity electrode material for rechargeable batteries, Li_2MnO_3–$LiCo_{1/3}Ni_{1/3}Mn_{1/3}O_2$. *Journal of the American Chemical Society, 133*(12), 4404-4419. doi:10.1021/ja108588y

Yang, P., Zhang, P., & Shi, C. et al. (2015). The functional separator coated with core–shell structured silica–poly(methyl methacrylate) sub-microspheres for lithium-ion batteries. *Journal of Membrane Science, 474*, 148-155. doi:http://dx.doi.org/10.1016/j.memsci.2014.09.047

Yi, T.-F., Xie, Y., & Shu, J. et al. (2011). Structure and electrochemical performance of niobium-substituted spinel lithium titanium oxide synthesized by solid-state method. *Journal of The Electrochemical Society, 158*(3), A266-A274. doi:10.1149/1.3533391

Yoo, H. D., Markevich, E., & Salitra, G. et al. (2014). On the challenge of developing advanced technologies for electrochemical energy storage and conversion. *Mater. Today, 17*(3), 110-121.

Yoshio, M., Tsumura, T., & Dimov, N. (2005). Electrochemical behaviors of silicon based anode material. *Journal of Power Sources, 146*(1–2), 10-14. doi:http://dx.doi.org/10.1016/j.jpowsour.2005.03.143

Zaghib, K., Simoneau, M., & Armand, M. et al. (1999). Electrochemical study of $Li_4Ti_5O_{12}$ as negative electrode for Li-ion polymer rechargeable batteries. *Journal of Power Sources, 81–82*, 300-305. doi:http://dx.doi.org/10.1016/S0378-7753(99)00209-8

Zhang, F., Ma, X., & Cao, C. et al. (2014). Poly(vinylidene fluoride)/SiO_2 composite membranes prepared by electrospinning and their excellent properties for nonwoven separators for lithium-ion batteries. *Journal of Power Sources, 251*, 423-431. doi:http://dx.doi.org/10.1016/j.jpowsour.2013.11.079

Zhang, S. S. (2007). A review on the separators of liquid electrolyte Li-ion batteries. *Journal of Power Sources, 164*(1), 351-364. doi:http://dx.doi.org/10.1016/j.jpowsour.2006.10.065

Zhang, W., Bi, E., & Li, M. et al. (2016). Synthesis of Ag/RGO composite as effective conductive ink filler for flexible inkjet printing electronics. *Colloids and Surfaces A: Physicochemical and Engineering Aspects, 490*, 232-240. doi:http://dx.doi.org/10.1016/j.colsurfa.2015.11.014

Zhang, Y., Lei, C., & Kim, W. S. (2013). Design optimized membrane-based flexible paper accelerometer with silver nano ink. *Applied Physics Letters, 103*(7), 073304.

Zielke, D., Hübler, A. C., & Hahn, U. et al. (2005). Polymer-based organic field-effect transistor using offset printed source/drain structures. *Applied Physics Letters, 87*(12), 123508. doi:http://dx.doi.org/10.1063/1.2056579

Zolriasatein, A., & Shokuhfar, A. (2015). Size effect on the melting temperature depression of Al 12 Mg 17 complex metallic alloy nanoparticles prepared by planetary ball milling. *Physica E: Low-dimensional Systems and Nanostructures, 74*, 101-107.